FORMATION OF ORGANIC AEROSOL THROUGH CLOUD CHEMISTRY: INSIGHTS FROM THE OH RADICAL OXIDATION OF FILTERED RAINWATER

by

ANJULI RAMOS-BUSOT

A thesis submitted to the

Graduate School-New Brunswick

Rutgers, The State University of New Jersey

in partial fulfillment of the requirements

for the degree of

Master of Science

Graduate Program in Environmental Sciences

written under the direction of

Barbara J. Turpin

and approved by

_____

_____

_____

New Brunswick, New Jersey

January, 2012

ABSTRACT OF THE THESIS

Formation of Organic Aerosol through Cloud Chemistry: Insights from the OH Radical Oxidation of Filtered Rainwater

By ANJULI RAMOS-BUSOT

Thesis Director:

Barbara J. Turpin

Organic particulate matter in the atmosphere plays an important role in climate forcing, visibility, and adverse health effects. Atmospheric organic aerosol is predominantly of secondary origin, formed in the atmosphere. Laboratory photooxidation experiments, atmospheric aerosol measurements below vs. above clouds and at increasing humidity, and modeling studies all suggest that secondary organic aerosol (SOA) forms from water-soluble gases through aqueous chemistry in clouds and wet aerosols (aqSOA). Previous laboratory experiments are simple compared to the atmospheric water media (single compound deionize water solutions), thus a more realistic approach is needed for the understanding of SOA formation through aqueous chemistry. We conducted batch photooxidation experiments with three different rainwater samples from Camden and Pinelands, NJ and hydroxyl radicals (formed from 150 μM H_2O_2 + UV radiation). We used rainwater (RW) as a surrogate for cloud water in these experiments.

SOA precursors and products were identified by real-time Electrospray Ionization – Mass Spectrometry (ESI-MS, continuous online sampling) and by Ion Chromatography (discrete samples). Precursors were found predominantly in the positive mode, suggesting the presence of aldehydes, alcohols and organic peroxides, and products were found predominantly in the negative mode, suggesting the presence of organic acids. A decrease in the abundance of ions with the same unit mass-to-charge ratio as standards of glyoxal, methylglyoxal and glycolaldehyde and an increase in the abundance of ions associated with organic acids (e.g., oxalic and pyruvic acid) suggest that these aldehydes were present and reacting. The evidence is strongest for methylglyoxal (three RW samples). Glyoxal oxidation appears to occur in two RW samples; evidence for glycolaldehyde is not as strong. Other potential contributors to SOA formation (precursor and products) were identified based on their percentage of change and absolute change in ion abundance across the reaction.

Acknowledgements

The past two years and a half have been the most fulfilling for both my personal life and scientific career. I give my gratitude to all the people that helped me to reach this milestone in my life, especially Dr. Evelyn Erenrich and Dr. Barbara Turpin. Dr. Erenrich enriched my scientific preparation through my participation in the Research in Science and Engineering (RISE) Program at Rutgers University in 2008. I am grateful for all of her scientific and personal advice, and for helping me become a Rutgers graduate student. Dr. Turpin was not only an incredible advisor and professor, but also someone that trusted me, and most importantly that I truly trust. She pushed me further in both my academic and research paths, and encouraged me to keep going no matter what. Her motivation, excitement and passion towards science inspired and showed me how to be a better researcher every day. I want to thank you both for being two of the most influential women in my life. I give my gratitude to Ron Lauck, his expertise in the IC and ESI-MS helped my experiments become extremely successful. My committee members, Dr. Annmarie Carlton and Dr. John Reinfelder were of great help in the improvement of my thesis work. Thank you Dr. Carlton for helping me to give better research presentations, the Atmospheric Chemistry project was of great help. Dr. Yong Lim, the postdoctoral fellow who's incredible expertise in organic chemistry made me believe he was an organic chemist, but in reality is a physical chemist (even better), helped me understand in more depth my research and experiments. Thank you Diana L. Ortiz, Jeffry R. Kirkland, Natasha Hodas, and Yi Tan for all the time that you helped me with my talk practices, for teaching me, for the advice, for the sushi during lunch, for

making the laboratory environment so great, and most importantly your friendship. Last but not least, my family, my close friend Kenneth and Gabriel for all your support, for believing in me, and for all your love. Gabriel, I could not have done it without you. Thank you all.

Table of Contents

List of tables

List of illustrations

Chapter 1. Introduction

1.1 Background

Atmospheric particulate matter (PM) has both direct and indirect effects on climate. The uncertainties in these are among the largest sources of uncertainty in climate change (IPCC, 2001). Absorption and scattering of radiation are direct effects. Particle properties such as size and composition, including water content, have a strong impact on the scattering or absorption of both incoming and outgoing solar radiation, cooling or heating the Earth's surface and atmosphere and affecting climate. Airborne particles (aerosols) also perturb climate through the modification of clouds and precipitation; this is considered the indirect effect (Twomey, 1991). Aerosol particles serve as nuclei for water condensation, consequently forming water droplets, hence clouds. It has been shown that the number of cloud condensation nuclei (CCN) has an impact in the formation, lifetime, and radiative properties of clouds (Twomey, 1974). PM also has a significant negative impact on human health, particularly to respiratory and cardiovascular systems (Harrison and Yin, 2000; Davidson et al., 2005; Pope and Dockery, 2006; EPA, 2004).

Organic compounds typically account for 20 - 70% of dry particle mass in the atmosphere, depending on location (Zhang et al., 2007). Organic particulate matter in the atmosphere is both directly emitted (Primary) and formed in the atmosphere from gaseous emissions (Secondary) (Turpin et al., 2000). Primary organic aerosol (POA) comes from sources like wind-driven soils and biological materials, volcanic eruptions, biomass burning, and fossil fuel combustion (Hallquist et al., 2009).

Secondary organic aerosol (SOA) is formed in the atmosphere from the photochemical oxidation of biogenic and anthropogenic gaseous organic emissions (Turpin et al., 2000; Seinfeld and Pankow, 2003; Fu et al., 2008). Several kinds of atmospheric measurements have verified and documented the importance of secondary organic aerosol formation. These include time resolved measurements of organic carbon (OC) and POA tracers (e.g., elemental carbon) (Turpin et al., 1991; Turpin and Huntzicker, 1995), factor analysis of organic mass fragments by Aerosol Mass Spectrometer (Zhang et al., 2005; Zhang et al., 2007; Ulbrich et al., 2009; Jimenez et al., 2009), and measurements of new particle growth (Riipinen et al., 2007; Smith et al., 2008; Metzger et al., 2010). For example, atmospheric measurements of the molecular composition of nanoparticles in a new particle formation and growth event during March in Tecamac, Mexico suggest that new particle growth was enhanced by organics and organics dominated the PM composition over sulfate and nitrate during the entire measurement period (11:14am – 3:45pm), with organics comprising 63 ± 15% to 98 ± 29% of the mass (Smith et al., 2008).

The formation of secondary inorganic aerosol is reasonable well understood compared to the formation of SOA (Hallquist et al., 2009). This is due, in part, to the complexity of organic aerosol. There are a large number of precursor compounds, reaction mechanisms and products. SOA is formed through two different mechanisms: gas-phase chemistry and vapor-pressure driven partitioning into particulate organic matter (gas SOA), and gas-phase chemistry followed by aqueous

chemistry (aqueous SOA). In the traditional theory of SOA formation (gas SOA) photochemical reactions in the gas phase produce products with a low enough vapor pressure that they partition into the organic matter in pre-existing particles (Seinfeld and Pankow, 2003). SOA formation through this mechanism highly depends on product volatility, temperature, and particulate organic mass. Precursors must have carbon numbers greater than C7 in order to produce products with low enough vapor pressure to give high SOA yields (Seinfeld and Pankow, 2003). Although this theory is a fundamental tool for modeling SOA (Seinfeld and Pankow, 2003; and Donahue et al., 2006) it does not produce O/C (oxygen/carbon) and OM/OC (organic matter/organic carbon) ratios as high as those found in ambient organic aerosol (Aiken et al., 2008; Lim et al., 2010). Models including only gas SOA and POA under predict OC concentrations (Tsigaridis and Kanakidou, 2003; and Heald et al., 2005). Model predictions show better agreement and higher correlations with measurements after incorporation of aqueous SOA formation (Carlton et al., 2008; Fu et al., 2008, 2009).

Aqueous SOA formation occurs when water soluble organics, formed through gas-phase chemistry, partition into atmospheric waters (aerosols, cloud droplets, and fogs), react with dissolved oxidants (e.g. OH radical, H_2O_2, O_3 and NO_3 radical) and form low volatility products. When these atmospheric waters evaporate, the low volatility products (e.g. carboxylic acids, and high molecular weight species) partly stay in the particle phase (Blando and Turpin, 2000). When conditions favor gas phase photochemistry and when liquid water is abundant, SOA formation

through aqueous chemistry is most likely to occur (Lim et al., 2010) because water-soluble aqueous SOA precursors are formed through gas phase photochemistry (Chang and Hill, 1980). Precursors of aqueous SOA are too volatile to contribute to SOA formation through gas-phase chemistry and vapor pressure based partitioning into organic matter (traditional theory). Thus, the addition of organic aqueous chemistry to models will increase the concentrations and change the spatial and temporal patterns of predicted organic aerosol concentrations.

High molecular weight compounds (HMWC) also called humic-like substances (HULIS), account for a substantial fraction of particulate matter, are often found in atmospheric waters, and their atmospheric dynamics suggest they are largely secondary (Zappoli et al., 1999; Krivacsy et al., 2000; Feng and Moller, 2004; Likens, 1983; Graber and Rudich, 2006). This material has some characteristics in common with humic and fulvic acids. HMWCs are a complex mixture of several classes of polyfunctional compounds, including oligomers, organosulfates and nitrooxy organosulfates (Hallquist et al., 2009). Lim et al (2010) predicted based on aqueous organic radical-radical reactions that HMWC forms through the aqueous OH radical oxidation of aldehydes in wet aerosols. They can also form through dark reactions in the presence of high concentrations of ammonium sulfate (Noziere et al., 2007; Shapiro et al., 2009). Altieri et al., (2009), found 26 high molecular weight CHO compounds in rainwater with the same elemental formulas as compounds formed from the aqueous OH radical oxidation of methylglyoxal. This suggests that the oligomerization of known biogenic and

anthropogenic organic precursors through in-cloud or aerosol-phase reactions could contribute to the complex HMWC measured in aerosols, fogs and rainwater.

Fog and cloud processing has been recognized as the major production pathway for sulfate (a major component of atmospheric aerosols) (Wolff et al., 1979; Graedel and Weschler, 1981; Graedel and Goldberg, 1983; Graedel et al., 1985,1986; Seigneur and Saxena, 1984; Karamchandani and Venkatram, 1992; McHenry and Dennis, 1994). Interestingly, a strong correlation between particulate sulfate and oxalate has been observed in East Asia and elsewhere (Yu et al., 2005). Oxalate is the most abundant water-soluble organic compound in both rural and urban aerosols (Facchini et al., 1999, Mader et al., 2004, Kawamura and Ikushima, 1993). And this correlation suggests a common dominant formation pathway for sulfate and oxalate (Yu et al., 2005), supporting the hypothesis that cloud processing is the predominant source of oxalate and a source of atmospheric SOA (Blando and Turpin, 2000). In fact, Myriokefalitakis et al. (2011) finds good agreement between measured oxalate and modeled oxalate produced globally through aqueous chemistry. During an aircraft study in the Houston area Sorooshian et al. (2007a, b) found that organic acids accounted for a larger fraction of the water-soluble PM mass above than below clouds, likely as a result of in-cloud chemistry followed by cloud droplet evaporation. These studies provide evidence that aqueous SOA contributes to the atmospheric SOA burden.

As previously mentioned, SOA is formed in the atmosphere from the oxidation of biogenic and anthropogenic organic emissions via oxidants formed photochemically. Bottom-up model estimates indicate an SOA flux of 12-70 Tg/yr from biogenic hydrocarbons (Kanakidou et al., 2005), 2-12 Tg/yr of SOA from anthropogenic hydrocarbons (Henze et al., 2008), a flux of 25 TgC/yr of POA from biomass burning and a flux of 9 TgC/yr of anthropogenic POA (Bond et al., 2004). This suggests that biogenic VOCs emissions contribute the most to SOA formation. Biogenic VOCs are derived from both marine and terrestrial ecosystems; including dimethylsulfide (Kettle and Andreae, 2000), carboxylic acids (Kawamura and Sakaguchi, 1999), dimethyl- and diethylammonium salts (Facchini et al., 2008) from marine ecosystems, and isoprene (which represents 38% of the VOC budget, Hallquist et al., 2009) from terrestrial ecosystems. Chen et al. (2007) suggests that SOA formation through cloud processing can be important at locations that are strongly influenced by monoterpene emissions; they calculated a 27% increase in SOA formation in a rural northeastern US scenario after adding aqueous SOA from isoprene to a 0-D model.

Atmospheric photo-oxidation of isoprene (and other alkenes and aromatics) produces water-soluble species (e.g., glyoxal, methylglyoxal and glycolaldehyde) (Lim et al., 2005). These species are too small (volatile) to contribute to gas SOA formation through gas-phase chemistry and vapor pressure based partitioning. However they are good candidates for aqueous SOA. Many studies have focused on characterizing the aqueous photo-oxidation products of these water-soluble species

through controlled laboratory experiments and chemical modeling (Lim et al., 2005; Altieri et al., 2006; Carlton et al., 2007; Tan et al., 2009, 2010; Perri et al., 2009; and Lim et al., 2010). These aldehydes react with OH radicals to produce less volatile species including oxalate, glycolate and HMWC with O/C ratios of 1-2, high enough to help explain the high atmospheric O/C ratios. Aqueous glyoxal, methylglyoxal, and glycolaldehyde OH radical oxidation pathways are shown in Figure 1.1. Aqueous chemistry is different from gas phase chemistry in part because these compounds are hydrated in the aqueous phase. Note that dissolved organics are present at very high concentrations in wet aerosols. At these high concentrations intermediate radical products can react with themselves rather than with O_2 and form HMWC (Altieri et al., 2006, Tan et al., 2010, and Lim et al., 2010).

1.2 Hypothesis, Specific Aims and Synopsis

To our knowledge controlled laboratory studies used to obtain insights concerning aqueous SOA formation have only been conducted with single compounds in deionized water. These experiments are simple compared to what happens in clouds and aerosols. The goal of the work described below is to use a more realistic cloud water surrogate, rainwater, to 1) see if the glyoxal, methylglyoxal and glycolaldehyde chemistry observed in previous single-compound laboratory experiments is observed in more realistic cloud water surrogates, and 2) see if there are other previously unrecognized precursors and products. For this purpose I produced OH radicals in filtered rainwater and examined changes in concentrations of constituents (i.e., precursors and products). I hypothesize that

organic compounds in the rainwater will oxidize forming lower volatility and higher molecular weight compounds (HMWC). I expect that glyoxal, methylglyoxal and glycolaldehyde would be consumed and organic acids would form. Additionally, I expect that other yet unrecognized precursors and products would also contribute to aqueous SOA formation, and that these experiments would help to identify them.

This study was done with New Jersey rainwater samples collected in Camden and Pinelands. Altieri et al. (2009) previously analyzed rainwater samples taken in these two locations; determining the elemental formula rainwater composition (47% CHO, 25% CHOS, 13% CHON, 9% other, and 5% CHONS for negative mass/charge species from 50-500 amu). Known components of aqueous SOA, including organic acids and HMWC were detected in these rainwater samples. Experiments were conducted in a batch reactor using a filtered rainwater sample and OH radicals. H_2O_2 photolysis was used to continuously produce the OH radicals. Note that OH radical oxidation is the major sink for organic compounds in cloud and fog water (Faust and Allen, 1993; Arakaki and Faust, 1998; Anastasio and McGregor, 2001; Arakaki et al., 2006). Continuous sampling was conducted during experiments with real time analysis by Electrospray Ionization–Mass Spectrometry (ESI-MS) (m/z 50 to 500) and discrete samples were taken for quantification of organic acids by Ion Chromatography (IC).

Results indicate that precursors are predominantly compounds found in the ESI-MS positive mode analyses suggesting that they are aldehydes, alcohols, and/or

organic peroxides, and that products are predominantly compounds found in the negative mode suggesting that they are organic acids. Strong evidence was found for the aqueous oxidation of methylglyoxal and the production of pyruvic and oxalic acids. This study provides more definitive evidence that organic acids with O/C ratios of 1-2 found predominately in the particle phase in the atmosphere (e.g., pyruvate, oxalate) are formed from the aqueous oxidation of aldehydes (e.g., methylglyoxal) in clouds by showing that this chemistry happens in filtered rainwater (a cloud water surrogate).

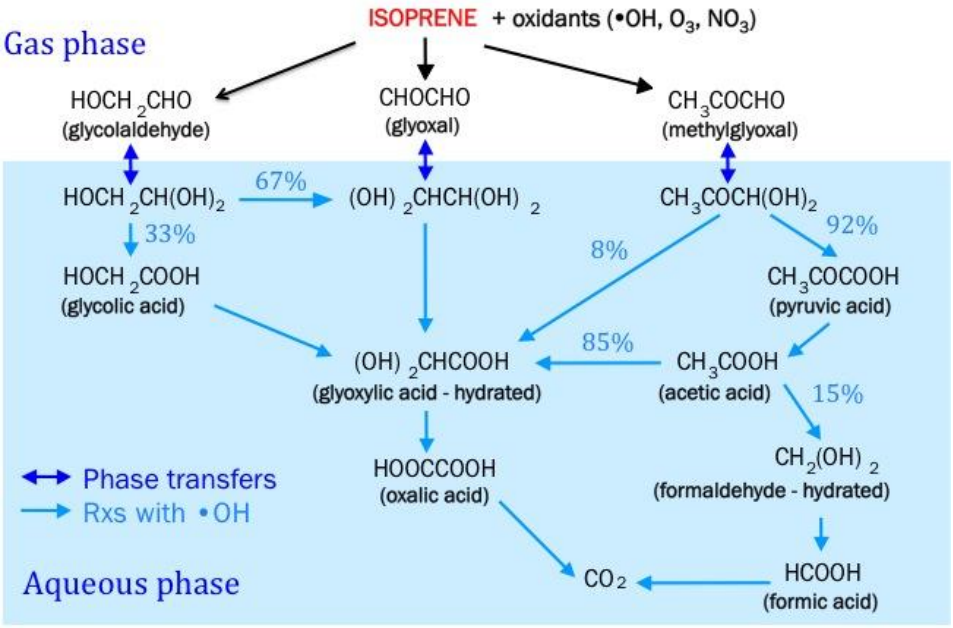

Figure 1.1. Aqueous OH radical oxidation of glycolaldehyde, glyoxal and methylglyoxal. All products of the gas-phase isoprene photochemistry (Lim et al., 2005).

Chapter 2. Methodology

2.1 Sample Collection

Three rainwater samples were used in this study (Table 2.1). Two were collected in Camden NJ in April and June 2003 (Latitude 39°56′57.45′′ N; Longitude 75°7′16.60′′ W; elevation 11 m) and the third was a composite of rainwater, collected in June and September 2003 from Pinelands, NJ (Latitude 39° 56′ 43.61′′ N; Longitude 74° 37′ 1.52′′ W; elevation 1 m) and Camden, NJ. Camden is a heavily industrialized city across the Delaware River and directly east of Philadelphia, PA. Pinelands is 30 miles east of Camden in the Lebanon State Forest. Camden and Pinelands rainwater are both impacted by similar regional air pollutants. I selected samples during spring and summer because I expect photochemistry to produce water-soluble organic compounds that can undergo aqueous atmospheric chemistry, and photochemical activity is greatest in the summer.

Samples were collected using wet-dry deposition collectors (Aerochem Metrics Model 301, Bushnell, FL. Rain collectors were fitted using stainless steel buckets and opened only during wetfall events. The collector's type and its placement at the site adhere to regulations outlined by the National Atmospheric Deposition Program (Bigelow et al., 2001). In order to minimize microbial degradation of DOM and consumption of inorganic nutrients the samples were retrieved within 12 hours of each rain event. Samples were filtered through pre-combusted glass fiber filters (Whatman GFF; baked for four hours at 500 °C; then rinsed with deionized water) ensuring analysis of the dissolved constituents only.

Contamination due to field sampling and laboratory sample processing was minimal (field and filter blanks <5% DOC-C). After collected, the rainwater was analyzed for nutrients and stored at −20°C in pre-cleaned polypropylene screw-capped tubes until analysis. For this study the samples were left overnight to thaw in the fridge; all samples were completely homogeneous before experimental use. Nutrient analyses were repeated to assess the chemical stability of the samples during storage (Table 2.1). A paired t-test indicates that the nutrient concentrations measured in 2003 and 2011 were not significantly different at the 95% confidence level for the two samples and one composite sample used in this work. The Pinelands September 19, 2003 sample (one of the samples used for the rainwater sample composite) nutrient concentrations were significantly higher on 2011 than 2003, but the composite concentrations were not.

2.2 Batch Photooxidation Reactions

OH radical oxidation of rainwater, a surrogate for cloud water, was used to gain insights into the photo-oxidation of organics in cloud water. Batch reactions were conducted in a 250 mL reaction vessel (250mL Reactor Vessel Jacketed, Ace Glass, Vineland, NJ). The vessel was cleaned with Alcanox (Fisher Cat No. or Electron Microscopy Sciences) and deionized (DI) water in a sonicator for 15 minutes and rinsed a minimum of three times with DI water before every use. I hypothesize that organic compounds in the rainwater will oxidize forming lower volatility and higher molecular weight compounds (HMWC). Continuous and discrete samples were collected for identification and characterization of the behavior of organic

precursors and products in the rainwater oxidation experiments. Each rainwater experiment was conducted four times, twice with negative-mode ESI-MS analysis and twice with positive-mode ESI-MS analysis. Control experiments were also conducted. Experiments were carried out for 4 hours. Rainwater alone was sampled for the first hour for the purpose of achieving a constant instrumental baseline. Then H_2O_2 was added and a UV lamp was placed in the quartz immersion well in the center of the reaction vessel to provide a continuous supply of OH radicals over the next 3 hours. The UV lamp was warmed up for at least 30 minutes before use. Air was constantly pumped through the immersion well for cooling purposes, and the samples were constantly mixed with a magnetic bar.

OH radicals were continuously formed *in situ* from photolysis of 150 μM H_2O_2 with a monochromatic mercury UV lamp (λ = 254 nm) (Strahler NN 8/15, Heraeus Noblelight, Inc. Duluth, GA). In previous experiments conducted with single compounds and the same type of lamp, H_2O_2 concentrations were usually five times the initial precursor concentration. In previous experiments conducted with 30 μM glyoxal or methylglyoxal and 150 μM H_2O_2, OH radical concentrations were approximately 10^{-12} M, based on a dilute aqueous chemistry model (Tan et al., 2009, 2010). Concentrations of glyoxal are typically a few μM in cloudwater and a few hundred μM in fogwater. The concentration of total dissolved organic carbon in these rainwater samples was 60 – 120 μM. Assuming that approximately on half to one quarter of this organic matter is as reactive as glyoxal, we expect the

concentration of OH radicals in the experiments reported herein to be approximately 10^{-12} M.

Throughout the experiment, sample was pulled continuously in real time into an ESI-MS, and discrete samples were taken for IC analysis. Temperature readings were recorded throughout the entire experiment, and dissolved oxygen (DO) and pH were recorded at the beginning and end of each experiment. Refer to Appendix A for temperature, pH and DO measurements. The pH averaged 5.2 ± 0.8 at the beginning of the reaction and 5.0 ± 0.6 at the end of the reaction. Dissolved oxygen (DO) averaged (107 ± 7)% at the beginning of the reaction and (107 ± 5)% at the end of the reaction.

Despite a constant flow of water through the vessel's water jacket, the temperature in the reaction vessel increased from ~20°C to ~39°C during the experiments with the first and second sample, and, as shown in Chapter 3, the oxalate time profiles for replicate experiments were not reproducible. One possible reason for the discrepancies between experiments is the heating of the rainwater sample during the experiments. (Note: Unlike previous experiments conducted in this laboratory, which started with 1 L, these experiments began with 250 mL.) Therefore, a chiller (Isotemp 2150 Nano Circulator, Fisher Scientific) was added to the system to bring ~25°C water through the water jacket. Constant temperature readings of ~25°C were obtained operating the chiller with a constant temperature of 12°C during a control experiment (DI water, and the UV lamp) with no sampling.

With the chiller, temperatures readings were maintained between 24°C and 29°C while conducting the batch photooxidation experiments with the third rainwater sample. Although this average temperature range is relatively constant, I believe that the later temperature readings are not true temperature measurements. Throughout the experiments the rainwater volume in the vessel decreases due to continuous sampling. This decrease in volume caused the thermometer to no longer be immersed in the rainwater, but just touching the vessel or be suspended in the air, thus, not indicating the appropriate temperature readings of the rainwater. Since the air heats up faster than water and the vessel is directly touching the casing surrounding the UV lamp, I think these later temperature readings are higher than the real rainwater readings. A three-hour control experiment (DI water, UV lamp, and no sampling) with the thermometer immersed in water was conducted in order to determine the true temperature. During this control experiment the temperature was (26.9 ± 0.9) °C. Refer to Appendix A for the detailed temperature measurements. This suggests that the chiller provided a constant temperature during experiments conducted with the third rainwater sample, and that the later temperature readings are not representative of the true temperature of the rainwater. This is considered a limitation of this work, however we do know all 4 replicate experiments were reproducible (based on oxalate time series) with the addition of the chiller to the system.

2.3 Product Analysis

The ESI-MS (HP-Agilent 1100) sampled continuously from the reaction vessel via an Agilent 1200 series isocratic high-pressure liquid chromatography (HPLC) pump (0.22 mL/min). The sample is mixed with the mobile phase (50%/50% mixture of 0.05% formic acid in water and methanol) pumped by a binary pump also at a flow of 0.22 mL/min. Note that a transit time of ~ 5 minutes (time it takes for the rainwater to reach the Electrospray chamber) was taken into account for the analysis of all rainwater samples. Nitrogen (10L/min, 350 °C) was used as the drying gas. A fragmenter voltage of 40 V and a capillary voltage of 3000 V were used. Data were recorded in Chemstation (version A.07.01) and processed using custom-made computer programs written in C++ by a former laboratory member. SOP and programs are provided in Appendix D.

The ESI-MS does not fragment compounds. Negative ions (e.g., deprotonated acids) are analyzed in the negative mode and positive ions (e.g., protonated aldehydes and alcohols) in the positive mode. Positive mode analysis is more challenging than negative mode analysis, because ions are sometimes detected as monomer plus proton, dimer plus a proton, monomer plus Na^+, or dimer plus Na^+. Negative mode ions are identified as molecular weight minus one (de-protonation of acidic proton). Ions from 50 to 1000 amu were detected in both negative and positive modes.

The IC system (ICS-3000, Dionex, Sunnyvale, CA; IonPac AS11-HC anion exchange column with AG11-HC guard column, 30°C) separates carboxylic acids based on their polarity. The mobile phase was an aqueous KOH solution (0.4 mL/min; 1–84 mM gradient over 35 min). Discrete samples were collected every 20 minutes through out the entire three-hour reaction, except at the beginning, when more samples were collected to capture the more rapid changes in concentration that are observed when OH radicals are first introduced. Samples were collected in the rainwater alone before introduction of OH radicals, at 0 min. (right after the H_2O_2 and UV lamp were added), 2 min., 5 min., 10 min., 20 min., and then every 20 minutes.

Every time experimental samples were analyzed by IC, DI water and a mixed standard were analyzed before and after the samples. Three time points during the reaction (20 min., 40 min., 120 min.) are considered particularly important due to concentration increases or decreases of specific species of interest, therefore these samples were analyzed in duplicate. Organic acids were identified and quantified based on a 7-point calibration curve done with acid standards, using Chromeleon software (Dionex). This IC column does not separate aldehydes or alcohols. In this work ESI-MS data were used to characterize the real-time behavior of precursors, intermediates, and products in order to gain a better understanding of what SOA precursors might be important in cloud water. IC data provide quantitative information on expected organic acids. Further details about sampling, instrumentation and software are provided in Appendix D.

2.4 Quality Control

Single-compound standards of glyoxal, methylglyoxal, and glycolaldehyde, and a mixed standard of glyoxylic acid, glycolic acid, pyruvic acid, oxalic acid, malonic acid, succinic acid, formic acid, and sulfate (25 μM each) were analyzed by ESI-MS (6 injections of each) for identification of these species in experimental data. The mean ion abundance (± SD) for each mass to charge (m/z) ratios was calculated from the 6 injections, and m/z ratios with abundances statistically greater than zero at the 0.05 level (t-test) were retained. Software processing details of the 6 injections are provided in Appendix D. The ion abundances of the m/z ratios identified in the DI water blank (6 injections) were subtracted from all standards. MS Spectra of aldehyde and acid standards are provided in Appendix A. Glyoxal is detected as its dimer plus H^+ (m/z $^+$ 117) and m/z $^+$ 131, methylglyoxal by m/z $^+$ 131 and its dimer plus a H^+ (m/z $^+$ 145), and glycoldehyde as m/z $^+$ 101 and m/z $^+$ 115. Organic acids were detected in the negative mode as molecular weight minus one: glyoxylic acid (m/z $^-$ 73), glycolic acid (m/z $^-$ 75), pyruvic acid (m/z $^-$ 87), oxalic acid (m/z $^-$ 89), sulfate (m/z $^-$ 97), malonic acid (m/z $^-$ 103), and succinic acid (m/z $^-$ 117). Formic acid (m/z $^-$ 45) was not detected since the detection limit of the instrument is m/z 50. Acetic acid (m/z $^-$ 59) was not present in the acids standard, however Altieri et al. (2006) analyzed acetic acid standards in this ESI-MS and found that it could not be detected despite having a molecular weight greater than 50.

Control experiments were conducted following the same methods previously mentioned (Section 2.2), with rainwater except without H_2O_2 (1st round, UV control)

and without UV (2nd round, H_2O_2 control). Both types of control experiments were conducted for each ESI-MS mode (+ and -), for a total of four control experiments. Continuous sampling was performed by ESI-MS, and discrete samples were taken for IC analysis. Mass Spectra and IC data for all control experiments are provided in Appendix C. Both IC and ESI-MS data showed that m/z $^-$ 89 (oxalate) was considerably consumed in rainwater with UV light but no H_2O_2,. However, m/z $^-$ 89 remains relatively constant in the presence of H_2O_2 but absence of UV.

A mixed standard of known concentration (50 μM each) containing: oxalic, pyruvic, malonic, glyoxylic, glycolic, succinic, formic acids and sulfate was analyzed by IC at the beginning and end of each sequence of experimental discrete samples to provide a measure of accuracy for quantified acids. Also at the end of the sequence, three samples from different experimental time points were analyzed for a second time to determine analytical precision. Pooled statistical analyses were performed for the third rainwater sample to report analytical precision, variability between replicate experiments and system accuracy. The analytical precision was 2%, expressed as a pooled relative standard deviation (pooled standard deviation/mean) of all acids' duplicate analyses. The variability between replicate experiments was 7%, expressed as the pooled relative standard deviation of organic acid concentrations across experiments. The pooled analytical precision and variability between replicate experiments analyses considered all acids except for malonic acid because of the relatively high values (20% and 75%) compared to the other acids (≤ 10%). The system accuracy was 9%, based on the pooled relative

standard deviation of all acids' mixed standard analyses. The pooled accuracy analysis considered all acids except for succinic and glycolic acid, again because of the relatively high values (26% for succinic and 62% for glycolic acid) compared to the other acids (≤ 13%). Refer to Appendix A for the complete detailed statistical analyses.

Dynamic blanks were taken before experiments conducted with the third rainwater sample (experimental and control experiments). To collect dynamic blanks, the reaction vessel was filled with deionized water after cleaning but before introducing the rainwater into the vessel. The dynamic blank samples were taken like regular experimental samples and used to determine whether there was any system contamination. No contamination was found for any acids except for malonic acid. In general the IC quantification of malonic acid in the 3rd rainwater sample (dynamic blanks were only performed for experiments with this sample) was poor, thus it was not included in the pooled statistical analyses discussed above. The analytical precision of malonic acid based on replicate sample analysis was 20%. The between-experiment variability in malonic acid concentrations was 75%, and the accuracy of malonic acid based on quantification of the mixed standard was 9%. The coefficient of determination (r) for the 7 point calibration curve was 0.983794. This suggests that malonic acid can be quantified accurately by IC, but the production and loss of malonic acid is more uncertain than other quantified acids.

2.5 Other potential reactants, intermediates and products

Glyoxal, methylglyoxal, glycoladehyde, and their organic acids products are found in cloud water (Munger et al., 1990; Munger et al., 1995; Bruggemann et al., 2005; Valverde- Canossa et al., 2005). The formation of organic acids (e.g., oxalic, glyoxylic and pyruvic acids) from the OH radical photo-oxidation of aldehydes was demonstrated in our experiments with natural rainwater. However, cloudwater contains many organic compounds, which could potentially form SOA through aqueous oxidation followed by droplet evaporation (Sorooshian et al. (2007a, b)). Thus, one goal of this research is to provide insights into the identities of other potential reactants, intermediates, and products. Potential contributors from 50 to 500 amu were identified using the third rainwater sample based on their percent change in ion abundance across the experiment. For this purpose the ion abundances 50, 130 and 210 minutes after the experiment began were used. About 50 minutes into control experiments (without UV or H_2O_2) mass spectral signals (ion abundance) have stabilized. In OH radical experiments this time point is before the introduction of OH radicals. Visual observations shows that about 130 minutes into the experiments reactants have decreased, and intermediates have increased. By about 210 minutes, reactants and intermediates have decreased, whereas products have increased compared to the beginning of the reaction. Table 2.2 shows the evaluation criteria used. Species that decreased 50 % or more between 50 and 210 minutes are considered reactants. Species that increased 30% or more from 50 to 130 minutes and decreased 30% or less from 130 to 210 minutes are considered intermediates. Species considered as products increased 25 % or more from 50 to

210 minutes. The 20 measurements of ion abundance made just before and after a time point (e.g., 50 min) were averaged to perform these analyses.

The approach of Table 2.2 documents potential contributors to SOA formation in cloudwater based on percent of changes in ion abundance of a cloudwater surrogate (rainwater sample #3). However information about the absolute change in ion abundance is not obtained by this approach. For this reason standard deviation calculations were also conducted for the same m/z ratio range (including time points from 50 minutes to the end of the experiment for each m/z ratio) for the third rainwater sample, in order to determine which species had the highest change in ion abundance across the experiment (e.g., high consumption or production)

				NH_4 (µM)		NO_3 (µM)		DOC (µM)		PO_4 (µM)	
Sample	Collection Date	Location (NJ)	Storm Trajectory	2003	2011	2003	2011	2003	2011	2003	2011
1	June/04/03	Camden	WSW	27.1	24.2	15.7	16.6	121.6	112.7	0	0
2	April/12/03	Camden	SE	9.6	8.9	12.4	13.4	21.5	27.9	0	0
3	June/04/03	Pinelands	WSW	15.3	14.9	8.9	8.6	81.0	81.5	0	0
	Sept./19/03	Pinelands	SE	11.2	11.1	10.7	10.5	61.4	82.1	0.1	0
	Sept./19/03	Camden	SE	13.2	13.2	10.1	10.7	66.1	61.3	0	0

Table 2.1: NJ rainwater collection details and nutrient properties.

	$\frac{\bar{x}_{130}-\bar{x}_{50}}{\max(\bar{x}_{130},\ \bar{x}_{50})}$	$\frac{\bar{x}_{130}-\bar{x}_{210}}{\max(\bar{x}_{130},\ \bar{x}_{210})}$	$\frac{\bar{x}_{50}-\bar{x}_{210}}{\max(\bar{x}_{50},\ \bar{x}_{210})}$	$\frac{\bar{x}_{210}-\bar{x}_{50}}{\max(\bar{x}_{210},\ \bar{x}_{50})}$
Product	--------	--------	--------	≥ 25%
Reactant	--------	--------	≥ 50%	--------
Intermediate	≥ 30%	≥ 30%	--------	--------

Table 2.2: Evaluation criteria for the identification of other potential reactants, intermediates and products. M/z ratios from 50 through 500 were evaluated for third rainwater sample. $\bar{x}_{50}$, $\bar{x}_{130}$, and $\bar{x}_{210}$ are the averaged ion abundances (over 20 measurements) of a specific unit mass at about 50, 130 and 210 minutes into the experiment.

Chapter 3. Preliminary Results

Results of batch photo-oxidation reactions conducted by reacting the 1st (June 04, 2003, Camden) and 2nd (April 12, 2003, Camden) rainwater samples with OH radicals are reported here. ESI- MS and IC results suggest that as organic precursors (aldehydes) were consumed, organic products (organic acids) were produced. The batch photo-oxidation reactions were conducted as described in Section 2.2, and sampling and analysis were conducted as described in Section 2.3. As shown in Figure 3.1, oxalate increases in concentration as the reaction proceeds. Oxalate concentration time series for the third experiment is different from the rest of the experiments conducted with the same rainwater sample (first) and with the second rainwater sample. The third experiment is not included in Figure 3.2 for a better visualization of the other experiments. Oxalate concentration time series shown in Figure 3.2 peaked about 40 to 60 minutes after OH radicals were introduced, except for the fourth experiment in which oxalate reaches a maximum 140 minutes after the addition of OH radicals. Oxalate concentrations in experiments conducted with the second rainwater sample (experiments 5 to 8) are lower than for the first rainwater sample (experiments 1 to 4); peaking at ~ 1μM while for the first rainwater sample oxalate peaked at ~ 4 μM (excluding the third experiment). This can be attributed to the difference in DOC concentrations for these two rainwater samples, the first sample having roughly a factor of 5 higher DOC concentrations than the second (Table 2.1). The large differences between oxalate time profiles across replicate experiments, especially for the first rainwater

sample, suggest that the reaction did not proceeding at a reproducible rate. This might occur because constant water circulation through the vessel water jacket might not have been sufficient to maintain a constant temperature in the reaction vessel.

The oxalate results above for the first rainwater sample suggest that the two experiments analyzed by positive mode ESI-MS and the two with negative mode ESI-MS probably did not all occur at the same rate. Figure 3.3 shows the results of those replicate experiments with the most similar oxalate profiles for each rainwater sample. For the first rainwater sample experiment # 1 and #2 were the most similar (Figure 3.3 A) experiments analyzed by ESI-MS in the negative and positive mode. The positive mode analysis of experiment # 2 is shown in Figure 3.3 B. The abundance of all ions associated with glyoxal, methylglyoxal and glycolaldehyde decreased as the reaction proceeded; m/z^+ 131, m/z^+ 145, m/z^+ 101 and m/z^+ 115 decreased abruptly relative to m/z^+ 117. The ions, m/z^+ 117 and m/z^+ 131, are the major ions in the ESI-MS analysis of the glyoxal standard, m/z^+ 131 and m/z^+ 145 are the major ions for the methylglyoxal standard, and m/z^+ 101 and m/z^+ 115 are the major ions for the glycolaldehyde standard (Appendix A). The fact that m/z^+ 131 behaves in the same way as m/z^+ 145 suggests that m/z^+131 is dominated by methylglyoxal. These results support the hypothesis that glyoxal, methylglyoxal and glycolaldehyde are precursors of SOA formation through aqueous oxidation. Figure 3.3 C shows the ESI-MS negative mode analysis of experiment #1. As expected, the abundances of several negative mode ions (i.e., organic acids)

increased as the reaction proceeds. A notable exception is glycolic acid. The decrease in m/z^+ 117 and 131 followed by an increase in m/z^- 73, then by m/z^- 89 is consistent with glyoxal + OH radical forming glyoxylic followed by oxalic acid (Tan et al., 2009). The decrease in m/z^+ 131 and 145 (methylglyoxal) and subsequent formation of m/z^- 87 followed by m/z^- 59, m/z^- 73, and then by m/z^- 89 provides strong evidence that methylglyoxal was oxidized by OH radicals and subsequently produced pyruvic, acetic, glyoxylic and oxalic acids. However, the evidence for the glycolaldehyde OH radical oxidation pathway is not as strong as for glyoxal and methylglyoxal. The ions, m/z^+ 101 and 115 decrease in ion abundance is consistent with glycolaldehyde OH radical oxidation, however m/z^- 75 decreased, being inconsistent with glycolic acid expected increase (Perri et al., 2009).

The second rainwater sample shows a better agreement for oxalate between replicate experiments. Figure 3.3 D shows the three most similar replicate experiments for the second rainwater sample. Experiments #6 and #8 were the most similar. ESI-MS positive mode analysis for experiment #7 is shown in Figure 3.3 E. Only a slight decrease in the ion abundance of m/z^+ 131 and 145 occurred in experiment #7, consistent with the oxidation of methylglyoxal. However none of the ions associated with these aldehydes decreased in experiment #8 (Figure 3.4). All organic acids shown in Figure 3.3 F increased except again for m/z^- 75 (glycolic acid). As with the first rainwater sample, the oxidation of methylglyoxal and subsequent formation of pyruvic, acetic, glyoxylic and subsequently oxalic acid is supported by the increase in the ion abundance of m/z^- 87, 59, 73, and then 89. The

lack of an increase in m/z^- 75 (glycolic acid) suggests the evidence for glycolaldehyde is not as strong.

Initial ion abundances of m/z^+ 131, m/z^+ 145 and m/z^+ 115 for experiment #7 were very similar to the initial ion abundances for the first rainwater sample, however m/z^+ 117 and m/z^+ 101 for experiment #7 were considerably higher than for the first rainwater sample. This does not mean that m/z^+ 117 and m/z^+ 101 were necessarily more concentrated for the second rainwater sample. It could be that the ionization efficiency is greater since the DOC concentration of the second rainwater sample is lower. Even though experiment #7 and #8 were conducted one after the other on the same day, the initial abundance of ions shown in Figure 3.4 were different in these two experiments.

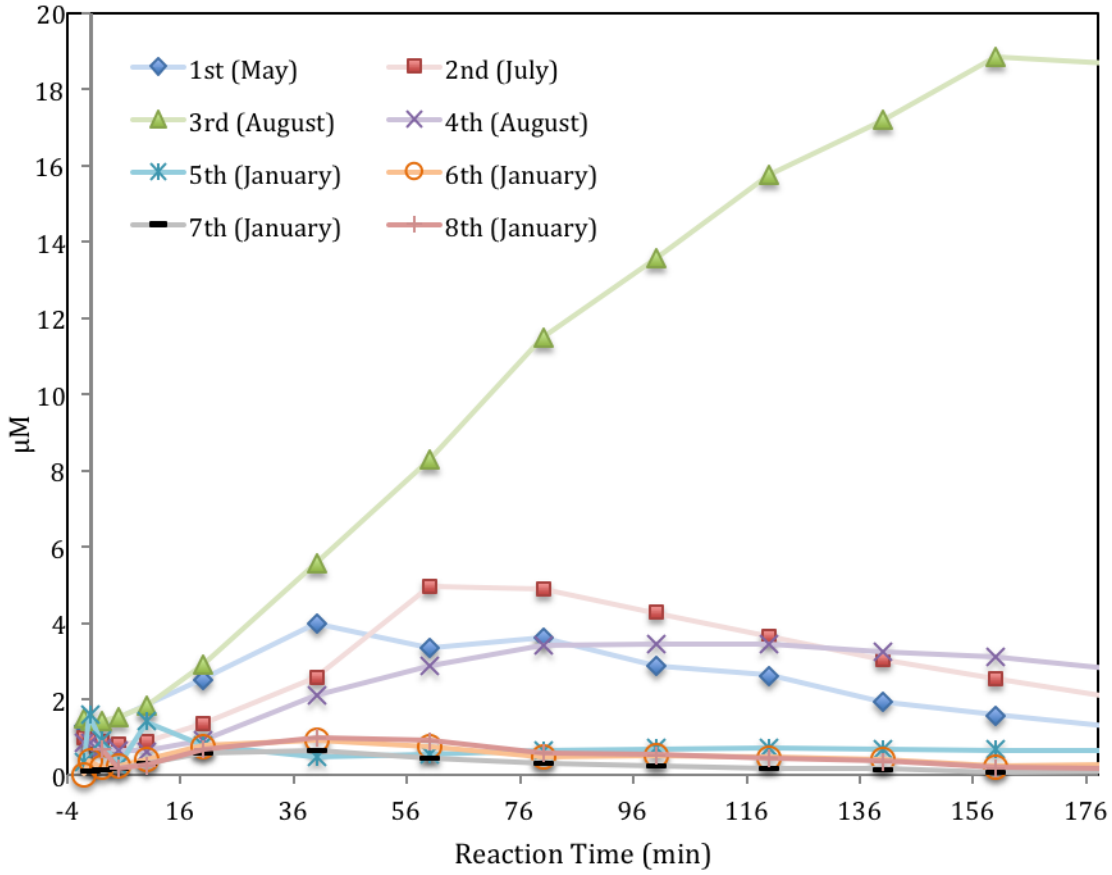

Figure 3.1: Oxalate concentration time series for experiments conducted with the first and second rainwater samples. Experiments 1-4 represent the first rainwater sample and experiments 5-8 represent the second rainwater samples. In this figure, t = 0 min indicates the time when OH radicals were introduced. The -2 time point is the pre-reaction quantification.

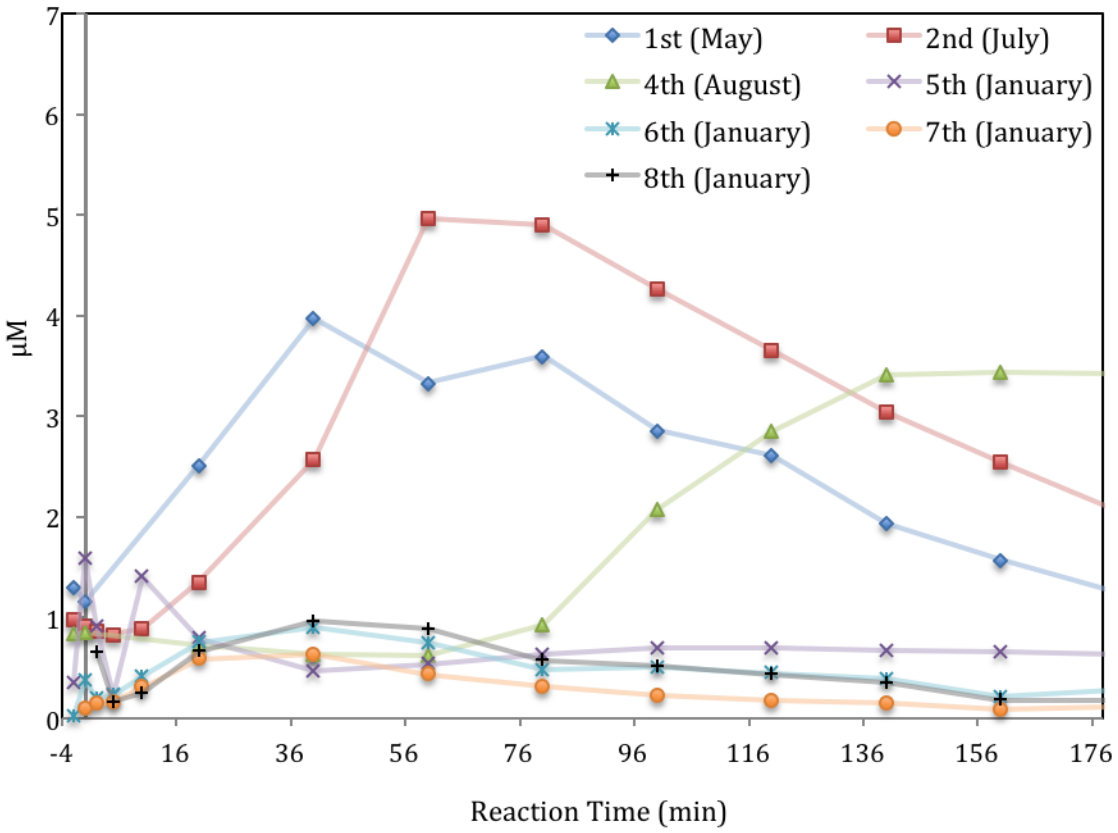

Figure 3.2: Oxalate concentration time series for experiments conducted with the first and second rainwater samples, with the exclusion of experiment #3. In this figure, t = 0 min indicates the time when OH radicals were introduced. The -2 time point is the pre-reaction quantification.

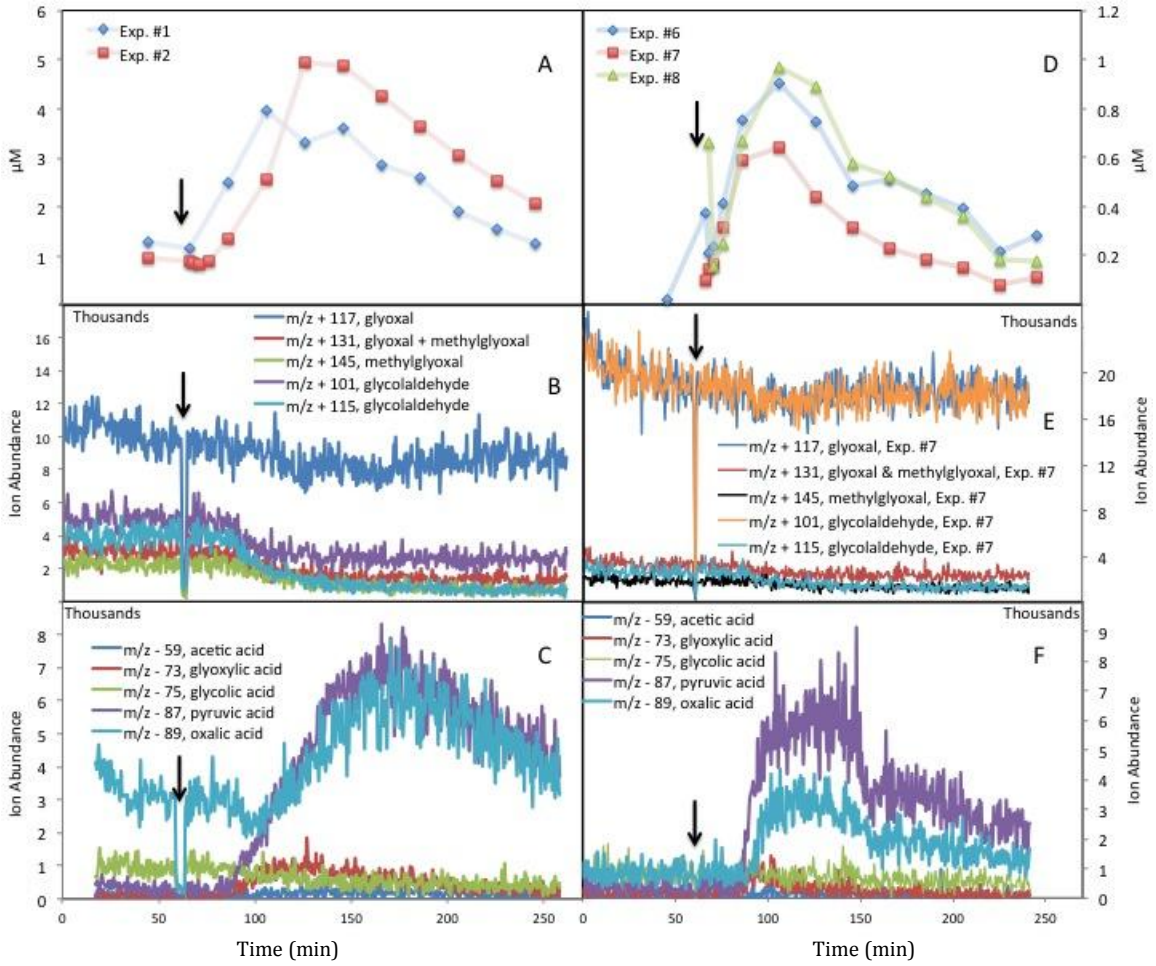

Figure 3.3: IC and ESI-MS analysis for the first and second rainwater samples. Oxalate concentrations time series for the most similar replicate experiments for the first (A) and second (D) rainwater samples. Abundance of several ions in the ESI-MS positive mode analysis of experiment #2 (B) for the first rainwater sample and of experiment #7 for the second rainwater sample (E). Abundance of several ions in the ESI-MS negative mode analysis of experiment #2 for the first rainwater sample (C) and #6 for the second rainwater sample (F). The black arrows indicate when H_2O_2 and the UV are added. OH radical reactions take place from this point further.

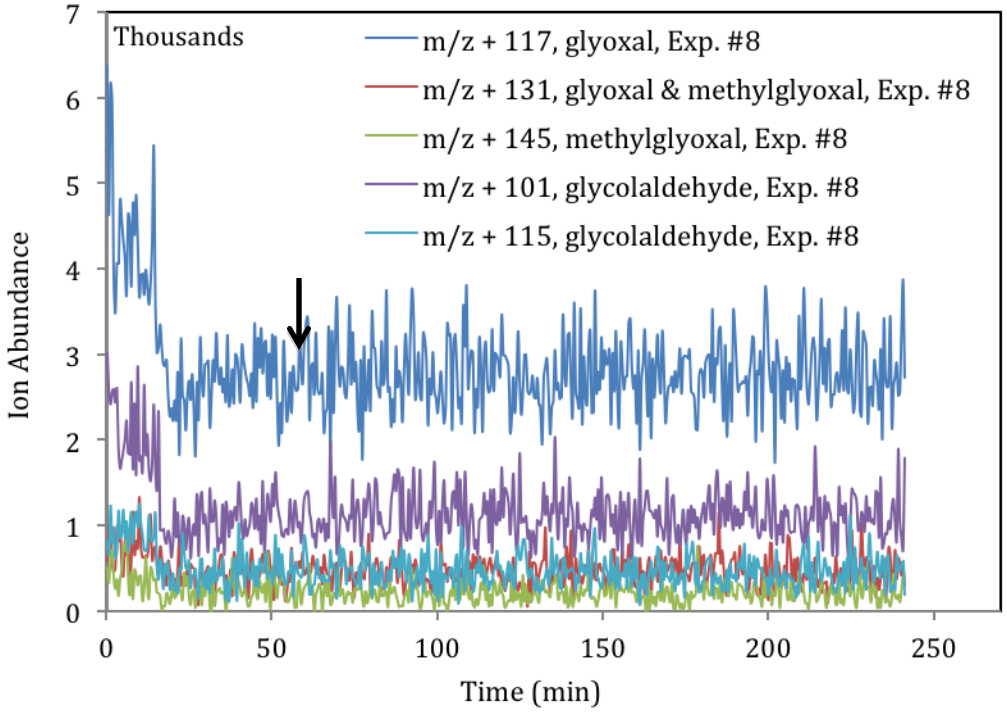

Figure 3.4: Abundance of several ions in the ESI-MS positive mode analysis of experiment #8 for the second rainwater sample. The black arrow indicates when H_2O_2 and the UV are added. OH radical reactions take place from this point further.

4. Results and Discussion

4.1 Filtered Rainwater Photooxidation Reactions

The good agreement across replicate experiments for oxalate (Figure 4.1 A) and other quantified species (Appendix B) conducted with OH radicals and the rainwater composite from Camden (Sept. 2003) and Pinelands (June and Sept. 2003) suggests that the reaction was proceeding at the same rate for all four replicate experiments. With the addition of the chiller to the experimental design, temperatures were maintained at (26.9 ± 0.9) °C, causing no differences in the reaction rates. Thus the time profiles for the two replicate experiments analyzed by positive mode (+) and the two by negative mode (-) ESI-MS can be compared with confidence. Glycolate, formate, succinate and/or malate, malonate and/or tartarate, oxalate and sulfate were measured by IC (Appendix B) in all four replicate experiments.

The greater than 50% decrease in m/z^+ 131 and 145 in both experiments analyzed in the positive mode is consistent with the loss of methylglyoxal by OH radical oxidation. Note that these are the major ions in the ESI-MS analysis of the methylglyoxal standard. (Appendix A) At cloud-relevant concentrations, the OH radical oxidation of methylglyoxal is expected to form pyruvic acid (m/z^- 87), followed by acetic acid (m/z^- 59), negligible concentrations of glyoxylic acid (m/z^- 73), and finally oxalic acid (m/z^- 89) according to the chemical modeling of Tan et al., (2010), which was validated with laboratory experiments. Consistent with this expectation, the decrease in m/z^+ 131 and 145 were accompanied by a substantial

increase in m/z^- 87, a modest increase in m/z^- 73 and subsequently an increase in m/z^- 89. The concentration of oxalate measured by IC and the abundance of m/z^- 89 both peak about 20 minutes after the addition of OH radicals (80 minutes into the experiment). These results strongly suggest that the OH radical oxidation of methylglyoxal took place in this rainwater experiment. Note the ion abundance of m/z^- 59 (acetic acid) was constant.

The case for glycolaldehyde is not quite as conclusive. If glycolaldehyde is an important precursor in this rainwater sample, we expect to see a decrease in m/z^+ 101 and 115 (glycolaldehyde), followed by a concurrent increase in glyoxal (m/z^+ 117 and 131) and glycolic acid (m/z^- 75). This would be followed by an increase in glyoxylic acid (m/z^- 73) and finally oxalic acid (m/z^- 89) (Perri et al., 2009). An immediate decrease is seen for m/z^+ 115 but not m/z^+ 101 (Figure 4.1 C), and an immediate increase in glycolate measured by IC (Appendix B). However m/z^- 75 (glycolic acid) and m/z^+ 117 (glyoxal) do not change. An increase in m/z^- 73 followed by m/z^- 89 (confirmed by IC to be oxalate) is consistent with the formation of glyoxylic acid followed by oxalic acid. It is possible that glycolaldehyde is present and reacting, but that other compounds with the same unit mass-to-charge (m/z^+ 101; m/z^- 75, 117) are obscuring the expected pattern. Alternatively, other precursors could have been responsible for the loss of m/z^+ 115 and the production of m/z^- 73 and 89.

While experiments from the first rainwater sample were consistent with the oxidation of glyoxal, this photo-oxidation pathway did not seem to be important in the third rainwater sample. Of the two major ions identified in the standard (m/z^+ 117 and 131) only one showed a decrease, however this ion (m/z^+ 131) was also a major ion for methylglyoxal. The behavior of m/z^+ 131 was similar to that of m/z^+ 145 (the other major ion for methylglyoxal), which suggests m/z^+ 131 was dominated by methylglyoxal and not glyoxal, showing then no decrease in ion abundance for glyoxal. If glyoxal photo-oxidation was indeed occurring, then a concurrent increase for glyoxylic acid (m/z^- 73) would be expected. As mentioned previously, m/z^- 73 did have an increase in ion abundance. However, other chemistry could be responsible for this increase (e.g., methylglyoxal or glycolaldehyde oxidation).

The formation of succinic and malonic acids in the third rainwater sample is suggested by both ESI-MS and IC analysis. Note that succinic and malonic acids are enriched in evaporated droplet residual particles in clouds (Sorooshian et al., 2007). As shown in Figure 4.2, there was an increase in m/z^- 103, consistent with the formation of malonic acid, and in m/z^- 117, consistent with the formation of succinic acid. Succinic and malic acids coelute in the IC, as do malonic and tartaric acids. After the addition of OH radical to the rainwater sample, the concentrations of succinic/malic and malonic/tartaric measured by IC increase (Appendix B). However, the IC analysis showed an intermediate behavior for the succininc/malic acids, suggesting the production and subsequent consumption of this material.

Interestingly, malic acid (m/z^- 133) also behaved as an intermediate in the ESI-MS negative mode analysis. In fact, only malic acid (m/z^- 133) peaked in ion abundance at the same time (~ 80 minutes) as the succinic/malic acids IC peak. Thus it is likely that the succinic/malic acid peak in the IC analysis is mostly dominated by malic acid. Note that if this IC peak had been dominated by succinic acid it would have been below the reported detection limit (Perri et al., 2009), (Appendix A). There was no evidence of an increase in ion abundance for tartaric acid (m/z^- 149), thus, suggesting that the malonic/tartaric increase measured by IC is mostly due to malonic acid.

Formic acid cannot be seen in the ESI-MS due to its low molecular weight (m/z^- 45). The ESI-MS detects ions greater than 50 amu. However, IC analysis suggests that formic acid is rapidly oxidized. Previous studies have identified and quantified the production of malonic acid at high concentration (3000 μM) methylglyoxal + OH radical (10^{-12} M) experiments but not in lower concentration experiments (30 and 300 μM) (Tan et al., 2010). Tan et al (2010) proposed that, at high concentration, products with higher carbon number than their precursors form through organic radical – radical reactions. Because the total carbon concentrations in this rainwater are low 112.7, 27.9 and ~75 μM, it is more likely that these 2, 3 and 4 carbon number products form from precursors with 2, 3, 4 or more carbons. The formation of acids with a carbon number higher than 2, suggest the dominance of methylglyoxal (3 carbons) over glyoxal and glycolaldehyde (2 carbons). Note that

these acids with a carbon number higher than 2 could also be formed from larger organic acids.

4.2 Control Experiments with Filtered Rainwater

Control experiments conducted with the same natural rainwater composite sample 1) in the presence of H_2O_2 but no UV and 2) in the presence of UV but no H_2O_2 were used to verify to what degree the changes described above were the result of OH radical reactions. Oxalate was not produced in either type of control experiment. It remained constant in the presence of H_2O_2 and was consumed in the presence of UV (Figure 4.3). No production or consumption of methylglyoxal (m/z^+ 131, 145) was observed for either type of control experiment (Appendix C). The abundance of m/z^+ 101 and 115 (glycolaldehyde) and m/z^+ 117 (glyoxal) were unchanged in the presence of UV, however a slight increase in the abundance of m/z^+ 101 and 115 (glycolaldehyde), and in m/z^+ 117 (glyoxal) were observed in the presence of H_2O_2 (Appendix C).

Most organic acid concentrations (IC) and ion abundances remained unchanged in control experiments; rainwater + H_2O_2 and rainwater + UV radiation (Appendix C). Rainwater + H_2O_2 showed a modest increase in m/z^- 87 (pyruvic) and an increase in m/z^- 103 (malonic), but not with the same magnitude as they did in experiments conducted with OH radicals (ion abundance of $\sim 1.5 \times 10^3$ vs. $\sim 1.0 \times 10^4$ for m/z – 87, and $\sim 6.0 \times 10^3$ vs. $\sim 1.4 \times 10^4$ for m/z - 103).

Previous methylglyoxal control studies have shown a slight increase in pyruvic acid under the presence of H_2O_2 or UV radiation (Tan et al., 2010) but no oxalate formation. In this work, oxalate and m/z- 89 decreased in the presence of UV. Since this is a natural rainwater sample, it is possible that small concentrations of H_2O_2 could have been present and photo-reacted when exposed to the UV lamp producing OH radicals. Another possible explanation for the oxalate decrease is the photo-degradation of species such as iron oxalate. Zuo and Holgné, 1992 showed that the photolysis of Fe(III)-oxalato complexes produces oxalate radicals, and subsequently these radicals reduce oxygen to the superoxide ion leading to the formation of H_2O_2. Overall, these results suggest that the depletion of aldehydes and formation of organic acids in the experiments (with OH radicals) were driven by OH radical chemistry.

4.3 Other Potential Reactants, Intermediates and Products

Cloud water (and natural rainwater) is a complex medium containing a vast number of components (Altieri et al., 2009). Thus, reactants, intermediates and products in addition to those I previously focused on are likely to contribute to SOA formation through cloud processing. These potential contributors were identified in the negative mode (Table 4.1) and positive mode (Table 4.2) mass spectral analyses of the third rainwater sample based on the evaluation criteria shown in Table 2.2. Figure 4.4 shows examples of how reactants, intermediates and products identified by these criteria behave in the presence of OH radicals. Ions in Tables 4.1 and 4.2 accompanied by an asterisk were identified in duplicate experiments. Because of

the less stringent criteria (30% and 25%) for the determination of intermediates and products, some ions were identified as both. These ions are check marked.

Table 4.1 shows that negative mode contributors are mostly intermediates and products; the ion abundance of negative mode ions most frequently increased. This suggests that intermediates and products are predominantly organic acids. Table 4.2 shows that positive mode contributors are mostly reactants; the ion abundance of positive mode ions most frequently decreased. This suggests that reactants (precursors) are mostly aldehydes, organic peroxides and/or alcohols. Several reactants were also identified in the negative mode, however only one product and three intermediates were identified in the positive mode. These results are indicative of a high number of possible precursors (identified reactants in the positive mode) that could contribute to SOA formation through cloud processing.

The ions with the twentieth highest standard deviations for both negative and positive mode are shown in Table 4.3. The highest standard deviations indicate the ions with the highest absolute change in ion abundance over the course of the experiment by either an increase or decrease. Some of the m/z ratios detected in the negative mode, and most of the ratios detected in the positive mode with the highest standard deviation were also identified by the percentage of change criteria. The m/z ratios marked with the number symbol (#) were detected using both approaches. Notably, m/z ratios detected in the negative mode were mostly

identified as products or intermediates, and m/z ratios detected in the positive mode were mostly identified as reactants.

The m/z ratios with high standard deviation that were not identified as reactants, intermediates or products based on the criteria of Table 2.2 are still considered as possible SOA contributors; but ones whose ion abundance changed less than the previously established criteria. For example m/z^- 81 (σ = 5065.40) increased only 9%, yet its increase in ion abundance is substantial (~50,000 to ~55,000). These results are indicate that other ions found in natural rainwater, a cloud water surrogate, different from those previously examined in this study (e.g. methylglyoxal, oxalate and pyruvate) participate in aqueous oxidation reactions that might lead to SOA formation through cloud processing. These ions were identified as aqueous OH radical reactants, intermediates or products based either on their relative change across the reaction or by their high concentration and absolute change in ion abundance. Please note that some ions identified by a large standard deviation were, on average, constant across the experiment.

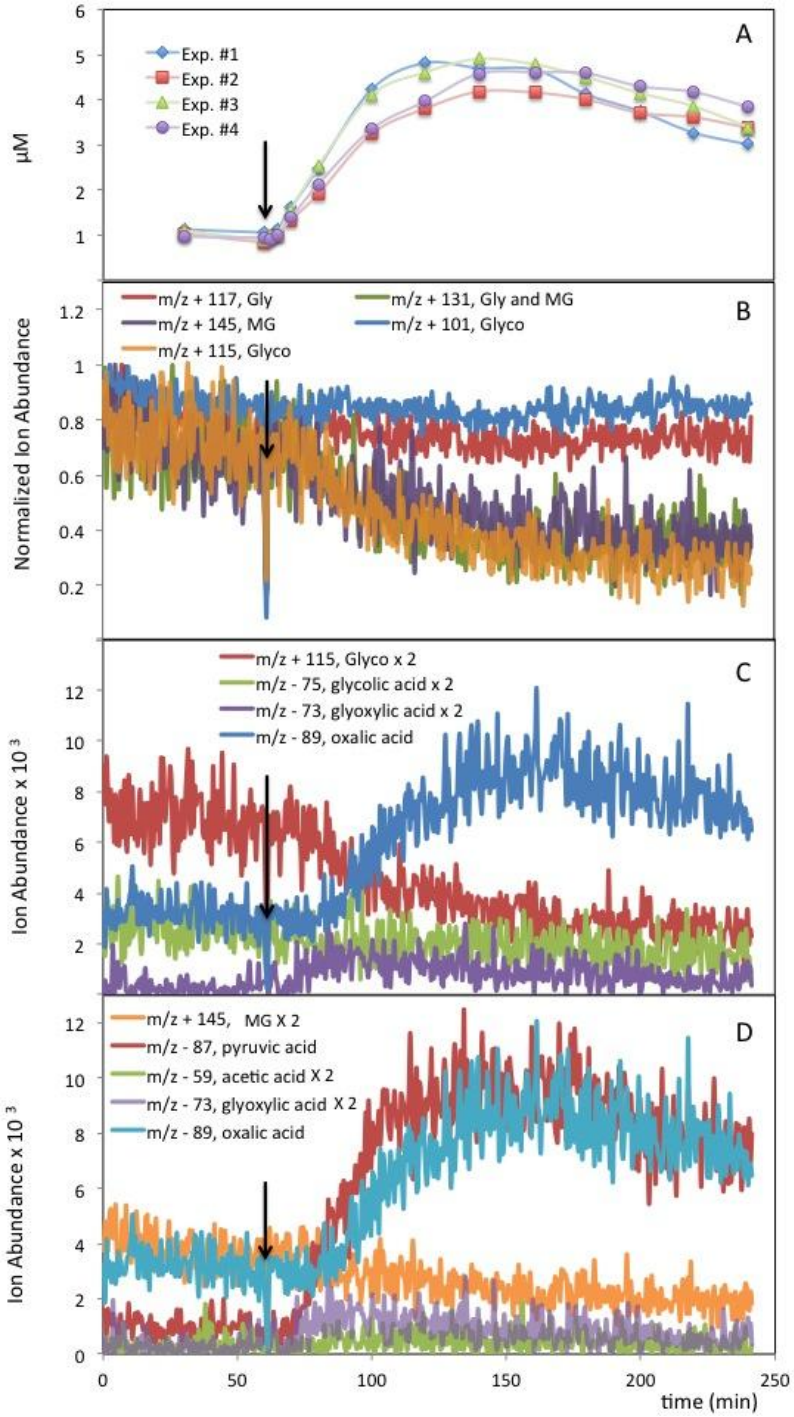

Figure 4.1: IC and ESI-MS analysis for the third rainwater sample. IC quantification of oxalate for four replicate experiments (A), aldehyde ESI-MS positive mode analysis (B), glycolaldehyde photo-oxidation pathway (C), and methylglyoxal photo-oxidation pathway (D). Figures C and D show positive mode (aldehydes) and negative mode (acids) analysis. The black arrow represent when H_2O_2 and the UV are added, the OH radical reactions can be seen from this point further.

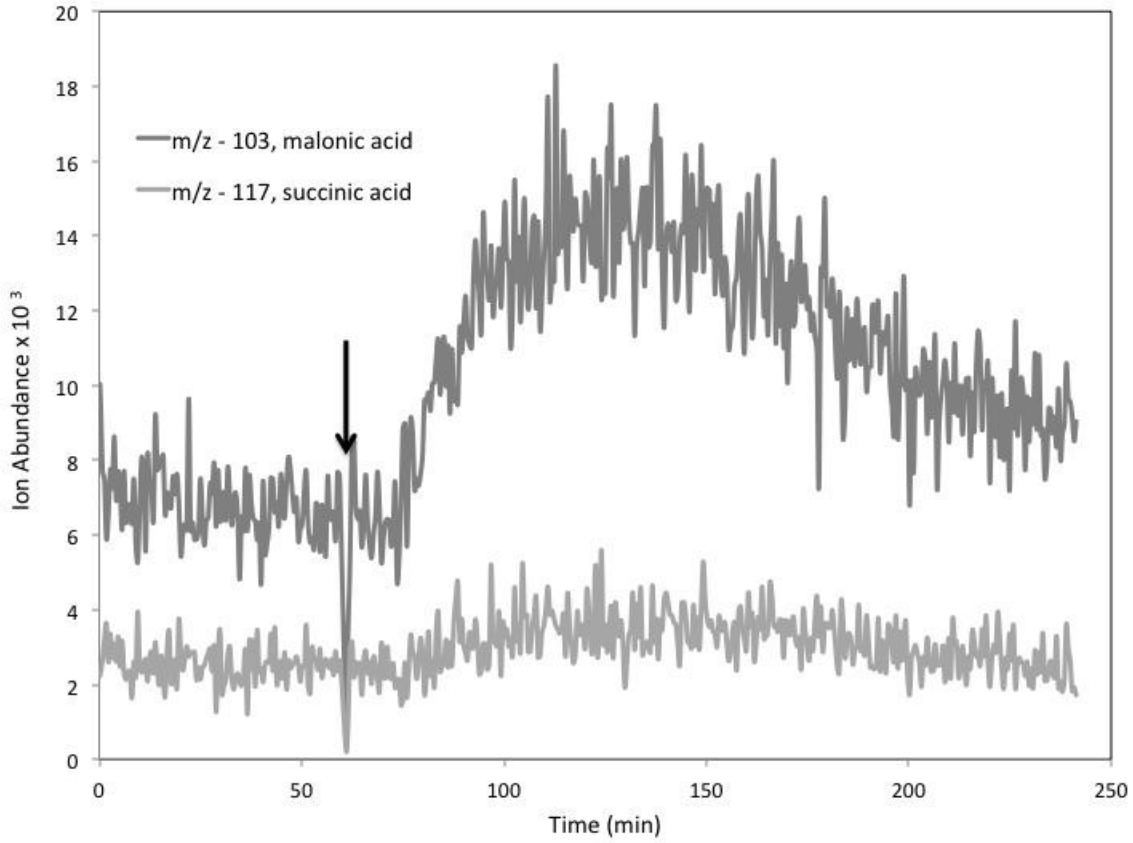

Figure 4.2: ESI-MS negative mode analysis of m/z- 103 (malonic) and m/z-117 (succinic acid). The black arrow represent when H_2O_2 and the UV are added, the OH radical reactions can be seen from this point further.

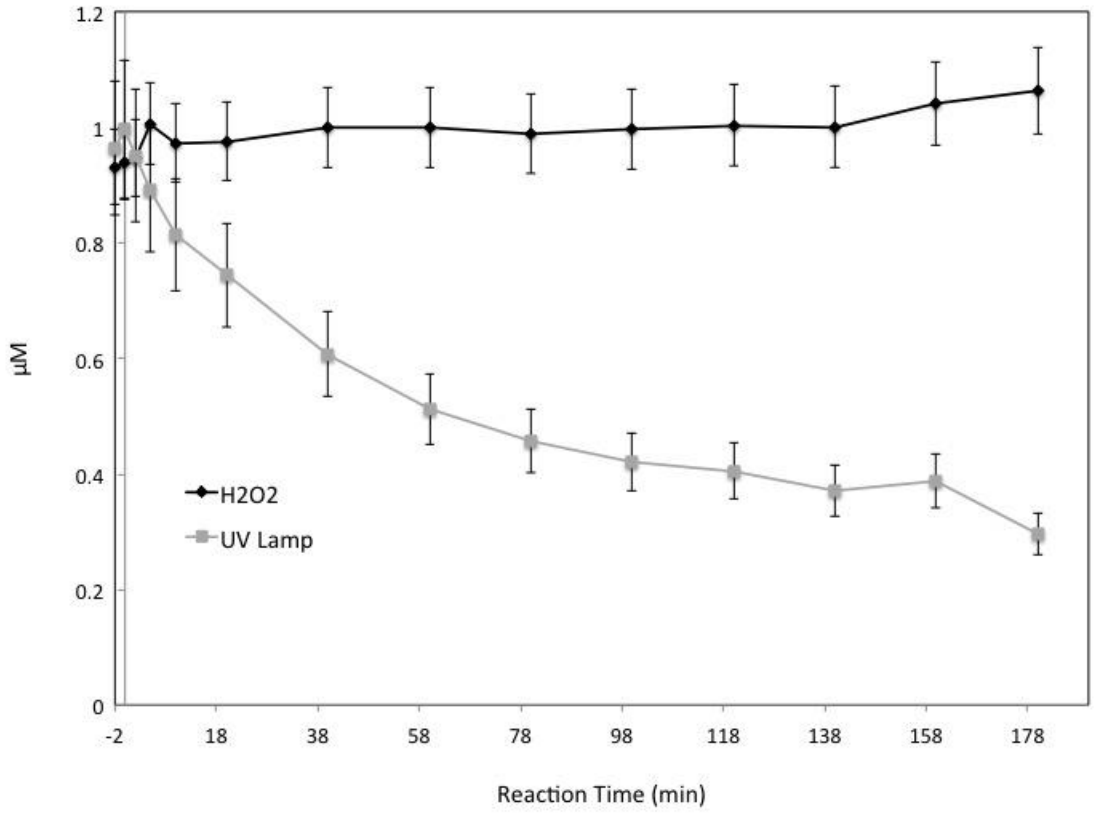

Figure 4.3: Oxalate concentration time series for control experiments. The black line represents rainwater + H_2O_2, and the gray line represents rainwater + UV radiation. The -2 time point is the pre-reaction quantification; the reactions can be seen from 0 and further. Error bars are the pooled standard deviation considering all oxalate time point for each experiment.

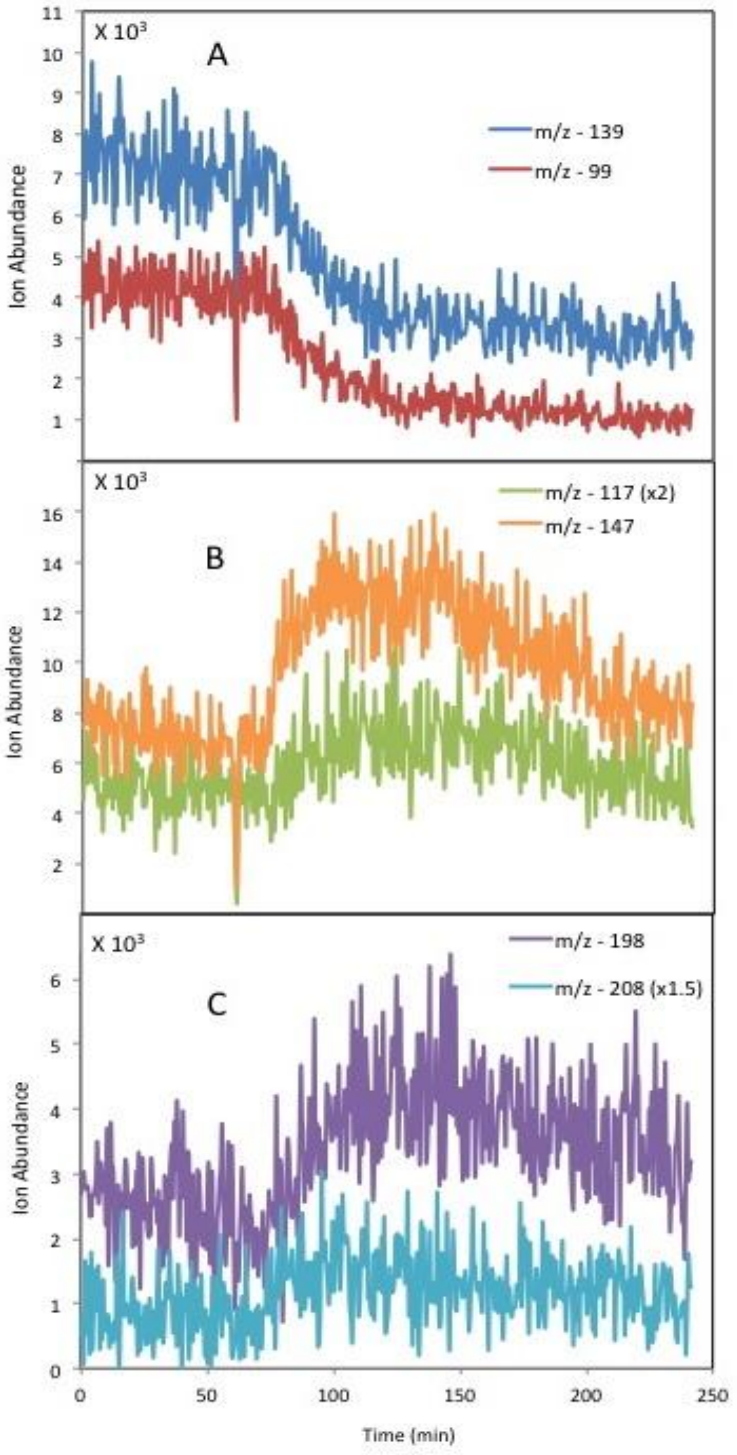

Figure 4.4: Examples of reactants (A), intermediates (B) and products (C) identified based on the criteria explained in Table 2.2.

Products				Intermediates		Reactants	
	51		200		50		50
	55	✓*	208		54		52
✓	57		232		56		56
✓	58		338	✓*	57		60
✓	59		422	✓	58		67
✓	60		458	✓	59		68
*	65		466	✓	60		77
	66		491	✓	67		78
✓	67			✓	71		85
	68			✓*	72		102
*	70			✓	73	*	111
✓*	71			✓	77		112
✓*	72				78	*	125
✓	73			✓	79	*	129
✓	77				99	*	137
✓*	79				100	*	138
	80			✓	101	*	143
	86			✓	102		152
*	87			✓*	103		154
*	88				104		221
*	89				105		230
	94				115		231
*	96				117		257
✓*	101			✓*	118		260
✓	102			✓	126		284
✓	103				127		294
*	116				133		300
✓	118				146		304
	124				147	*	312
✓*	126			✓	196		316
	142			✓	198		356
	144			✓	208	*	362
	162				239		372
	164						389
✓	196						412
✓*	198						484

Table 4.1: Negative mode potential contributors identified based on the percentage of change criteria. Listed m/z ratios represent potential reactants, intermediates or products for the third rainwater. The m/z^- ratios marked with an asterisk were identified in both duplicate experiments. The check indicates m/z ratios that were identified as both intermediates and products.

Prod.	Int.	Reac.								
* 63	54	50	152	* 194	* 231	* 267	* 312	* 347	* 389	464
	58	* 51	* 153	* 195	232	* 268	* 313	* 349	393	465
	82	* 52	154	* 196	234	269	* 314	* 350	396	467
		54	* 155	* 197	* 236	* 270	* 315	* 351	398	* 468
		56	156	* 198	* 237	* 271	* 316	352	399	469
		57	* 157	* 199	* 238	* 272	* 317	353	405	* 473
		58	* 158	200	* 239	* 273	318	354	* 407	475
		68	* 159	* 201	* 240	* 274	319	* 355	* 409	477
		69	162	* 202	* 241	* 275	320	356	411	479
		70	164	* 203	* 242	276	* 321	* 357	412	481
		71	* 167	* 204	* 243	* 277	322	* 358	416	482
		77	168	206	244	278	* 323	359	417	485
		78	* 169	* 207	* 245	282	* 324	* 360	418	490
		79	* 171	208	* 246	* 284	* 325	361	419	498
		84	172	* 209	* 247	* 287	* 327	363	421	499
		96	* 173	* 210	* 248	290	* 328	* 365	424	500
		* 99	* 174	* 211	250	* 291	* 329	366	* 425	
		* 100	176	* 213	* 251	* 292	* 330	* 367	428	
		110	* 179	* 215	* 253	* 293	* 331	369	433	
		* 113	* 180	* 216	* 254	294	* 332	370	436	
		114	* 181	* 218	* 255	295	333	371	438	
		* 115	* 182	* 219	256	* 296	* 334	373	439	
		127	* 183	* 220	257	* 297	335	* 374	444	
		129	184	221	258	* 298	* 336	375	446	
		130	* 185	* 222	* 259	299	337	377	447	

		131	186	* 223	* 260	302	* 339	379	451	
		* 137	* 187	* 225	261	* 303	340	* 381	452	
		139	* 188	226	* 262	* 304	* 341	* 383	453	
		* 141	* 190	* 227	263	* 305	* 342	384	455	
		142	* 191	* 228	* 264	* 309	343	386	* 458	
		146	* 192	* 229	* 265	310	345	387	462	
		151	193	* 230	266	* 311	* 346	388	463	

Table 4.2: Positive mode potential contributors identified based on the percentage of change criteria. Listed m/z ratios represent potential reactants, intermediates or products for the third rainwater. M/z ratios marked with an asterisk were also identified in duplicate experiment, and check indicates m/z ratios that were identified as both intermediates and products

(- mode)				(+ mode)			
	m/z	type	σ		m/z	type	σ
✓	62	P	3118	✓	60	R	1386
✓	81	P	5065		61	I	1090
✓	83	P	1972	✓	65	R	4616
✓#	87	P	2921	✓#	69	R	9936
✓#	89	P	2482	#	70	R	1158
✓	91	R	12047	✓	81	R	1207
	93	C	931	✓#	99	R	1097
✓	97	P	5740	✓	101	R	3114
✓#	103	P	3403		103	C	928
✓	113	R	4973	✓	117	R	1657
✓#	147	I	3198		123	R	930
✓	155	C	1080	✓	133	R	2003
✓	165	P	2489	✓#	139	R	1450
	171	P	920	✓#	141	R	1441
✓	183	P	1987	✓#	153	R	1144
✓	185	P	1338	✓#	155	R	1294
#	196	P	1091	✓#	157	R	1266
✓#	198	P	1268	✓#	167	R	1196
✓	210	P	3325	✓#	169	R	1068
✓	211	P	1085	#	179	R	1091
✓	213	I	1093	✓#	181	R	1121
	215	P	1083	✓#	185	R	1271
	217	C	1042	✓#	195	R	1152
	223	C	900	#	211	R	927

Table 4.3: Negative and positive mode potential contributors identified based on the standard deviation criteria. The listed m/z ratios represent the twentieth highest standard deviations (σ) of potential reactants, intermediates or products for the third rainwater in the 50 – 500 m/z ratio range. Check marked m/z ratios were detected in both rounds of duplicate experiments, and m/z ratios marked with the number symbol (#) were also identified by the percentage of change criteria. The m/z ratios of type P are identified as products, type I as intermediates, and type R as reactants. Type C had large standard deviations that, on average, did not change across the experiment.

5.Conclusions and Implications

Rainwater, a more realistic cloud water surrogate than single compound laboratory experiments, was used to develop a better understanding of cloud chemistry that could contribute to SOA formation. To our knowledge, previously only controlled laboratory experiments with single compounds had been conducted for this purpose. Three samples of New Jersey rainwater oxidized by OH radicals showed the consumption and production of key previously studied organic species. Oxalate, the most abundant dicarboxylic acid in both rural and urban aerosols (Facchini et al., 1999, Mader et al., 2004, Kawamura and Ikushima, 1993), was previously shown to be a major product of the aqueous OH radical oxidation of glyoxal, methylglyoxal and glycolaldehyde. In this work, oxalate production followed the depletion of unit mass ions associated with methylglyoxal and their intermediate organic acid products for all rainwater samples. The evidence for the presence and oxidation of glycolaldehyde was not as strong and for glyoxal was only shown for the first rainwater sample.

Evidence for the photo-oxidation mechanisms proposed by single compound controlled laboratory experiments for glyoxal, methylglyoxal and glycolaldehyde (Lim et al., 2005; Altieri et al., 2006; Carlton et al., 2007; Tan et al., 2009, 2010; Perri et al., 2009; and Lim et al., 2010) was suggested by the IC and ESI-MS analysis results of the studied NJ rainwater samples. IC quantification of oxalate indicated that its production in replicate experiments for the first and second rainwater samples was occurring at different reaction rates. This effect was eliminated (i.e., for

the third rainwater sample) after a chiller was added to keep the temperature of the rainwater more constant during the experiment.

OH radical oxidation of the third rainwater sample was conducted after incorporation of a chiller to avoid temperature increases during the experiment. Oxalate concentrations were reproducible across the four experiments conducted with this rainwater sample. Strong evidence for methylglyoxal oxidation was observed upon introduction of OH radicals to the third rainwater sample (Figure 4.4 B). Evidence for the presence and OH radical oxidation of glycolaldehyde was not as strong due to the decrease in ion abundance of only one of its major ions and the constant ion abundance of glyoxal and m/z^- 75 (glycolic acid) (Figure 4.4 C). Please note that the IC analysis for glycolate showed an increase in concentration. Glyoxal photo-oxidation pathway did not seem to be important for this rainwater sample because of the decrease of only one of its major ions, an ion (m/z^+ 131) one that is also a major ion for methylglyoxal and which behaved in the same way as m/z^+ 145 (the other major ion for methylglyoxal). This suggests that m/z^+ 131 in this sample is dominated by methylglyoxal and not glyoxal, and suggests that glyoxal is not present and reacting with OH radicals in this rainwater sample. Controlled experiments conducted with the third rainwater sample showed that the presence of OH radical is indeed necessary for the consumption of aldehydes and the production of organic acids, in particular oxalic acid.

Because of the complex media that cloudwater and rainwater are and the large amount of unidentified DOC, I hypothesized that there are additional contributors

(besides glyoxal, methylglyoxal and glycolaldehyde) to SOA formation through OH radical photo-oxidation. Two criteria (Section 2.5) were employed in order to identify other possible precursors and products in the third rainwater sample. Based on these criteria, several species were identified that participated in oxidation chemistry (as reactants, intermediates or products) based on either their relative change across the reaction or by their high abundance and absolute change in ion abundance. Contributors identified in the positive mode were mostly reactants suggesting that reactants are mostly aldehydes, alcohols and/or organic peroxides. Contributors identified in the negative mode were mostly intermediates and products, suggesting that intermediates and products are mostly organic acids.

Further proof of other potential contributors is provided by the production of succinic and malonic acids. Previous single-compound laboratory experiments have shown the formation of small amounts of succinic acid and larger amounts of malonic acid from methylglyoxal in 1 mM and 3 mM experiments (Altieri et al., 2008, and Tan et al., 2010), however the formation was not observed in lower concentration experiments that simulated rainwater conditions; 30 μM and 300 μM (Tan et al., 2010). Interestingly, the formation of malonic (m/z^- 103) and succinic acids (m/z^-117) were observed in the IC and ESI-MS negative mode analysis of the third rainwater sample. The timing of the peak in ion abundance (ESI-MS) and concentration (IC) agreed for malonic acid, ~120 minutes, but not for succinate. This formation may not necessarily be from the oxidation of methylglyoxal, but from other unknown organic species. Herrmann et al., 2005 determined that malonic acid

is a product of OH radical oxidation of succinic acid. For succinic acid oxidation to be the source of malonic acid in this rainwater experiment, the malonate peak would have to follow the peak in succinate. However, in fact, the peak in ion abundance of succinic and malonic acids occur at the same time in the ESI-MS analysis.

Blando et al (1999) suggested a list of potential precursors and products derived from the literature. The unit mass ions corresponding to some of these potential precursors and products were also identified by the two criteria used in this study, thus suggesting that they could be participating in oxidation chemistry in this rainwater sample. Table 5.1 shows the potential intermediates and products suggested by Blando et al, 1999. Other organic acids studied by Sorooshian et al. (2007) are also included. Some of these ions were also identified as potential intermediates and products by the "percentage of change" criteria. As previously mentioned, organic acids are identified in the ESI-MS negative mode as their molecular weight minus one. Table 5.1 shows the m/z by which these species are identified. However, the identification of species in the positive mode is more complicated than in the negative mode. Species can be seen as molecular weight plus a proton (+1) or a Sodium (+23), they could be in their dimer form (2MW), and other complicated forms. Table 5.2 shows several possible m/z's (e.g., species plus a proton or plus a Sodium) for potential precursors suggested by Blando et al., 1999. Some precursors were also identified by the percentage of change and the standard deviation criteria used in this study. Almost all potential contributors suggested and

studied by the previous studies were identified as precursors, intermediates and products for the third rainwater sample.

This study provides evidence for the photo-oxidation of methylglyoxal and glyoxyl in a cloudwater surrogate, natural rainwater; the evidence for glycolaldehyde is mixed. It must be recognized that rainwater is not a perfect cloudwater surrogate because below cloud scavenging of gases and particles can also contribute solutes to rainwater. The production of malonic and succinic acids and the identification of other possible contributors of unknown composition provide evidence for additional aqueous chemistry that may contribute to SOA formation and alleviate the discrepancies between atmospheric models and ambient measurements.

For future work, I proposed additional OH radical experiments in which glyoxal, methylglyoxal and glycolaldehyde are all present at cloud-relevant concentrations. These experiments will help determine if the oxidation of one of these aldehydes dominates over the others. It is important to note that the reaction vessel is a closed system with an air headspace that increases as the experiment (and sampling) proceeds. Losses of semivolatile gases could occur through volatilization into the head space. Future experiments of this type should measure the headspace throughout the experiment. I also recommend that samples stored frozen from the third rainwater experiments conducted as part of this thesis be analyzed by IC-ESI-MS. This should be conducted for the purpose of verifying the

identities of many negative mode species seen by ESI-MS. Another smart step for this study would quantification of aldehydes, ketones and organic peroxides. These lists of potential contributors indicate that, for a better understanding of the cloud water chemistry, a more detailed analysis of natural rainwater or cloudwater samples should be done. Species that were identified by this study's criteria, species suggested by Blando et al., 1999 and species analyzed by other studies should be prioritized for quantitation.

	Organic Acids	MW - 1
I	malic acid	133.1
*	methyl succininc acid	131.11
*	methyl glutaric acid	145.14
I	methyl malonic acid	117.09
I	oxo-malonic acid	117.05
I	furmaric acid	115.07
*	glutaric acid	131.12
*	pimelic acid	159.17
**	lactate	89.08
**	maleic acid	115.07
*	adipic acid	145.14
*	suberic acid	173.2
P	acetate	59.05
I	propionate	73.08

Table 5.1: Other potential intermediates and products suggested by the literature. Listed species represent potential intermediates and products suggested by Blando et al., 1999 identified by the percentage of change criteria used in this study, as well as others studied from the recent literature. Species marked with an I or a P are intermediates and products identified by this study's criteria. Species marked with an asterisk (intermediates) and two asterisks (products) were not identified by the criteria. [1]Species suggested by Blando et al., 1999. [2]Species studied by Sorooshian et al., 2007.

Species	plus H+		plus Na+	
ALDEHYDES				
formaldehyde	ND	31.03	N	53.03
acetaldehyde	ND	45.05	C	67.05
propanal	R	59.08	σ R	81.08
benzaldehyde	R	107.12	✓	129.12
methacrolein	✓	71.09	R	93.09
KETONES				
acetone	R	59.08	σ R	81.08
2-butanone	P	73.11	R	95.11
ALCOHOLS				
phenol	R	95.11	I	117.11
ORGANIC PEROXIDES				
hydroxymethylhydroperoxide	σ P	65.32	R	87.32
1-hydroxymethyl hydroperoxide	σ P	65.32	R	87.32
methyl hydroperoxide	ND	49.0413	✓	71.0413

Table 5.2: Other potential precursors suggested by the literature. Listed species represent potential precursors suggested by Blando et al., 1999 whose m/z's were identified by the percentage of change criteria and the standard deviation criteria used in this study. Species with the check mark were identified as reactants by the percentage of change criteria and species marked with the sigma letter (σ) were identified as reactants by the standard deviation criteria. Species marked with R, I, P, or C were reactants, intermediates, products and constant species that were not identified by this study's criteria. Species marked with a C stayed constant, and species marked with an N, were noise.

Appendix A. Supporting Information for Chapter 2

Appendix A.1

Temperature readings for the third rainwater sample

Temperature readings (°C) for all experimental and control experiments for the 3rd rainwater sample. Dates represent the day of analysis.

	Experiments				Controls			
	June 8th (°C)		June 9th (°C)		June 14th (°C)		June 15th (°C)	
Time (min)	1st round	2nd round	1st round	2nd round	LAMP	H_2O_2	LAMP	H_2O_2
Pre-0	25	24.5	25	25	24	25	25	25
0	25	24.5	20	25	20	25	21	25
2	30	24.5	19.5	25.5	21	25	23	25
5	27	24.5	21.5	27	21.5	25	22	25
10	27	24.5	23	27.5	22.5	25	23	25
20	29	24.5	25	28	24	25	22	25
40	30.5	25	26	27	26	25	23.5	25
60	30	26	27	27.5	27	25	24	25
80	30	26.5	27.5	27.5	28	24.5	24.5	24.5
100	31.5	26.5	27.5	27.5	28.5	24.5	24.5	24.5
120	31.5	25.5	28	27.5	29	24.5	25.5	24.5
140	31.5	26.5	29	26.5	30	24.5	26	24.5
160	31.5	26.5	29	26.5	30	24.5	26	24.5
180	32	26	29	27	30	24.5	26.5	24.5

Appendix A.2

Average temperature readings for the third rainwater sample

Average temperature readings in °C for all experiments conducted for the 3rd rainwater sample. Errors bars are shown for experimental (n=4) and control with UV lamp (n=2) experiments. Control experiment with H_2O_2 (n=2) had a σ of 0 for all time points.

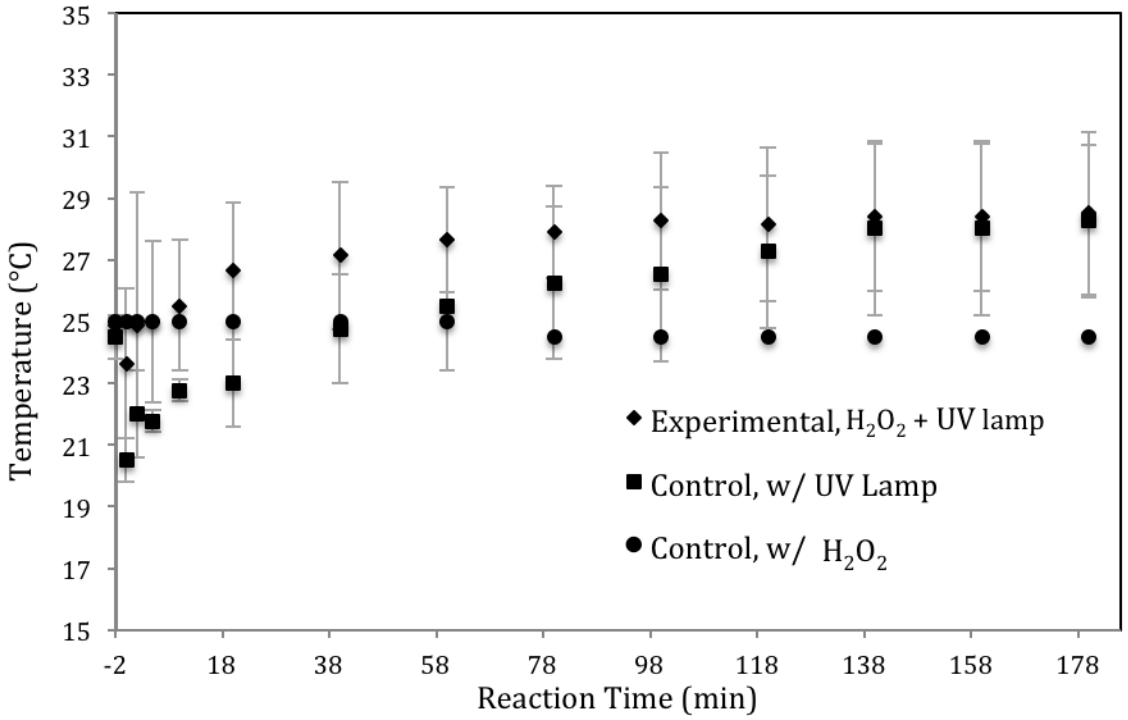

Appendix A.3

pH readings for all rainwater samples

Table A.2: pH readings at the beginning and end of all experimental and control experiments.

	Rainwater Sample	Date	Round	Beginning	End
Experiments	#1	May 27th, 2010	1st	-	-
		July 8th, 2010		6.1	5
		August 6th, 2010		4.47	4.32
		August 10th, 2010		3.66	3.55
	#2	January 13th, 2010	1st	5.2	5.4
			2nd	5.2	5.1
		January 14th, 2010	1st	5.14	5.1
			2nd	5.2	5.1
	#3	June 8th, 2011	1st	7	5.8
			2nd	5	5.2
		June 9th, 2011	1st	5.1	5.2
			2nd	4.8	4.9
Controls	#3	June 14th, 2011	1st	4.6	4.5
			2nd	4.7	4.6
		June 15th, 2011	1st	4.6	4.7
			2nd	4.5	4.6

Appendix A.4

Dissolved oxygen readings for all rainwater samples

Dissolved oxygen percentage (DO) readings at the beginning and end of all experimental and control experiments.

	Rainwater Sample	Date	Round	Beginning (%)	End (%)
Experiments	#1	May 27th, 2010	1st	-	-
		July 8th, 2010		114	105.8
		August 6th, 2010		107	106.3
		August 10th, 2010		108	106
	#2	January 13th, 2010	1st	111.1	115
			2nd	111.4	113
		January 14th, 2010	1st	113	109
			2nd	114	113
	#3	June 8th, 2011	1st	97.5	98
			2nd	97	100.5
		June 9th, 2011	1st	100	103
			2nd	99	109
Controls	#3	June 14th, 2011	1st	101	106
			2nd	100	100
		June 15th, 2011	1st	102	106
			2nd	102	102

Appendix A.5

Temperature readings for the Chiller control experiment

Table 4: Temperature readings (°C) obtained during a control experiment (DI water, UV lamp, and no sampling) with the addition of the Chiller in the experimental set-up.

Reaction Time (min)	Temperature (°C)
pre-0	25.0
0	25.0
2	28.0
5	28.0
10	28.0
20	27.0
40	26.5
60	26.5
80	27.0
100	27.0
120	27.0
140	27.0
160	27.0
180	27.0

Appendix A.6

Statistical analysis for the third rainwater sample

Statistical analyses for all mixed standard acids for the 3rd rainwater sample. The method detection limits for each acid were obtained by Perri et al., 2009. The pooled analytical precision and variability between replicate experiments analyses considered all acids except for malonic acid. The pooled accuracy analysis considered all acids except for succinic and glycolic acid.

Rainwater Sample	Acid	Coefficient of determination r^2	Analytical precision (%)	Accuracy (%)	Variability (%)	Method detection limit (μM)
#3 Pinelands (June/04/2003) Pinelands (Sept./19/2003) Camden (April/19/2003)	glycolic	0.987872	< 1	62	4	0.6
	formic	0.996801	5	9	8	0.7
	pyruvic	0.999643	– – –	– – –	– – –	
	glyoxylic	0.997393	– – –	– – –	– – –	0.2
	succinic	0.994149	9	26	10	4.3
	malonic	0.983794	20	9	75	0.3
	sulfate	0.997928	1	5	4	
	oxalic	0.999634	3	13	10	0.1

Analytical Precision	pooled standard deviations of all duplicate analyses = 2% (n=54)
Variability between replicate experiments	pooled standard deviations of all replicate analyses = 7% (n_i= 271)
Accuracy	pooled standard deviation of all mixed standard analyses = 9% (n = 32)

n = number of pairs

n_i = number of data points

Appendix A.7

Mass Spectra of mixed acid standard

Mass Spectra of a mixed organic acid and sulfate standard of glyoxylic acid (m/z - 73), glycolic acid (m/z - 75), pyruvic acid (m/z - 87), oxalic acid (m/z - 89), malonic acid (m/z - 103), succinic acid (m/z - 117), and sulfate (m/z - 97).

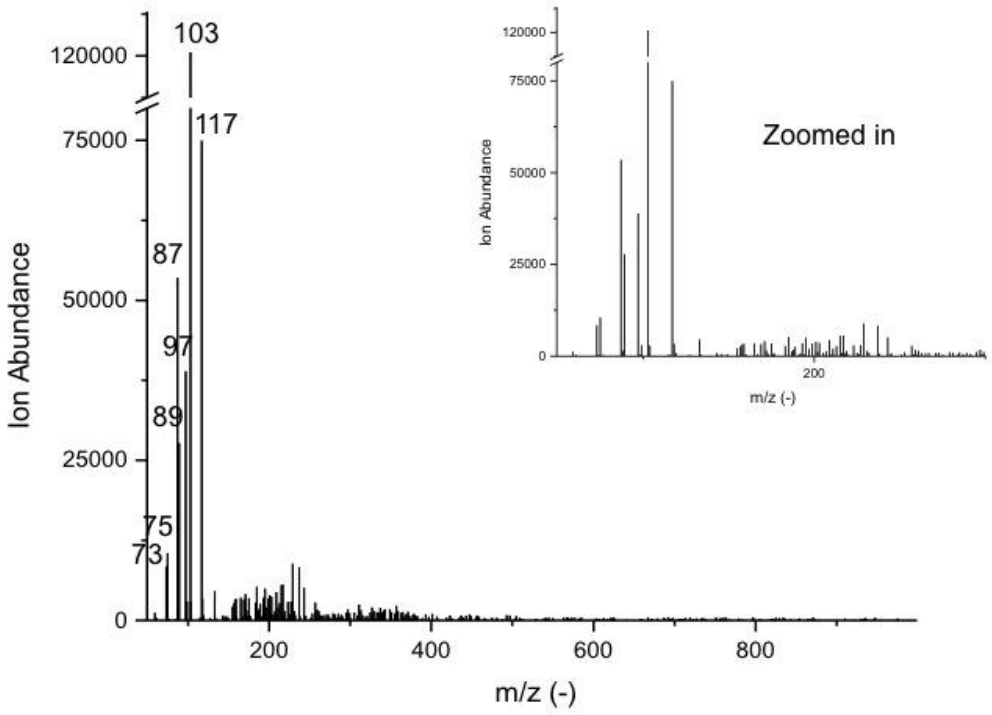

Appendix A.8

Mass Spectra of glyoxal standard

Mass Spectra of a glyoxal standard. Glyoxal is identified by its dimer plus H^+ (m/z^+ 117), and m/z^+ 131. M/z^+ 409 is considered a system impurity.

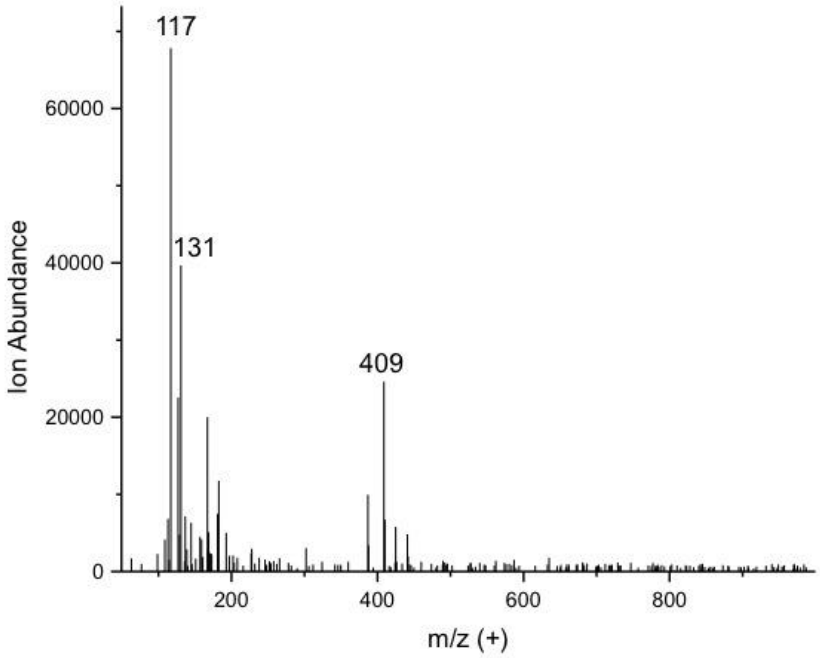

Appendix A.9

Mass Spectra of methylglyoxal standard

Mass Spectra of a methylglyoxal standard. Methylglyoxal is identified by its dimer plus H^+ (m/z $^+$ 145), and m/z $^+$ 131. m/z $^+$ 409 is a contaminant.

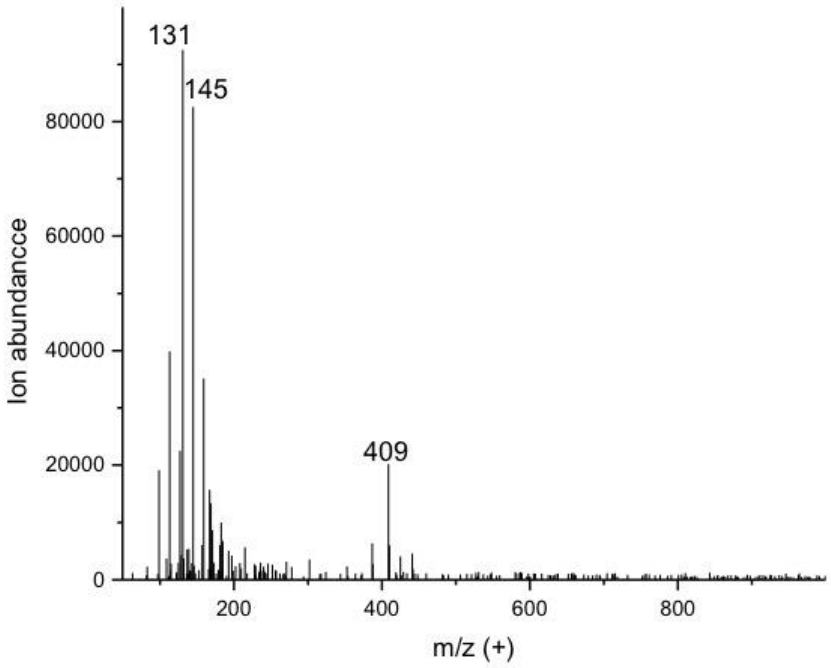

Appendix A.10

Mass Spectra of glycolaldehyde standard

Mass Spectra of a glycolaldehyde standard. Glycolaldehyde is identified by m/z $^{+}$ 101 and m/z $^{+}$ 115. M/z $^{+}$ 409 is impurity contaminant.

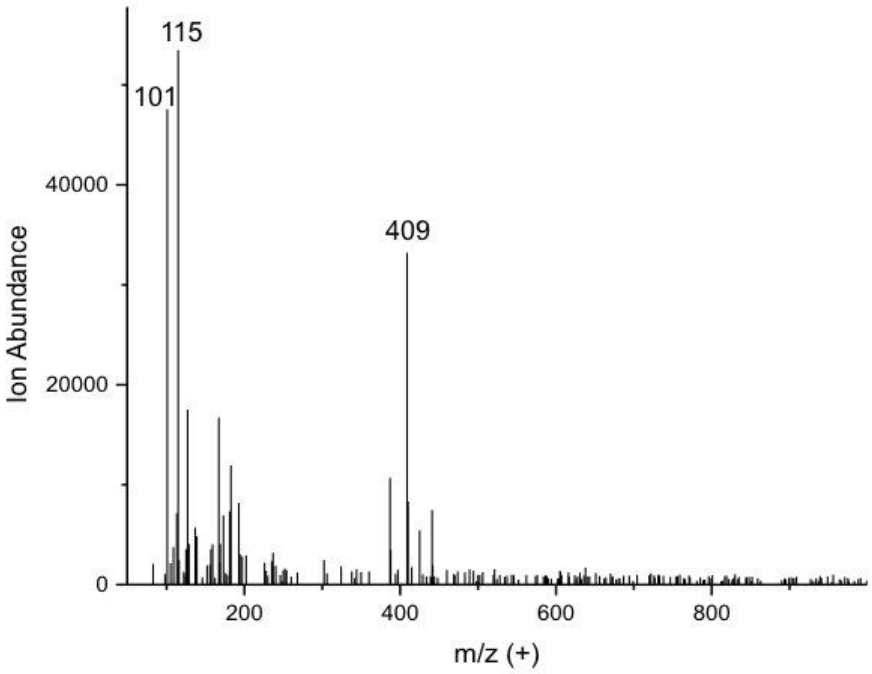

Appendix B. Supporting Information for Chapter 4.1

Appendix B.1

IC average concentration time series of glycolate and sulfate

IC average concentration time series of glycolate and sulfate of the rainwater sample #3 + OH radicals experiments. Errors bars are the percentage coefficient of variation (variability between experiments) for each acid

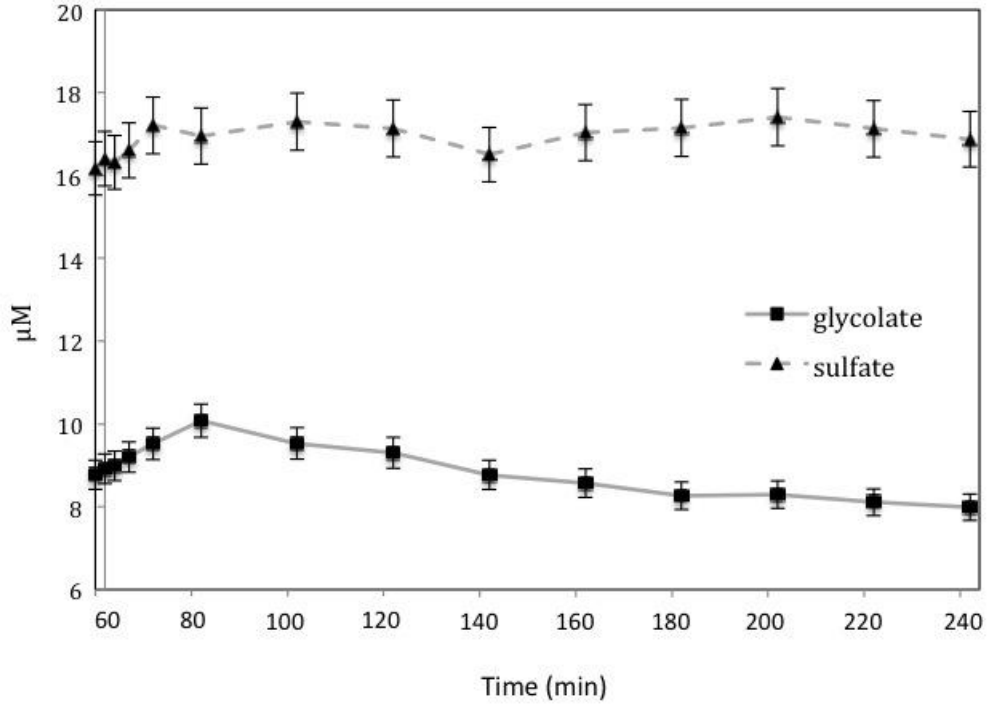

Appendix B.2

IC average concentration time series of formate, succinate and oxalate

IC average concentration time series of formate, succinate/malate and oxalate of the rainwater sample #3 + OH radicals experiments. Errors bars are the percentage coefficient of variation (variability between experiments) for each acid. Note that succinate and malate co-elude.

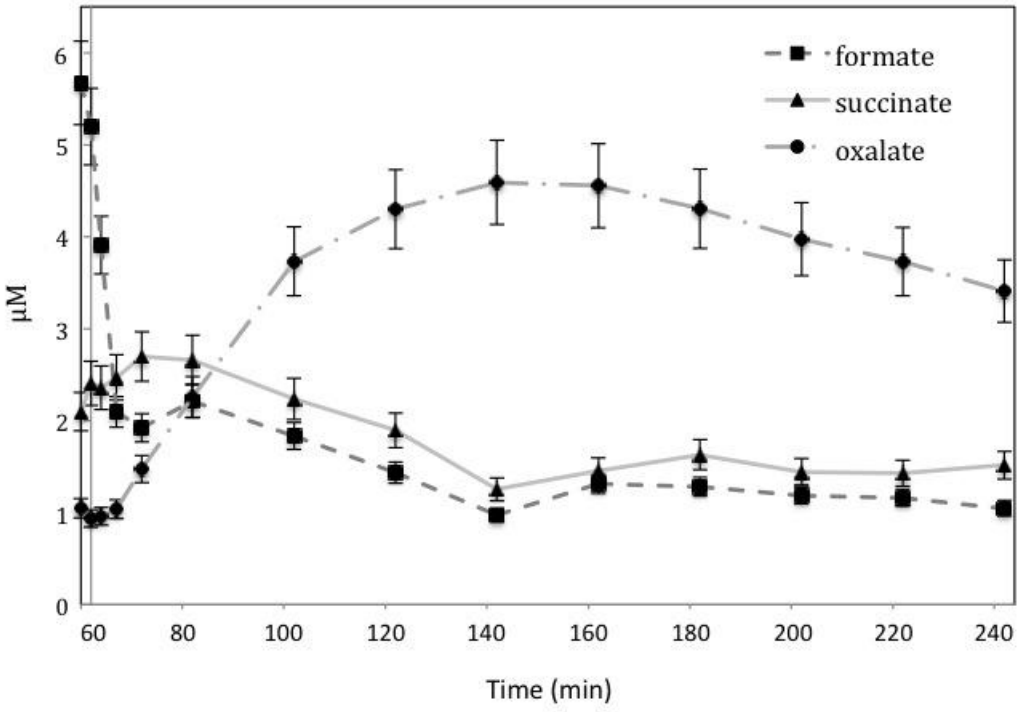

Appendix B.3

IC average concentration time series of malonate

IC average concentration time series of malonate/tartarate of the rainwater sample #3 + OH radicals experiments. Errors bars are the percentage coefficient of variation (variability between experiments) for the specific acid. Note that malonate and tararate coelute.

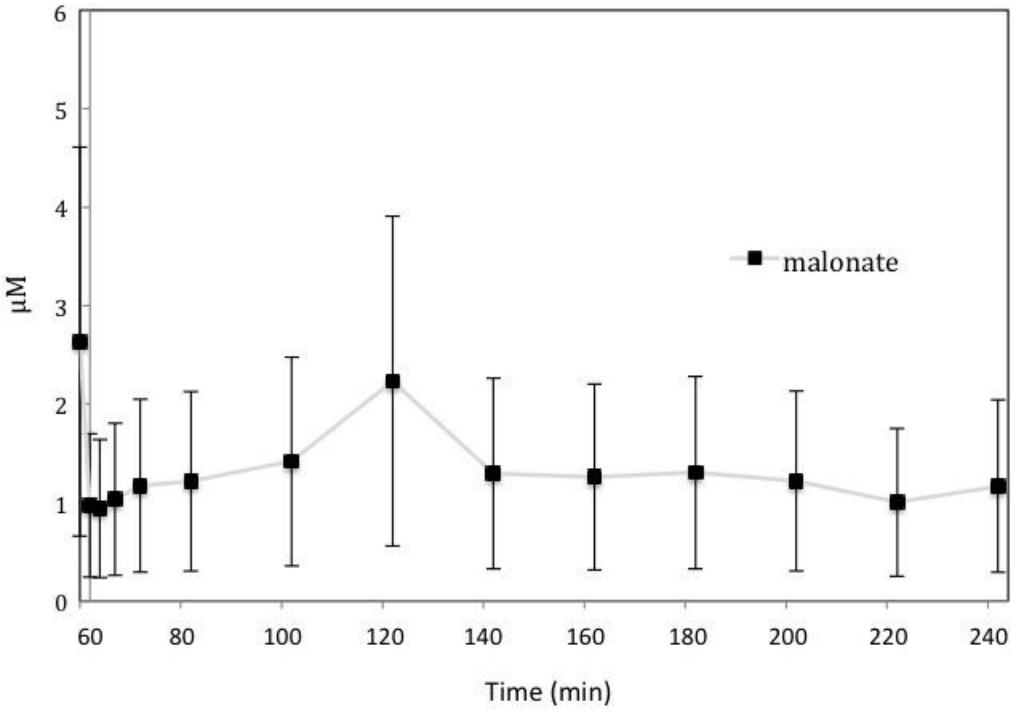

Appendix C. Supporting Information for Chapter 4.2

Appendix C.1

IC concentration time series of oxalate for all control experiments

Oxalate measured by IC in control experiments of the third rainwater sample with H_2O_2 or UV radiation. Black lines represent rainwater + H_2O_2, and gray lines represent rainwater + UV radiation. At t = 60 the lamp was inserted or H_2O_2 added.

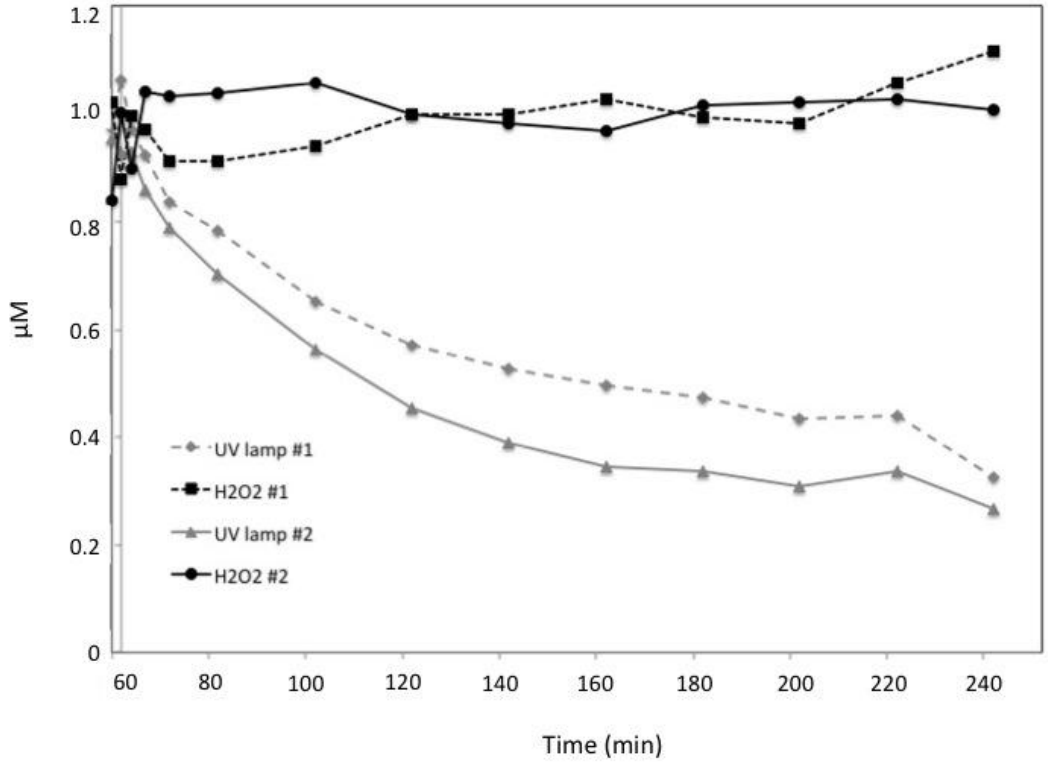

Appendix C.2

ESI-MS positive mode analysis of m/z $^+$ 117 and 101 for the H_2O_2 control experiment

ESI-MS positive mode analysis of the third rainwater sample + H_2O_2 reaction. The black arrow indicates when H_2O_2 was added.

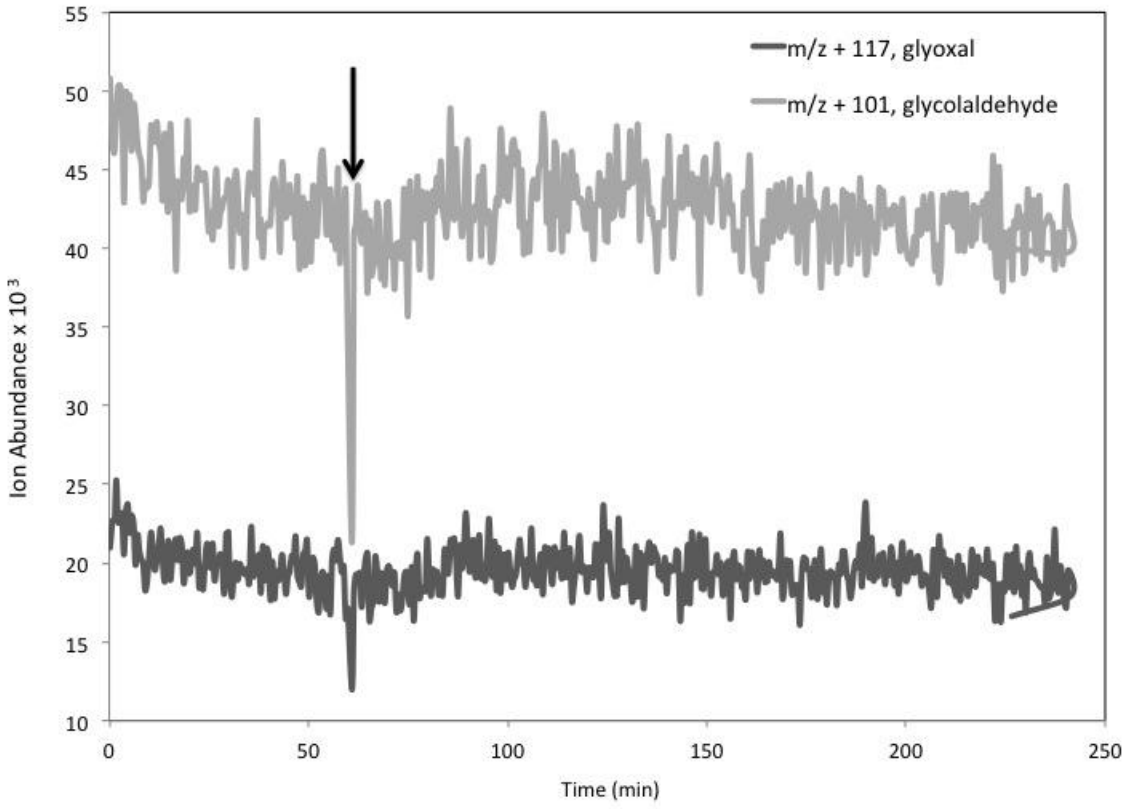

Appendix C.3

ESI-MS positive mode analysis of m/z $^+$ 115, 131 and 145 for the H_2O_2 control experiment

ESI-MS positive mode analysis of the third rainwater sample + H_2O_2 reaction. The black arrow indicates when H_2O_2 was added.

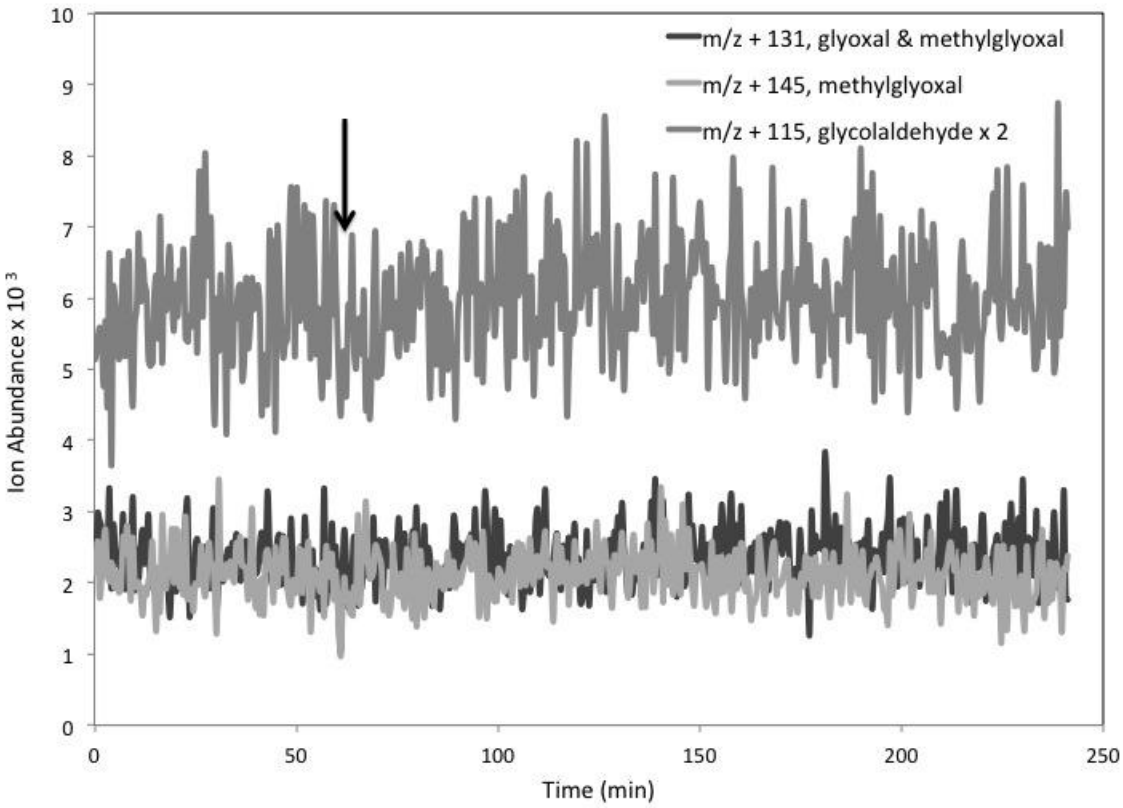

Appendix C.4

ESI-MS positive mode analysis of m/z + 117, and 101 for the UV radiation control experiment

ESI-MS positive mode analysis of the third rainwater sample + UV radiation reaction. The black arrows indicate when the UV lamp is added.

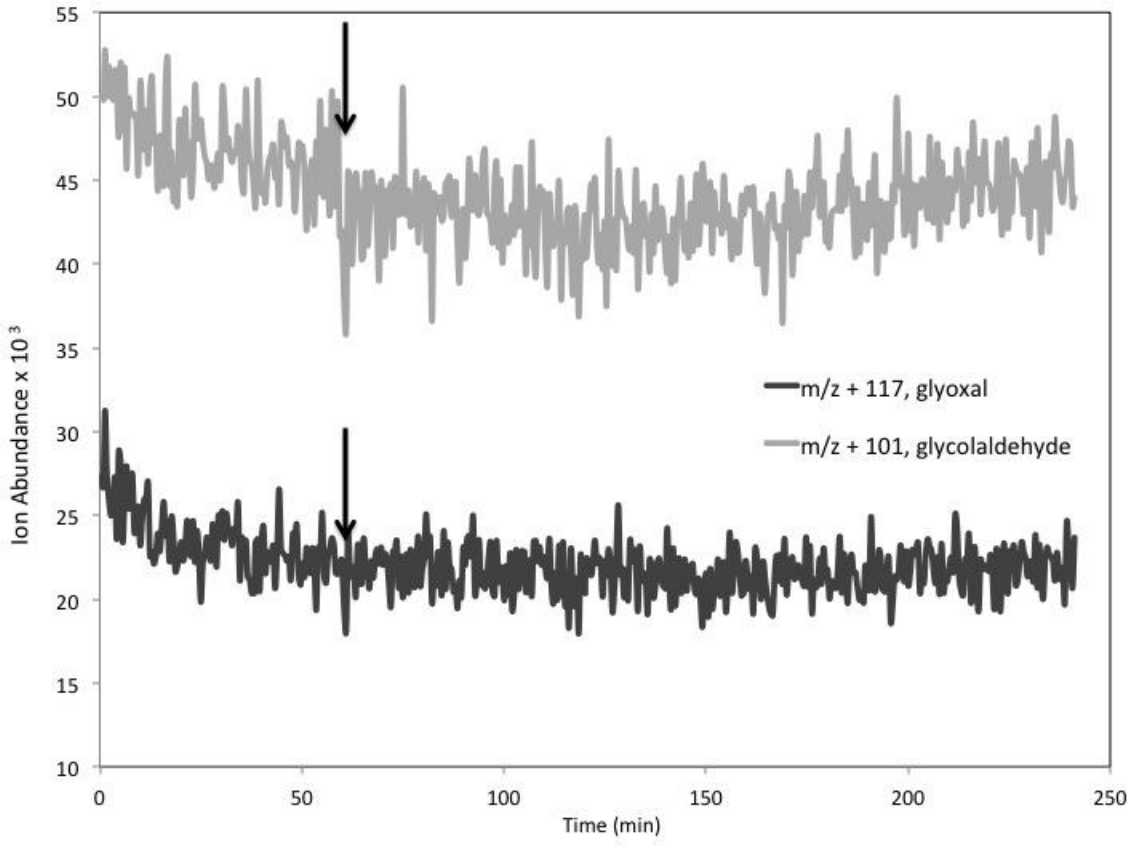

Appendix C.5

ESI-MS positive mode analysis of m/z $^{+}$ 115, 131 and 145 for the UV radiation control experiment

Figure C.5: ESI-MS positive mode analysis of the third rainwater sample + UV radiation reaction. The black arrows indicate when the UV lamp is added.

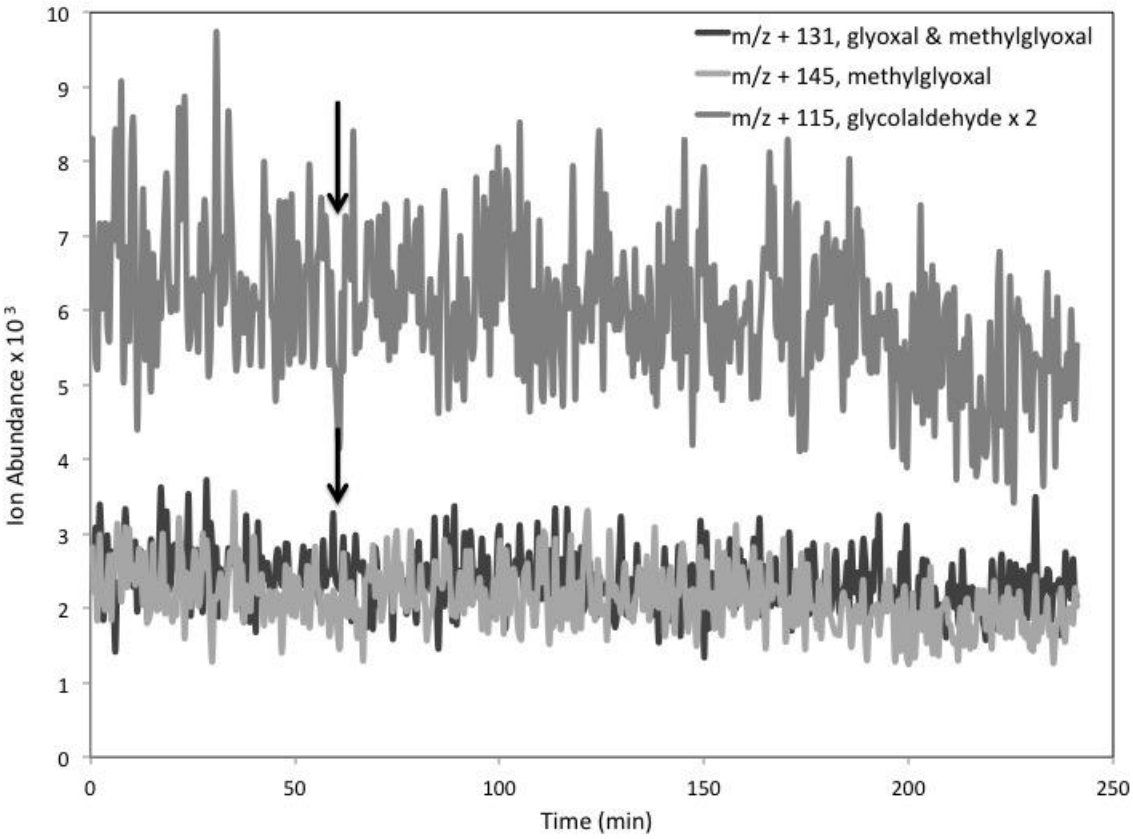

Appendix C.6

ESI-MS negative mode analysis of m/z - 59, 73, 75, 87 and 89 for the H_2O_2 control experiment

ESI-MS negative mode analysis of the third rainwater sample + H_2O_2 reaction. The black arrow indicates when H_2O_2 is added.

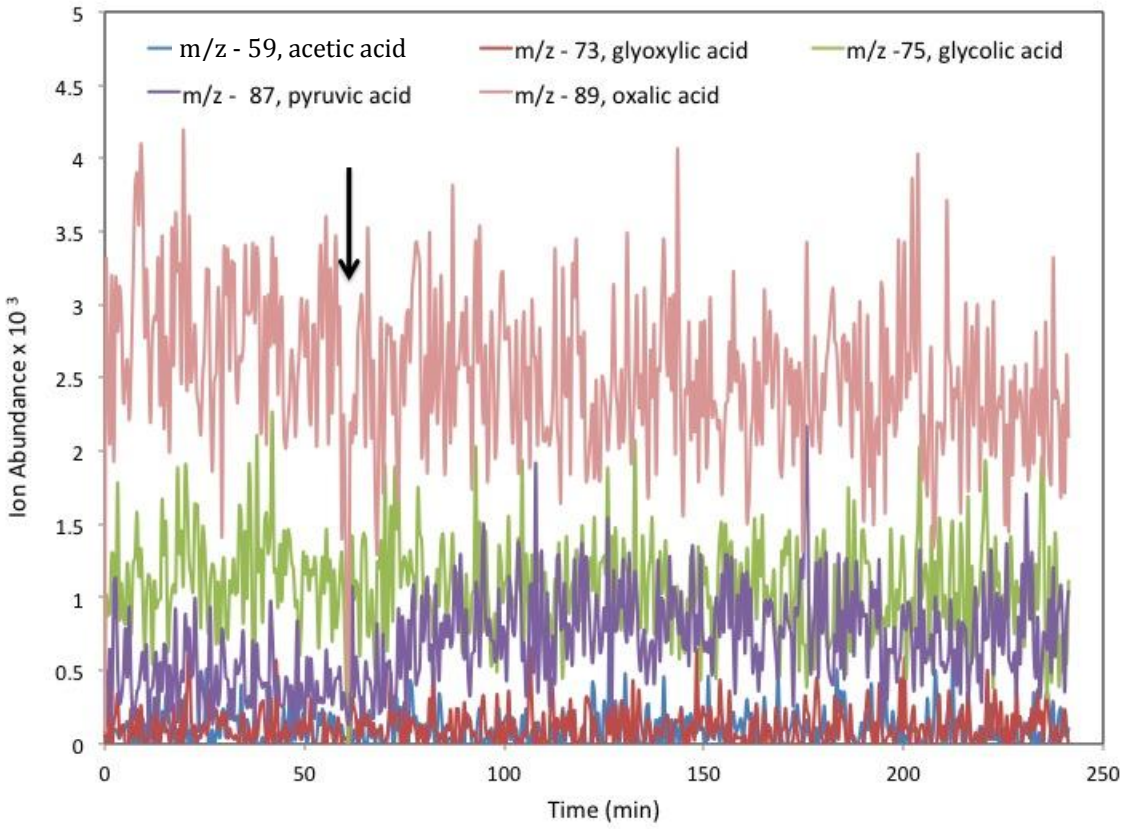

Appendix C.7

ESI-MS negative mode analysis of m/z $^-$ 103 and 117 for the H_2O_2 control experiment

ESI-MS negative mode analysis of the third rainwater sample + H_2O_2 reaction. The black arrow indicates when H_2O_2 is added.

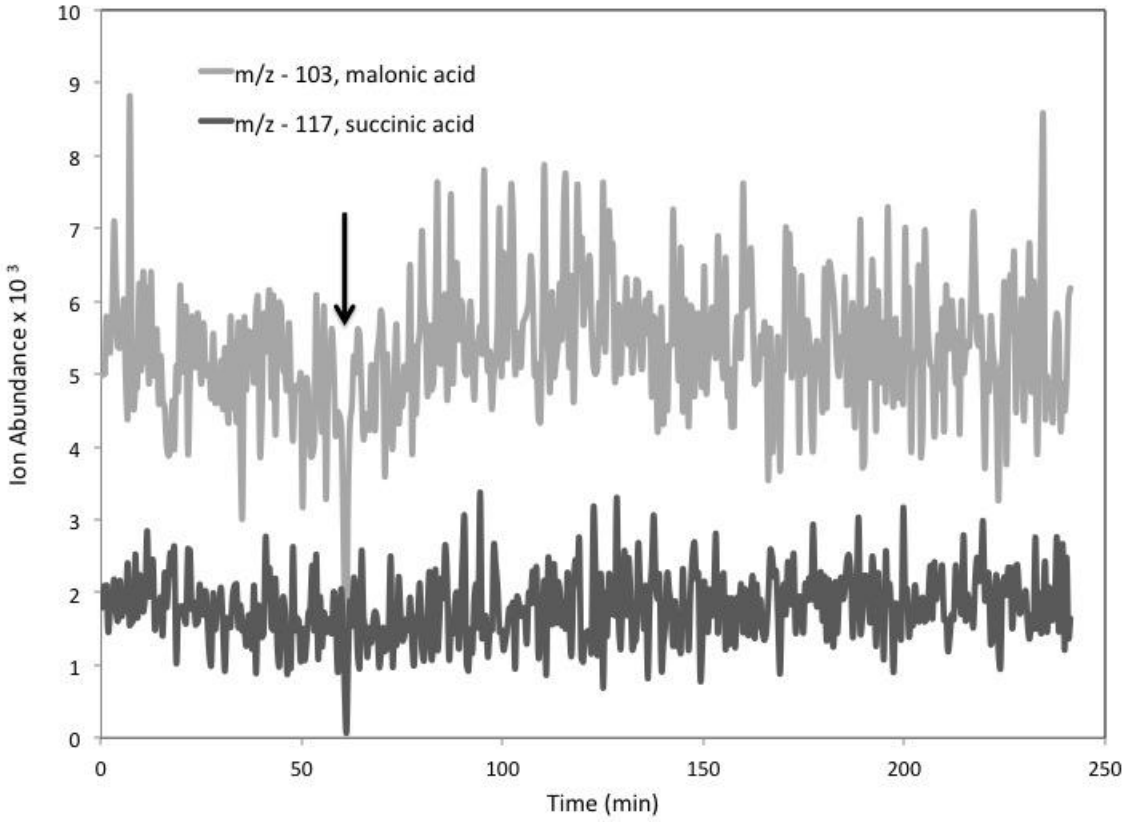

Appendix C.8

ESI-MS negative mode analysis of m/z - 59, 73, 75, 87 and 89 for the UV radiation control experiment

ESI-MS negative mode analysis of the third rainwater sample + UV radiation reaction. The black arrows indicate when the UV lamp is added.

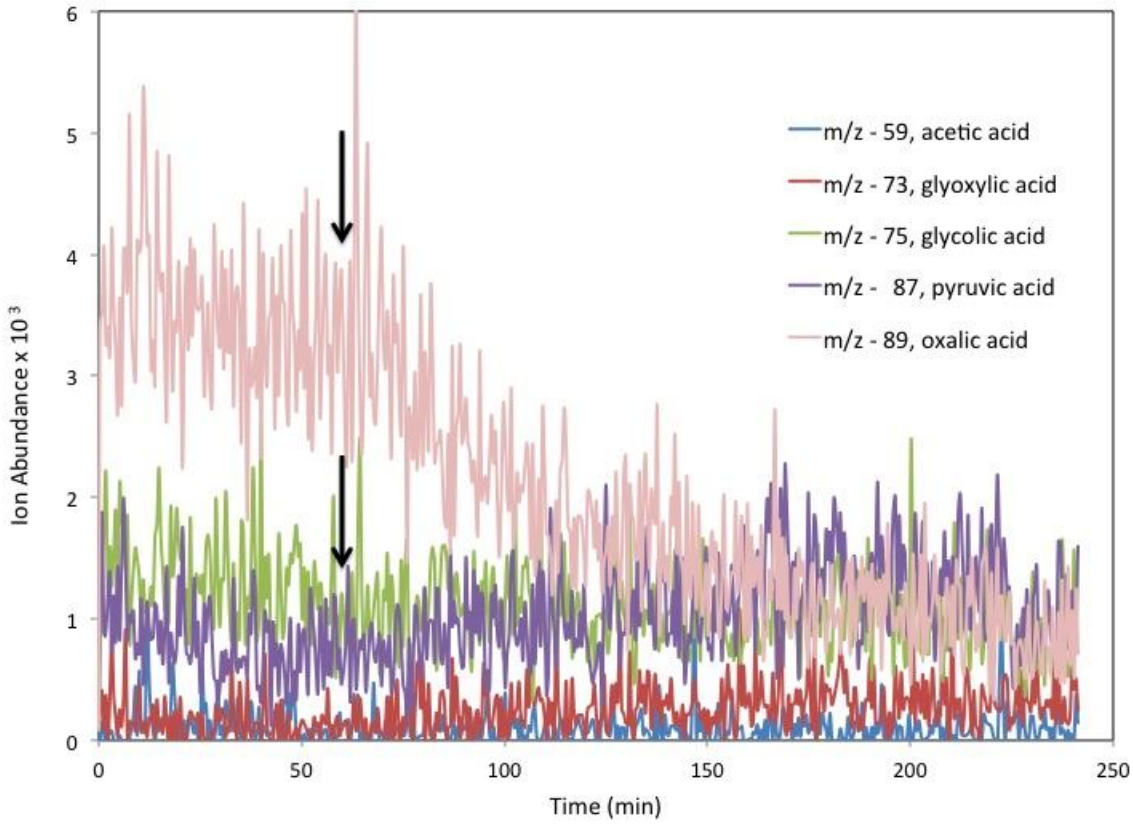

Appendix C.9

ESI-MS negative mode analysis of m/z $^{-}$ 103 and 117 for the UV radiation control experiment

ESI-MS negative mode analysis of the third rainwater sample + UV radiation reaction. The black arrows indicate when the UV lamp is added.

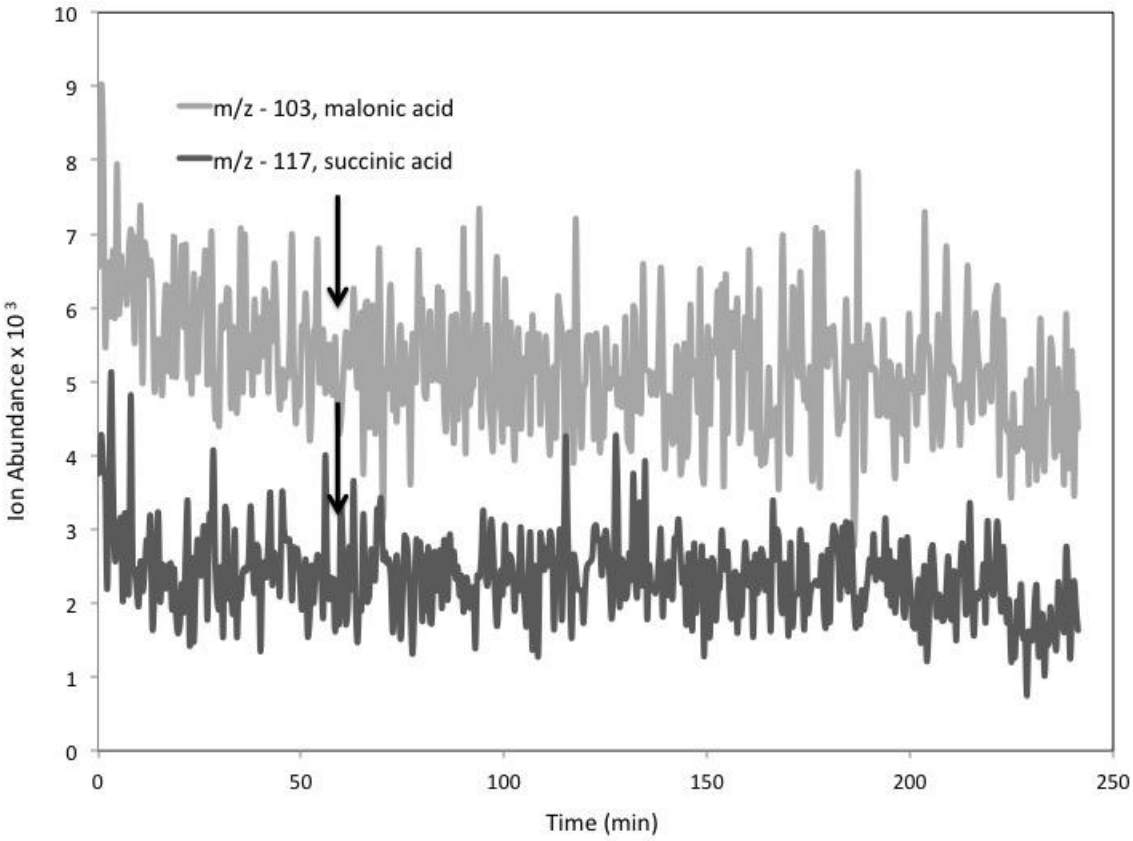

Appendix D: SOP Materials

Appendix D.1

APESI (LC-DAD-CLND-MSD) SOP

Power up from long term (>3 days) shut down

A. Open ChemStation Software LC-MS-CLND online #1

1. Open black valve on LC Binary Pump so that mobile phase flows to waste (turn it counter-clockwise)

B. MSD power up

1. Open valve on liquid N2 tank

2. Check gas flow (left gauge on regulator), if pressure is < 80 psi, open PB (pressure build-up) valve on tank & monitor pressure until it is stable @ 80 psi. (Proceed to step #3 right away but continue to monitor pressure)

3. Switch on power button (bottom left hand corner of the MSD), rough pump will start automatically.

4. If power button already on (but rough pump is off) then start pump down of MSD by going to Diagnosis screen of Chemstation software, pull down the Maintenance menu and click on MSD Pumpdown. System will turn on rough pump ad begin pump down procedure.

5. MSD needs >8 hours after pump down to warm up; data not reliable if you run before this warm up period (High vacuum needs to be ~5.6E-006 Torr)

6. Run 'Check Tune' under MSD Tune screen. If Check Tune fails, 'Autotune' should be run immediately.

7. Go to 'Diagnosis" screen and check the EMF (Early Maintenance Feedback) Info Pad. Any yellow highlighted items need attention.

8. Run a DI water blank for >40 min. to allow system to settle. (MSD detector does not turn on until a sample is introduced to the system)

9. Any obvious noise, baseline, signal, vacuum, or electronics problems detected during the initial blank and standard sample runs need to be resolved.

10. If a problem is detected it can be diagnosed by going to the 'Diagnosis' screen and selecting 'Tests' under the 'Diagnosis' menu. Each instrument component module (Pump, Sampler/Injector, Thermostat, & Detector) has tests associated with it. See ESI-MS Maintenance Schedule file for further details on running routine or diagnostic tests.

C. CLND power up

1. Attach nebulizer to pyrotube (fitting tightens counter clock-wise)

2. Attach nebulizer gas lines to swagelock fittings

3. Attach peek tubing line (coming from splitter) to the end of the nebulizer

4. Open the top cover of the instrument and attach membrane dryer

5. Open the valves on the O_2 and He gas tanks (don't do anything to the regulators)

6. Open the flow restrictor valve

7. Plug in the vacuum pump

8. Turn on the O_3 generator (switch on front panel of instrument)

Power up from short term (1 to 3 days) shut down

A. Open ChemStation Software LC-MS-CLND online #1

1. Open black valve on LC Binary Pump so that mobile phase flows to waste (turn it counter-clockwise)

B. MSD power up

1. Check Liquid Nitrogen (gas) flow (left gauge on regulator), if pressure is < 80 psi, open PB (pressure build-up) valve on tank & monitor pressure until it is stable @ 80 psi. (Proceed to step #3 right away but continue to monitor pressure)

2. On Chemstation software, click on the system "on" button (bottom right side of system diagram).

3. Make sure high vacuum is ~5.6E-006 Torr

4. Run a Checktune, if it fails run an Autotune immediately.

5. Check the EMF for yellow highlighted items & attend to them.

6. Run a DI water blank for >40 min. to allow system to settle. (MSD detector does not turn on until a sample is introduced to the system)

7. If any problems are noticed in baseline, noise, signal, etc., follow directions for diagnosing and resolving problems (#9 under **Power up from long term (>3 days) shut down** above)

C. CLND power up

1. Attach nebulizer to pyrotube (fitting tightens counter clock-wise)

2. Attach nebulizer gas lines to swagelock fittings

3. Attach peek tubing line (coming from splitter) to the end of the nebulizer

4. Open the top cover of the instrument and attach membrane dryer

5. Open the valves on the O_2 and He gas tanks (don't do anything to the regulators)

6. Open the flow restrictor valve

7. Plug in the vacuum pump

8. Turn on the O_3 generator (switch on front panel of instrument)

Terms/Definitions:

Long term shut-down- instrument shut down so that no gases are flowing and no mobile phase is flowing through the system. This is done when the instrument won't be run over a period of >2-3 days.

Appendix D.2

Online ESI checklist and SOP

Time

_____ Lamp on in unused vessel

_____ MS On
_____ Check Tune +, - mode
_____ Check volumes in mobile phase bottles, fill if needed
_____ DI Blank 30 min (from mobile phase bottle) (0.11 mL/min each pump) (using 2pumpsN.m or 2pumpsP.m)

_____ Rinse reaction vessel / let dry upside down for a while
_____ Start tubing flush with rainin rabbit from DI water in beaker
_____ Makeup solution in 250 mL volumetric flask

_____ Setup reaction vessel by MS
_____ Cover bottom 2/3 with foil
_____ Stir bar on at 300 RPM
_____ Check cooling water connections on vessel
_____ Cooling water on

_____ Insert Rainin Rabbit tubing
_____ Set Isocratic pump to 0 mL/min
_____ Put HPLC pump inlet into reaction vessel at the bottom
_____ Make sure rabbit tubing is above the HPLC inlet tubing
_____ Pour reaction solution into vessel

_____ Purge HPLC pump for 2 min at 5 mL/min
_____ Set isocratic pump to 0.22 mL/min; **Close waste valve**
_____ Setup sequence with n runs of 2Pumps(N/P), 60 min each
_____ Start analysis, start stopwatch timer, leave for at least 60 min

_____ Set Isocratic pump to 0 mL/min
_____ Pour H_2O_2 in, mix, turn lamp on (note time)
_____ Set Isocratic pump to 0.22 mL / min
_____ Turn on cooling air
_____ Cover the top portion with foil

Monitor cooling water for leaks! Make sure stir bar is stirring properly
Sample every now and then, run samples on IC ASAP
Sample for ESI and HPLC both
Don't forget to take duplicates!

Cleanup

_____ Turn lamp off, stored in its container

_____ Set isocratic pump to 0 mL/min (it'll probably already be on standby)
_____ Put isocratic pump inlet into a clean beaker with DI water
_____ Purge isocratic pump for 5-10 min at 5 mL/min
_____ Put isocratic pump inlet back into DI mobile phase bottle
_____ Purge isocratic pump for 5-10 min at 5 mL/min
_____ Switch to MS at 0.22 mL/min
_____ Run DI Blank for 30 min (from mobile phase bottle) (0.22 mL/min each pump) using 2pumpsN.m or 2pumpsP.m

_____ Empty reaction vessel, sampling waste into waste bottle
_____ Start tubing flush with rainin rabbit from DI water in beaker

_____ Clean reaction vessel, red cap, and stir bar in 1% alconox solution for 15 minutes in sonicator

_____ Rinse reaction vessel, stir bar, thermometer, and red cap at least 3x in DI water and fill with DI water overnight, insert rabbit tubing into it as well

Appendix D.3

SOP for Processing ESI Data using PERRI Program

(Processing protocol for data collected using ESI-MS autosampler)
Created: 28-OCT-2010 RJL
Updated: 02-NOV-2010 RJL

A. Open Chemstation (Instrument Offline) for data processing

B. Copy/Save the ESI-MS Data, Sequence, and Method files of the sample run to be processed in a new folder on desktop of pc to be used for processing.

NOTE: All ESI-MS files are located on the ESI-MS PC hard drive:
masspec/Vol_Second (D:)/hpchem/1/

C. Create a "Positive" and "Negative" mode subfolders within the new desktop folder.

D. Separate (cut and paste) the positive and negative mode sample raw data into the appropriate subfolders.

E. Copy the following data processing application and programs into the ESI-MS data subfolders created above (sections C and D):
CDFpinky.exe
netcdf.dll
sequence.xls
CheckData.exe

NOTE: ESI-MS Data Processing Application is named PERRI
PERRI and the associated programs/tools mentioned above can be found here:
xserve.envsci.rutgers.edu
/Volumes/des/turpin_lab/turpinlab/ESI/Perri Programs
Your subfolder(s) should now look similar to Figure 1 below.

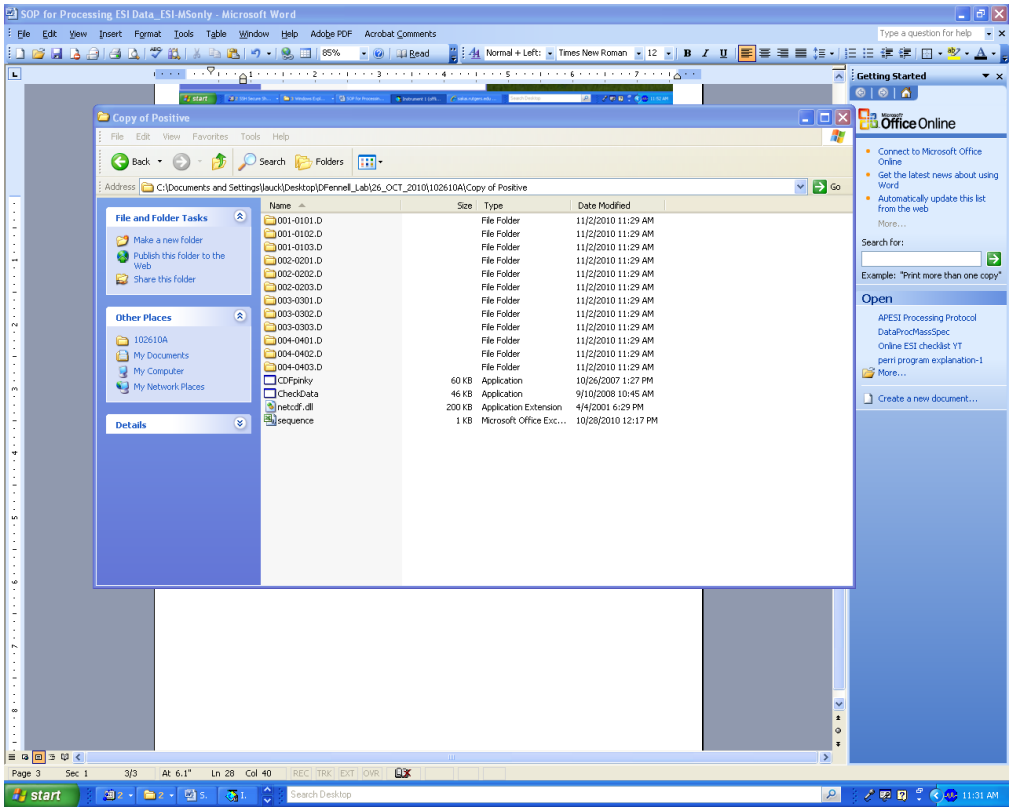

Figure 1. Subfolder containing data, PERRI applications, and associated files

F. In Chemstation, select 'File' > 'Batch Convert MS Data to AIA'

G. Browse for location of data set (positive or negative subfolder above) in the 'Target Directory' section of the Batch Convert window (Figure 2)

H. 'ADD' the same path (copy or browse for same path as in section G above), to the 'Selected Files' section of the Batch Convert window (Figure 2).

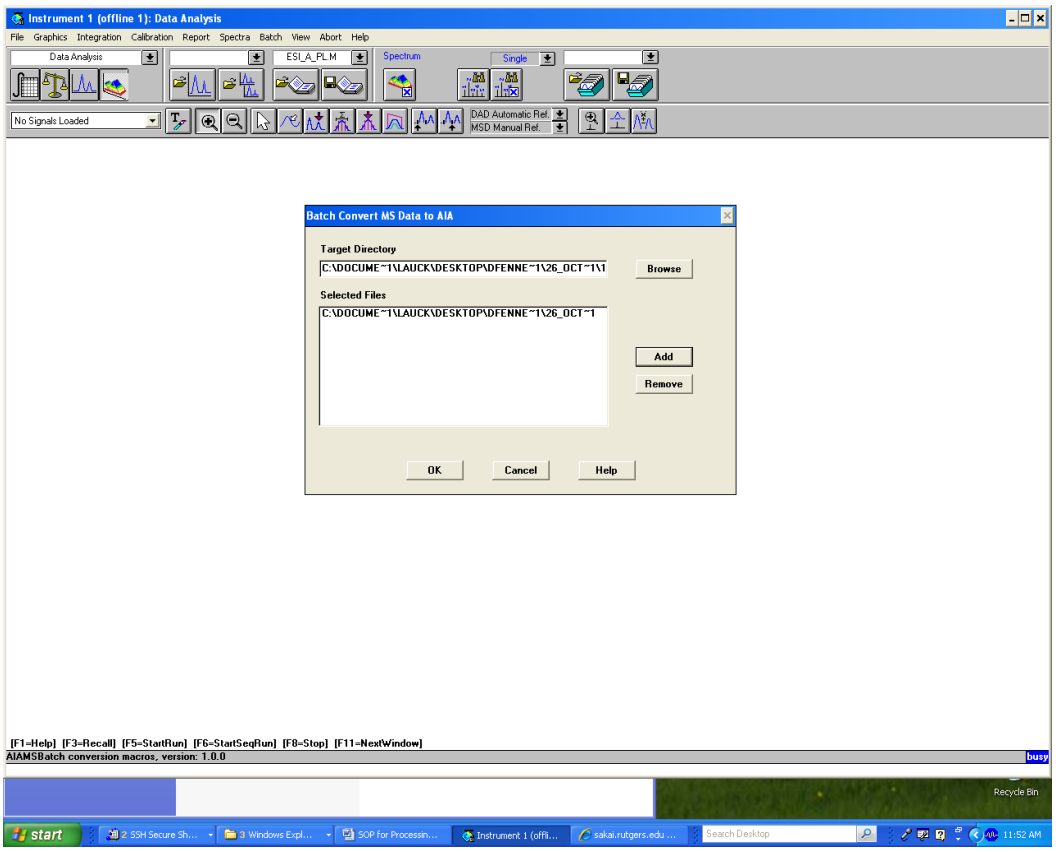

Figure 2. Batch Converting Data Files

I. Select 'OK' and the batch conversion will begin. Each ESI-MS-TIC peak will be visible on screen for a second or two as batch conversion proceeds (check peaks for Gaussian shape).

NOTE: Upon completion of batch conversion, files with *.AIA extentions should be visible in the
ESI-MS Data folder on desktop. The subfolder should now look similar to
(Figure 3 below). Chemstation can be closed at this point if desired.

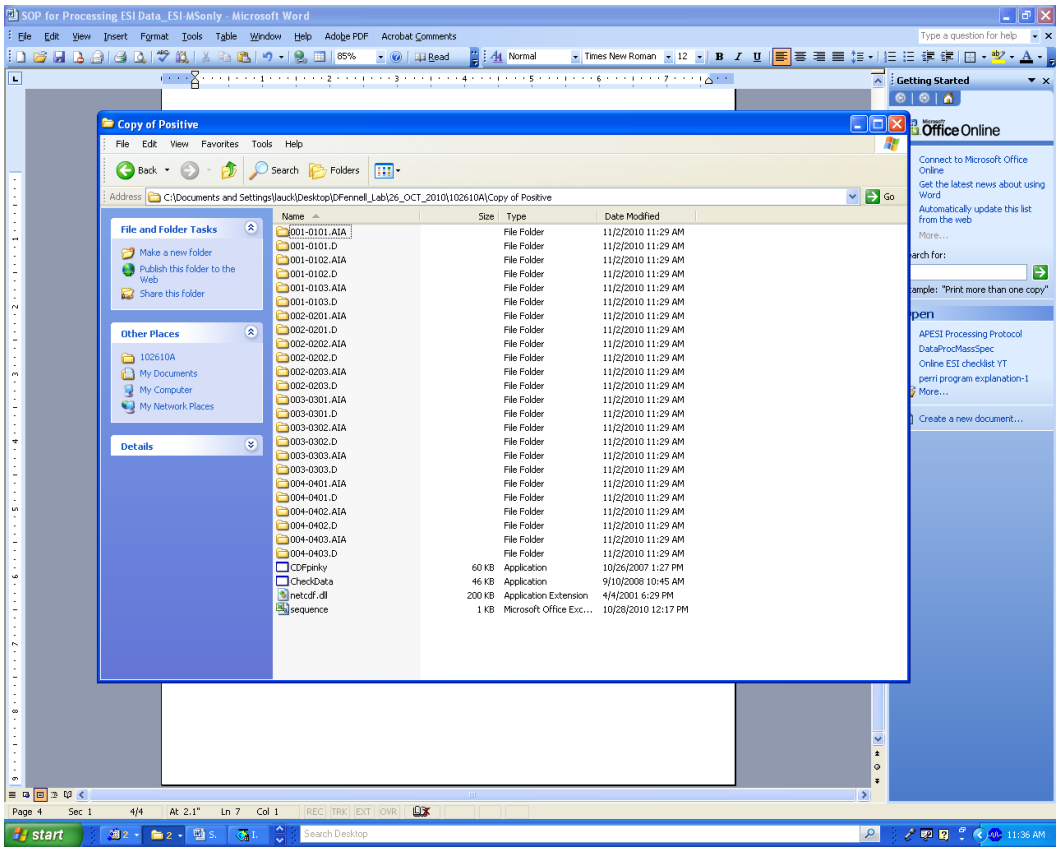

Figure 3. Batch converted data files

J. At this point the 'Sequence' file in the subfolder needs to be modified to match your samples.

NOTE: The format of the sequence file must remain the same as the template sequence file in order for the PERRI applications to operate properly. You must enter your sample IDs, line numbers, and vial numbers in the appropriate format and locations within the sequence file or the template sequence file located here: xserve.envsci.rutgers.edu/Volumes/des/turpin_lab/turpinlab/ESI/Perri Programs to develop your new sequence file (the template sequence file helps if you have a rather large sequence that was run on ESI-MS). **Also note** that the new sequence file name must contain the word "sequence".

K. In the subfolder containing batch converted data (positive or negative mode subfolder) and newly developed sequence.xls file, double click on 'CDFpinky' application.

L. Follow directions that appear in new application window.

M. In the same subfolder that 'CDFpinky' was executed above in section J (positive or negative mode subfolder), double click on 'CheckData' application.

N. Follow directions that appear in new application window.

NOTE: Several files will be created after the applications CDFpinky and CheckData are run. The summary output file will have the last two path entries as part of its name.
For example: If the data folder has the following path – **C:\Documents and Settings\Lauck\Desktop\ESI_run\PosMode_test_02-NOV-2010**
Then the summary output file will be named **ESI_run-PosMode_test_02-NOV-2010**

N. The entire data folder (created in section B) including all subfolders can now be moved to an appropriate location on the hard drive.

Appendix D.4

Ion Chromatography System SOP

This SOP was originally written by Diana Ortiz and modified by Yi Tan, Ron J. Lauck and Jeffrey Kirkland.

1. Overview

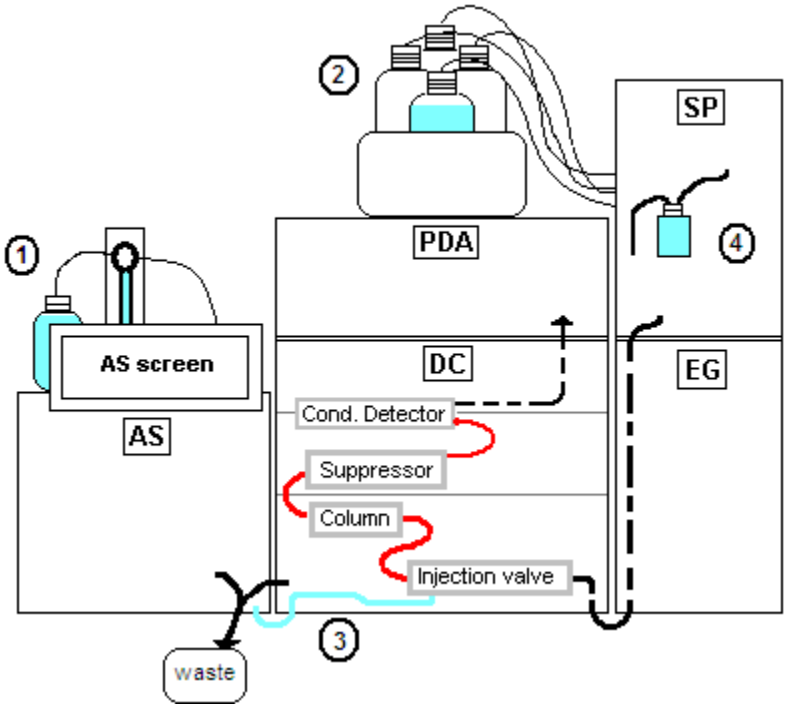

Legend:

SP - Single Pump, with gradient pump.
EG - Eluent Generator generates high purity OH eluents in deionized water.
DC - Detector/Chromatography Module, with the following components:
Injection valve, Column, Suppressor, and Conductivity Detector
PDA - Photodiode Array Detector, measures absorbance spectrum (190-800 nm).
AS - Autosampler

Red tubing - contains sample plus eluent.

① - Deionized water and syringe used to push sample into the system

(NOTE: This water must be change WEEKLY)

② - Deionized water that is used to generate the eluent.
(NOTE: This water must be change WEEKLY)

③ - Sample that gets pushed by the deionized water from the AS into the injection valve in the DC. **(NOTE: This transparent tubing must NOT have bubbles)**

④ - Deionized water used to rinse pump seal.
(NOTE: This water must be change WEEKLY)

Software:

1. Click the **"Chromeleon"** shortcut on the desktop. In addition to the Chromeleon window, a small window with "The Tip of the Day" will pop out then select "Close".

2. On the left side of the window, create a subfolder with your name in the **"2_Data"** folder. See Figure 2, #1.

3. *Copy and paste one of the latest sequence of any of the other subfolders or go to **"File"** then **"New"**, and select **"Sequence (using Wizard)"** to create a new sequence from scratch, see section 5.6.1 of ICS-3000 Manual for more details (attached in SOP). This is important for section C "Sample Run" of this SOP, page 13.

   NOTE: See "Sequence Additions" under the IC – QA/QC section for samples that must be included in every sequence

   NOTE: If using a copy of a previous sequence, be aware of deleting the finished samples that don't correspond to your experiment, or if writing on top of the information make sure to change the "Name", "Type", "Position", "Status", "Program", etc. See Figure 2, #2.

4. Go to **"Default Panel Tabset"** on the **"Chromeleon"** window. See Figure 2, #3.

5. A new small window will pop out, click on **"My Computer"**, then click on the **"Chromeleon Server"**, and finally **"Ok"**. See Figure 3.

6. The Chromeleon [Panel Tabset1] will open; this is the main Control panel. Go to **"File"**, then **"Save As"**, and change the name.

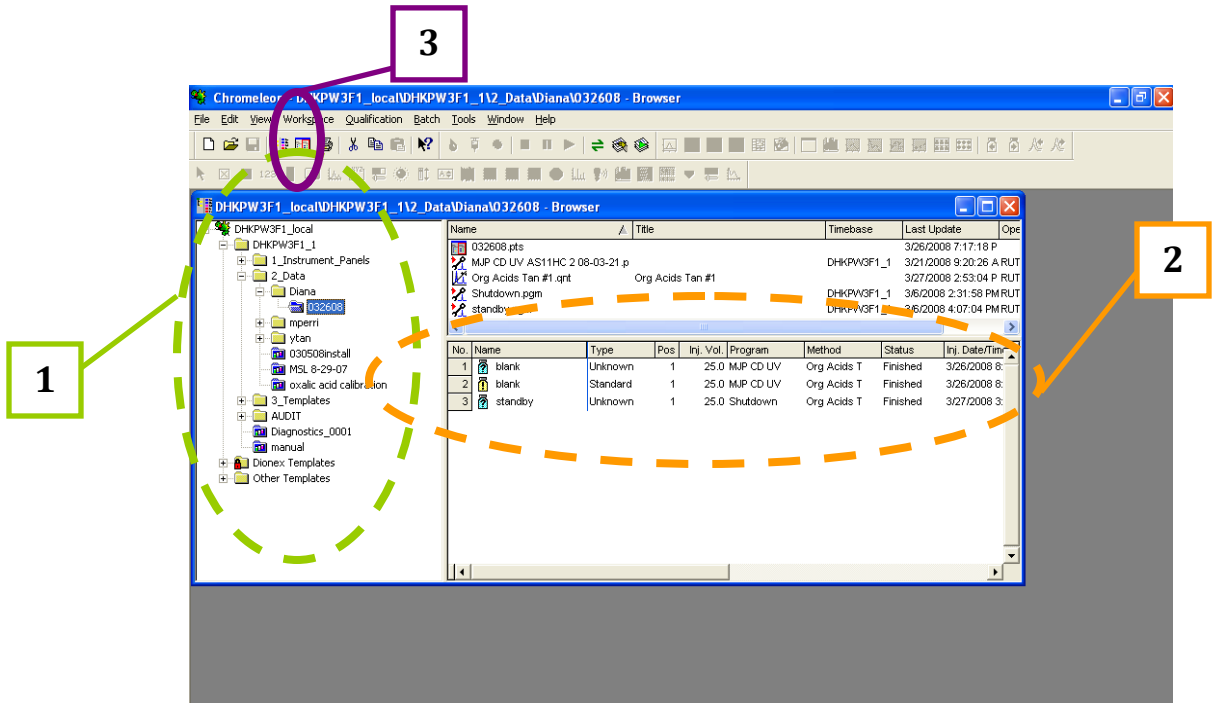

Figure 2. Chromeleon window

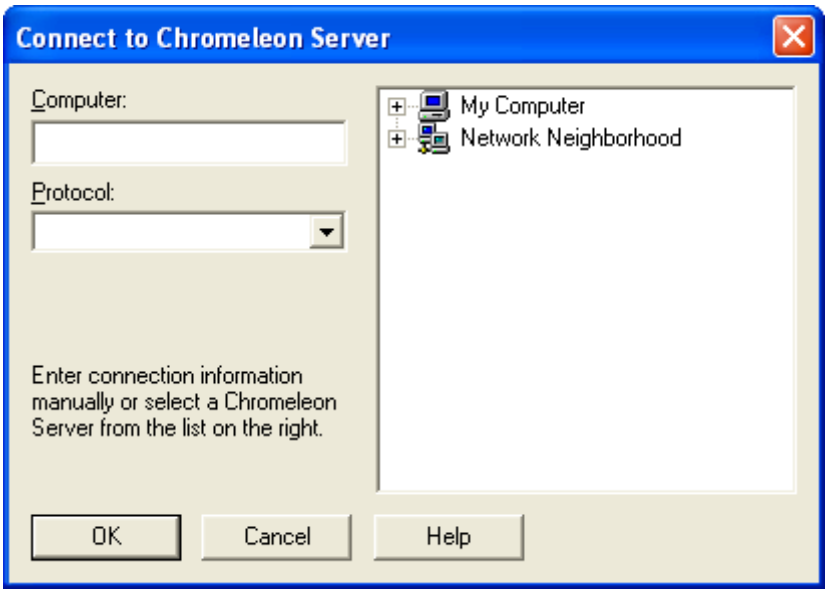

Figure 3. Small window that pops out after clicking "Default Panel Tabset"

2. Pre-Setup (This should be done every morning)

CHECK: Make sure of proper line configuration IC only or IC/MS (see attachment#).

Also check Argon tank/pressure. It is not mandatory that Argon is on when running IC only, however, if Argon is on it is displacing CO2 in the mobile phase containers (important for IC/MS – see section with further details of IC/MS setup).

A. Single Pump (SP) Prime

1. Open Chromeleon's control panel, **[Panel Tablet 1]**, go to the pump Control panel, **"Gradient Pump"** tab (See Figure 4).

NOTE: Make sure Pump is set to 'OFF' and Prime Control is also set to 'OFF'

NOTE: You can switch between local folder file screen (DHKPW3F1_local) and Panel Tabset screen by pushing 'cntrl tab' or by using appropriate buttons in the menu bar.

2. Set the following parameters on the pump Control panel:

- ***Prime Control***

  Duration: 300 sec

  Prime rate: 6.0 ml/min

- ***Gradient Control***

  If isocratic mode is desired: A = **100.0** and the rest =**0.0**

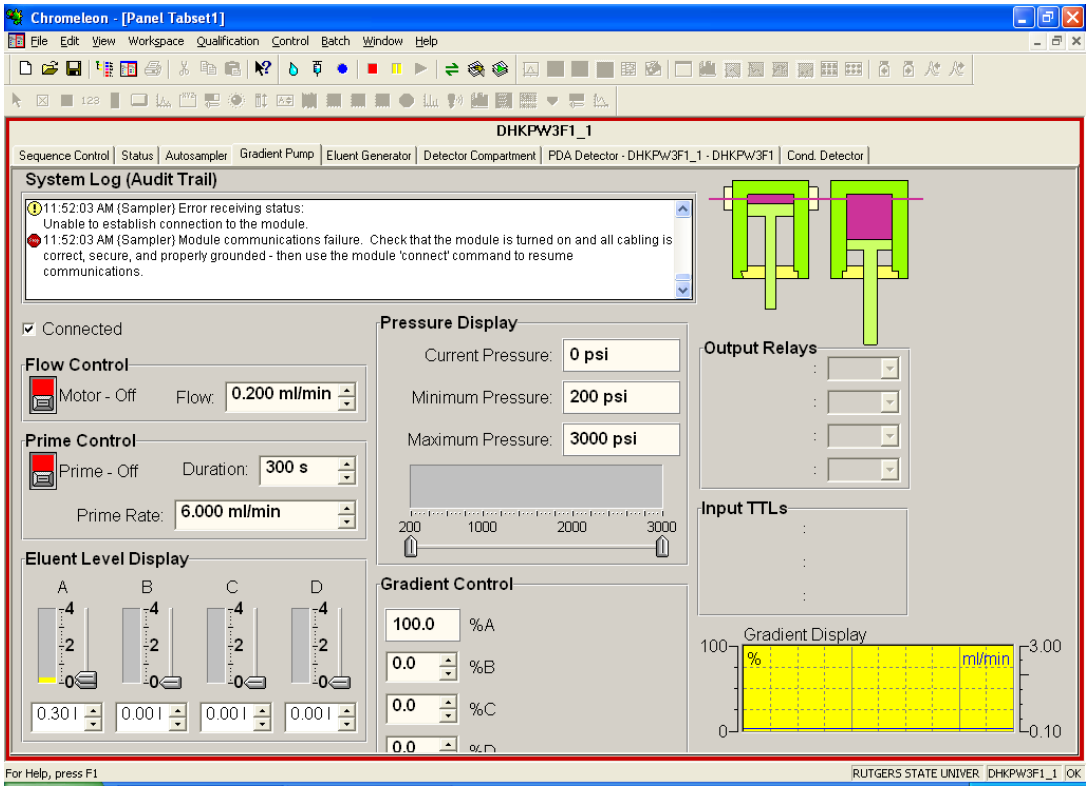

Figure 4. Gradient Pump control panel

3. Open the SP door and then open the priming valve by turning it one-half turn counterclockwise. See Figure 5.

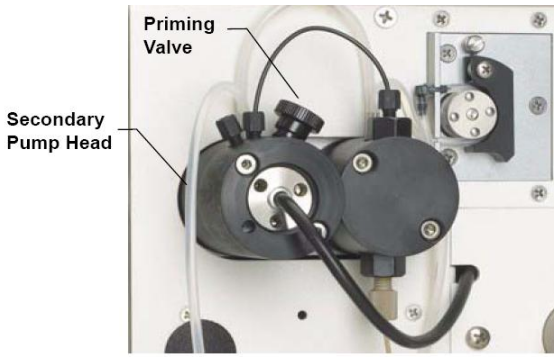

Figure 5. SP priming valve

NOTE: If the priming valve is opened too much, air is drawn through the valve and air bubbles can be seen exiting the waste line.

3. To enable priming, switch the **"Prime"** button to **"On"** on the pump Control panel.
   NOTE: "check results" window comes up (like "ready check" for a sequence.

5. Continue priming the pump until all air and previous eluents are purged and no air bubbles can be seen exiting the waste line.

6. When finished priming, make sure the **"Prime"** button is back to **"Off"**.

7. Close the priming valve by closing it clockwise.
   CHECK: (DO NOT OVERTIGHTEN THE PRIMING VALVE.)

   NOTE: When closing Prime Valve more bubbles will come through, try slowly closing valve & then shut off Prime Button 2 x to clear bubbles.

8. Set the following settings on the pump Control panel:

   - ***Flow Control (In Gradient Pump Tab)***

Flow: **0.400** ml/min

Switch Motor **"On"**

- ***Pressure Display***

Verify, Current Pressure: ~**2000** psi

(For Standby Mode – 0.2 ml/min: pressure ~1300 psi)

NOTE: Pressure can vary over time. If the pressure is too low, there may be a leak somewhere in the system. If the pressure is too high, there may be a clogged/dirty filter.

B. Autosampler (AS) Flush/Prime

1. On the Chromeleon Control panel, **[Panel Tablet1]**, click on the **"Autosampler"** tab. See Figure 6.

2. Make sure the **"Connect"** box is checked, so that the AS is connected to the software. See green circle in Figure 6.

3. Set the prime volume:
   - If daily use: 2000 ?L
   - If non-daily use: 3000 ?L

<If priming doesn't get rid of bubbles, prime by hand, don't tap the syringe. (Remove from assembly by stopping on upstroke and unscrewing syringe)>

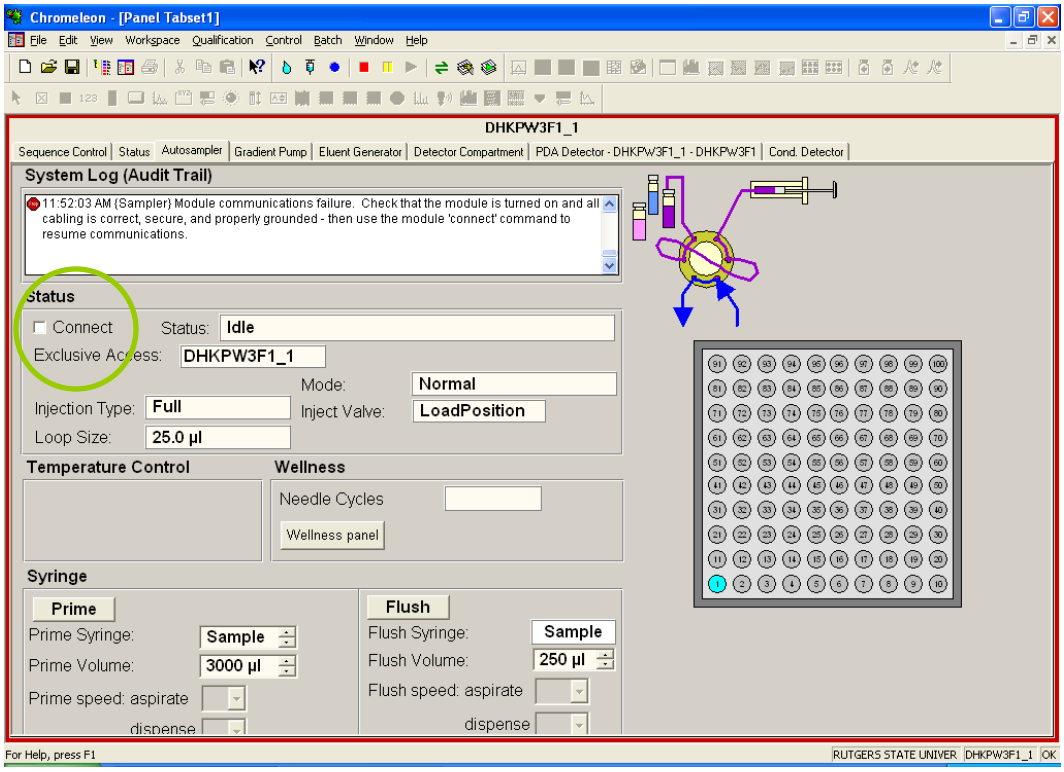

Figure 6. Autosampler control panel

4. Setup

C. Parameters

Open the Chromeleon Control Panel and set the following parameters:

1. **Autosampler Tab** (See Figure 6)

   Make sure the **"Connect"** box is checked

2. **Gradient Pump Tab** (See Figure 4)

   - Make sure the **"Connected"** box is checked
   - Flow Control:
     - ⇨ Flow: **0.400 ml/min**
     - ⇨ Turn "Motor" **On**

- Verify, Pressure*: **~2000 psi** (ideal: 2200 psi)

***must wait a couple of minutes so that the pressure gets ~2000psi**

3. **Eluent Generator Tab** (See Figure 7)

- Make sure the **"Connected"** box is checked
- EGC_1 Control:
  - ⇨ Turn "`**On**"
  - ⇨ EluGen-OH Target Concentration: **1 mM**
  - ⇨ CR-TC: **On**
- EGC_1 Information:
  - ⇨ Check, Remaining Ion Count*: **%**

  *Write it down on the "IC Record" binder, see part b.

4. **Detector Compartment Tab** (See Figure 8)

- Make sure the **"Connected"** box is checked
- Suppressor1 Settings:
  - ⇨ Type: **ASRS-2mm**
  - ⇨ Mode: **On**
- Column_TC:
  - ⇨ Set Point: **30ºC**
  - ⇨ Mode: **On**

*** NOTE: If you open doors to column compartment, temperature in there will change & temp. controller will shut down if temp increases 0.01º**

NOTE: If you look at the suppressor when it is on, small bubbles from Regen Out signifies it is working.

5. **Conductivity Detector Tab** (See Figure 9)

   - Cell Heater:

     ⇨ Cell Heater Mode: **On**

   - Conductivity Detector Settings:

     ⇨ Verify, Total Signal*: **< 1 µS**

     *** Click on the blue dot on top of the tabs (see red circle in Figure 9) to check the stability of the baseline.**

     NOTE: If starting the IC fresh, the conductivity will settle below 1 µS if left overnight.

6. **DOUBLE CHECK FLUID LEVELS**

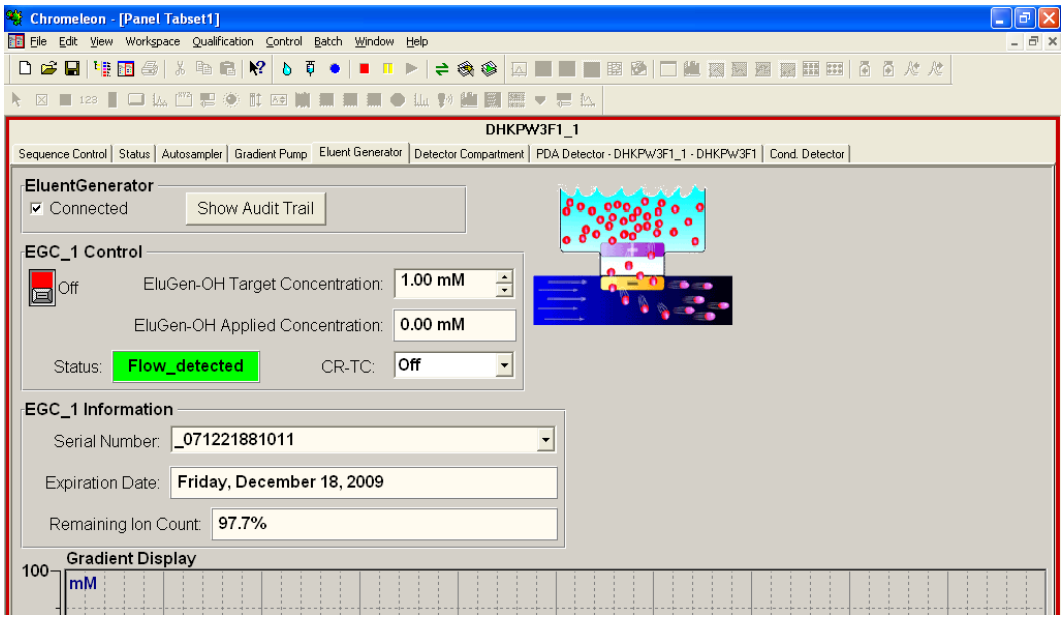

Figure 7. Eluent Generator control panel

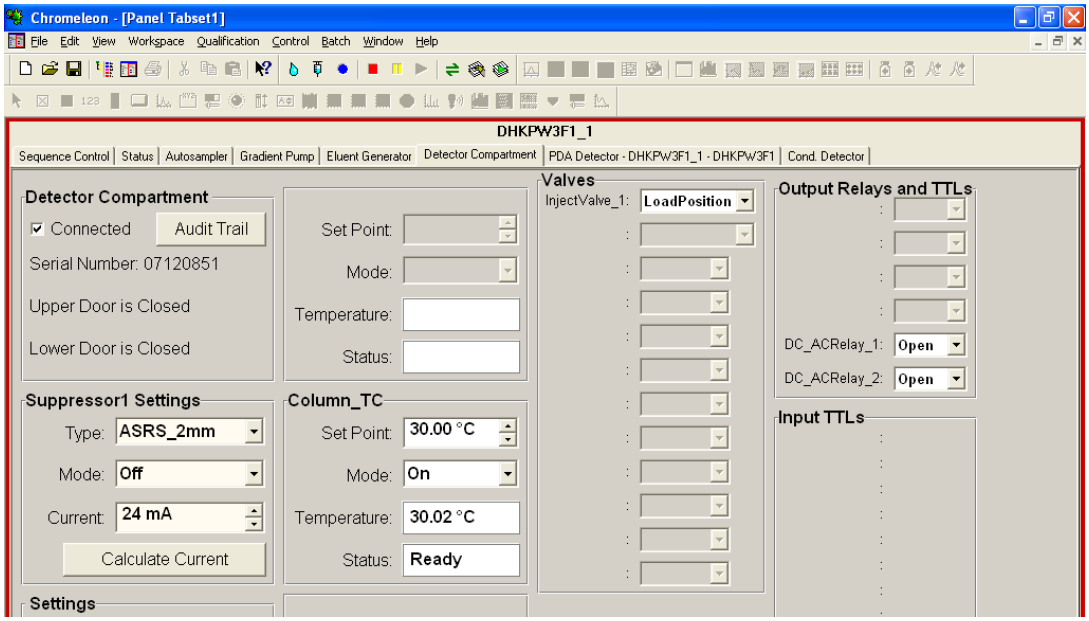

Figure 8. Detector Compartment control panel

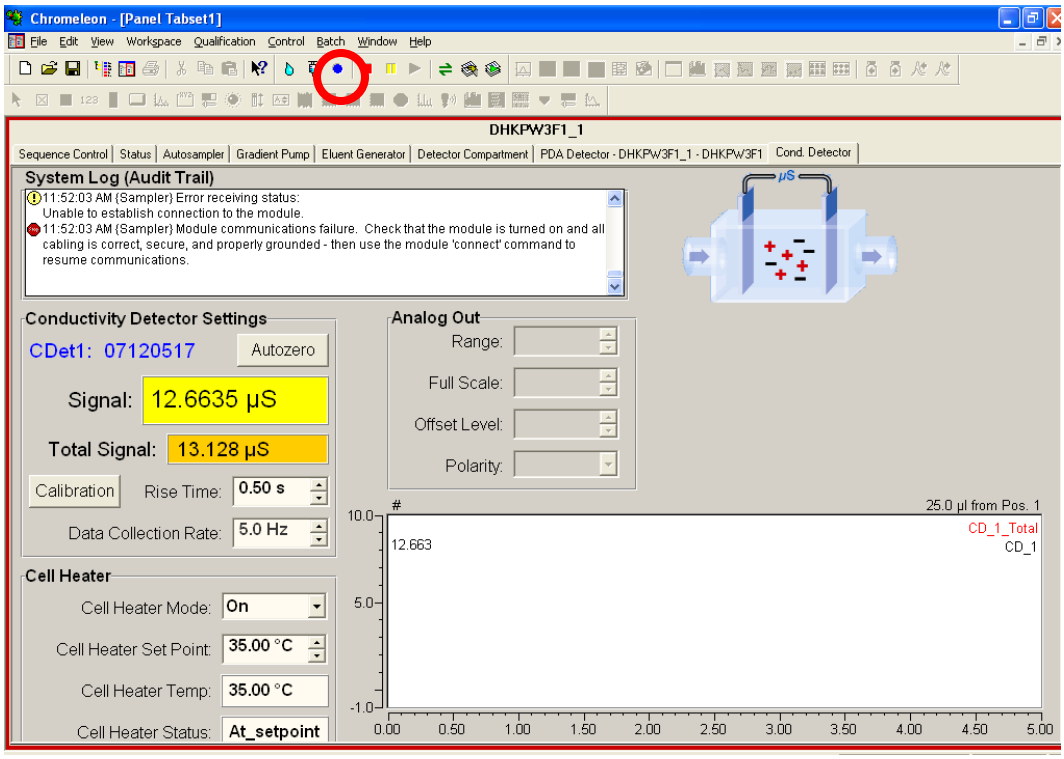

Figure 9. Conductivity Detector control panel

5. Sample Run

A. Overview

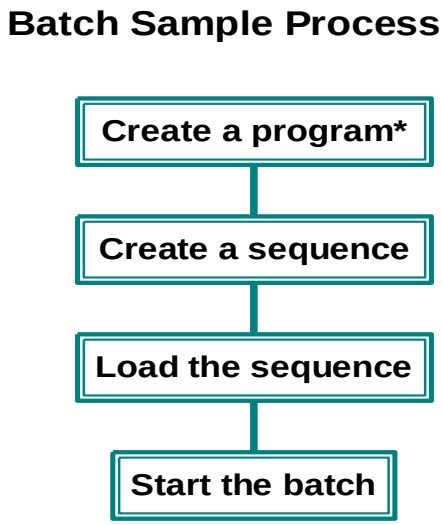

*Includes commands for sampling loading, autozero, injection, and data adquisition.

B. Loading Samples into the Autosampler

a. Prepare the samples: filter sample solutions with 0.45μm filter.

b. Fill the 1.8 mL sample vials at least halfway thorough and place them in the autosampler tray.

NOTE: -Place septum before putting the caps, WHITE SIDE FACING OUTSIDE.

-Each vial position has a corresponding number in the tray.

C. Automatic (Batch) Sample Processing

c. Use Chromeleon to create a list of samples (a sequence) to be processed automatically. See page 4 of SOP, "Software".

For each sample, the sequence includes a program with commands and parameters for controlling ICS-3000 modules and acquiring sample data. To create a program go to Chromeleon's Control Panel, open the **"Sequence Control"** tab and click **"Create Program"**.

d. Run STANDARDS FIRST to create a quantification method, in case there is no previous quantification method that you could use.

NOTE: in the Chromeleon window, use the dropdown menu for sample type to select "Standard" (further instructions on running standards can be found in the "Developing a Calibration Curve" section)

The sequence also includes a quantification method for peak identification and area determination. To create a quantification method, go to the **File** menu and select **"New"**, then select **"Method File"** from the list.

e. After creating the sequence, you can start batch processing.

    i. In the Chromeleon window, click on **"Start/Stop Batch"**.

    ii. A dialog box appears to check that the instrument is ready, then click **"ÖK"**. It will run automatically.

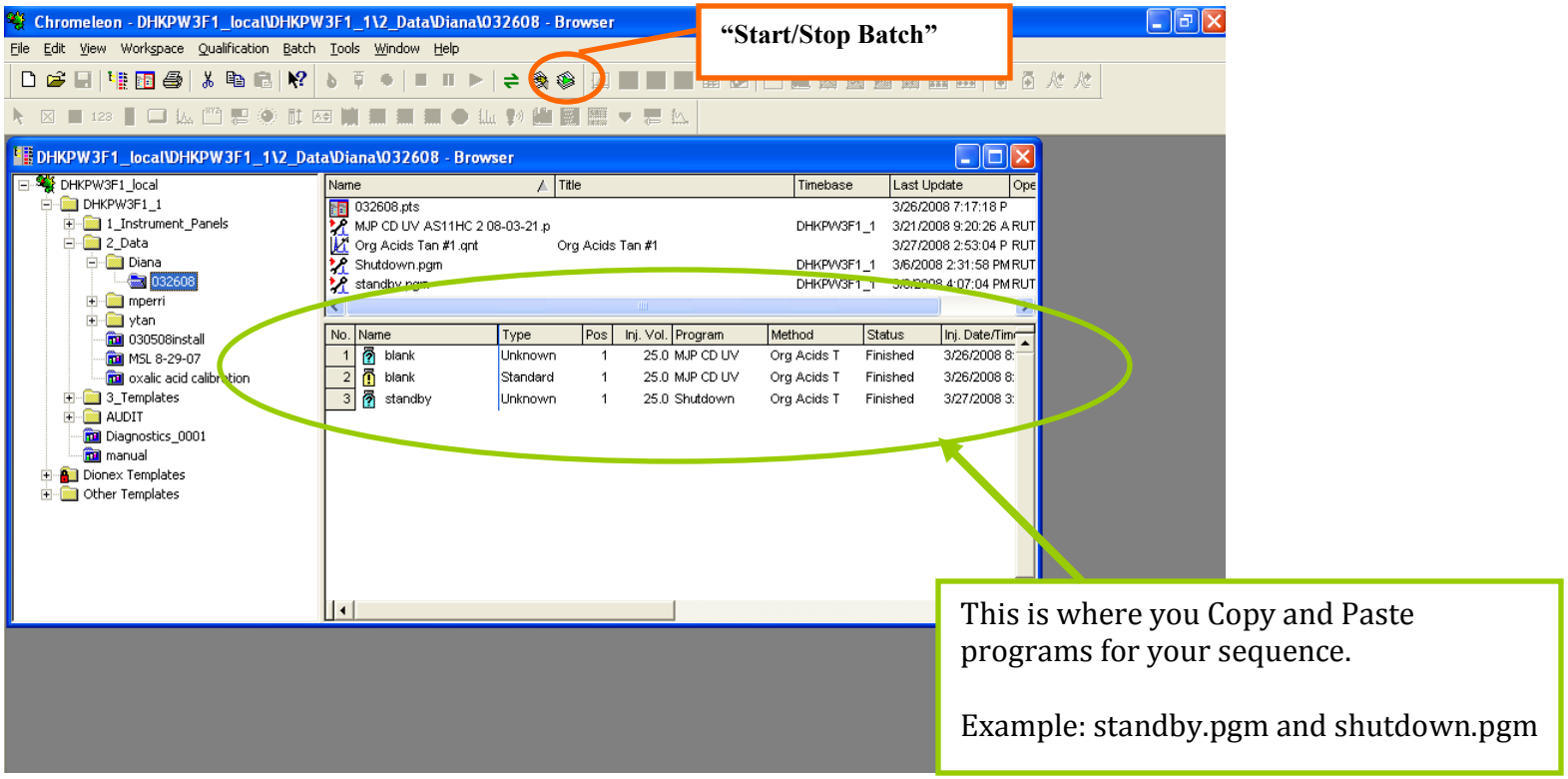

D. Record Entry

- Keep a record in the IC notebook.
- Fill out the form in the "IC Record" binder. (See attachment)
- Print your sequence and store it in the "IC Record" binder.

6. Developing a Standard Curve
NOTE: This is done after running samples of type "Standard"
NOTE: This should be done every ~6 months (the same amount of time that elapses before purchasing new solutions) or when the any change is made to the IC system (i.e.; new column)

1) In Chromeleon: File → New → Method File
    a. General Tab
        i. Give method a name (ex. Mixed Stnd 110315)
        ii. ✓ Absolute Signal
        iii. Fixed @ 25.0 µL
        iv. Autorecalibrate

NOTE: You may refer to old methods to choose settings

    b. Detection Tab
        i. Parameter Value: 0.01 (Detection of Peak)
        ii. Save with method name (same name as 6.1.a.i: Mixed Stnd 110315)
    c. Sample Sequence (Chromeleon sequence window)
        i. Change sample methods (w/ dropdown menu) to method created
        ii. Fill column
        iii. SAVE
        iv. Double Click Sample (non-zero standard: to make sure peaks are present)
            1. Select peak of interest (double click one at a time)
            2. Name peak in window that pops up (ex. Oxalic acid)
            3. Click icon to activate (| → [])
            4. Peak should then appear labeled in the spectrum
            5. Record the retention time of the peak
    d. Detection Tab (back in the New Method File): Input Retention times for each organic acid
    e. Peak Table Tab
        i. Delete Peak 1 = 0
        ii. Window – double click
            1. Check "Relative", "Nearest", "5%"
            2. Fill Column
        iii. Calibration Type
            1. "Quadratic", "Force function through 0"
            2. Fill Column
    f. Amount Table Tab
        i. Right Click peak name
        ii. Columns → Edit amount columns
        iii. Assign Standards based on name
        iv. Click "Autogenerate"
        v. Dropdown – "generate EACH standard" – click apply, OK

vi. Enter amounts for each standard (**IN µM; reads mM**) (ex. 1000 = 1mM)

g. Chromatogram (in chromeleon sample window)
   i. Click "show calibration curve" icon on toolbar (axes w/ line of slope ~1)
   ii. View summary tab to view concentrations
   iii. View calibration tab to view R^2 values of curve
   iv. Close and re-open chromatogram window to ensure application of method parameters

7. Coupling IC/MS (Refer to IC/MS QA/QC for additional details)

A. IC
   a. Make sure IC is "Shut Down" and PUMP is OFF
   b. Remove tube from "cellout" completely (both ends) and place in plastic bag
   c. From bag (in drawer left of IC computer), plug in orange/red tubing to cellout (leads IC outlet to MS)
   d. From bag, plug in large clear tube into "regen" to regenerate suppressor
   e. Auxiliary bottle should be full of milli-q to regenerate suppressor
   f. He/Ar: Pink tubed pressure gauge should read near 10 psi (~8 psi)
   g. Tank pressure should also read near 10 psi

B. MS
   a. T-joint from IC plugged into MS inlet (other end of orange/red tube)
   b. Communication cable (9 pin) spliced from IC to MS and Autosampler
   c. Nitrogen Tank
      i. should read near ~80 psi (Gas Use Valve)
      ii. PB: pressure builder nozzle – increase to 80 if necessary
   d. Re-boot MS computer/program to update chemstation and system

8. Standby & Shutdown

A. Standby

Use when the instrument will be running regularly, for example during the week.

a. Copy the standby program (**standby.pgm**) from a previous sequence and paste it in your sequence. See previous figure (green).

b. Make the last sample of your sequence a "standby" sample by selecting its program as **"standby"**. When the instrument gets to this sample it will automatically turn to standby mode.

B. Shutdown

Use when the instrument isn't going to be used for some days, for example during the weekend.

c. Copy the shutdown program (**shutdown.pgm**) from a previous sequence and paste it in your sequence. See previous figure (green).

d. Make the last sample of your sequence a "shutdown" sample by selecting the program: **"shutdown"**. When the instrument gets to this sample it will automatically shutdown.

9. IC Data Analysis and QA/QC

A. Sequence Additions

i. *Water Blank*

1. Should be run at the beginning and end of every sequence

ii. *Dynamic Blank*

1. Should be run at the beginning and end of every sequence

2. To prepare a dynamic blank, a clean, empty reaction vessel should be filled with E-pure 17.5 megaohm (milli-q) water. A dynamic blank should be drawn from the reaction vessel (executing the same habits/steps as a regular sample)

iii. *Mixed Standard*

1. Quantification of the mixed standard should be within 10% of the desired amount
2. Should be run at the beginning and end of short sequences
3. Should be run every 20 samples for long sequences

*****NOTE: Standards should be replaced every year.**

iv. *Independent Standard*

1. Quantification of the independent standard should be within 10% of the desired amount
2. The independent standard should include the following compounds (for MGLY, GLY, and GLYDE experiments): Formic acid, glycolic acid, pyruvic acid, succinic acid, tartaric acid, and oxalic acid.

v. *Raw Data From Calibration*

1. The samples used to develop the calibration curve must be copy/pasted into the sequence to get the method to function properly (tick "all including raw data" when inserting the copied samples)

vi. *Certified Reference Sample*

1. A certified reference sample (additional independent standard) should be included in the sequence Xtimes/runs (to be determined…) and within 10%

vii. Repeated Samples

1. At least 10% of samples should be run in duplicate (duplicates should be run at the end of the sequence to determine if there is any variation from the position in the sequence to the end of the run)

B. Data Processing

i. Double click the mixed standard to open the chromatogram
ii. Select the first peak in the chromatogram and zoom-in to manually check the integration
    1. Cursor tool with a peak next to it can be used to change the integration (the automatic integration must be deleted before assigning a new one)
    2. The left and right arrow tools can be used to navigate to the next chromatogram and through the entire sequence
    3. When leaving a chromatogram, chromeleon will automatically ask if the changes should be saved, SAVE changes as necessary
    4. Continue through the sequence to check the integration on the single peak for each sample
iii. Zoom-out in the mixed standard chromatogram and zoom-in to the next peak in the chromatogram (Repeat the manual check for each peak in the sequence)
iv. In the mixed standard chromatogram, select the first peak and select the summary tab in the worksheet on the bottom half of the screen
    1. The summary tab includes sample name, peak area, amount, etc.
    2. This information should be copy/pasted into an excel spreadsheet
v. Selecting the next peak in the chromatogram will bring up a new set of summary data, copy/paste until all peak data is transferred to an excel spreadsheet
vi. Manipulate data as necessary in excel or import to other workbook software

C. QA/QC Experiments (to be determined)

a. Percent Recovery Experiments
b. Gradient Mobile Phase Experiments
c. Detection Limit Experiments

10. IC/MS Data Analysis and QA/QC

A. Sequence Additions

a. The same quality control measures should be executed for IC/MS as were for IC alone.

B. Data Analysis

a. MS Computer
    i. Chemstation online 1
    ii. Go into “Data Analysis” (in the Run Control dropdown menu)
        1. Open folder (select: STD00001.D)

        2. Should look like a data bomb
    iii. Integration Dropdown menu: Autointegrate cleans the spectrum
    iv. Find folder in D:; copy/paste into xserve/turpinlab/ESI (to access the file from the IC computer)

b. IC Computer
    i. Find file on xserve and copy/paste to C:/ESI
    ii. Instrument 1 Offline (start menu)
    iii. Find folder in: C:/ESI; Date; STD00001.D again (autointegrate again)
    iv. Chromeleon: open sequence named by date
    v. Look at sample (chromatogram) – ESI vs IC spectrum
        1. Sample number in sequence – not vial position
    vi. Count shark fins in ESI spectrum (sample 13 corresponds to the spectrum before the 13th shark fin)
    vii. Check IC to match the IC record with the IC/MS record
    viii. Note peak retention times of compounds of interest

c. MS Computer
    i. Find peak retention times in ESI data (zoom-zoom)
    ii. Integrate MS peak (Riemann sum icon)
    iii. Spectra Tab – Tabulate mass spectrum
        1. Provides table – File/Print/Tabular mass spectrum (save name)
    iv. Start Tab – Programs – Exploring – to find folder destination
        1. SAVE: ex. F:/ICMS/JKIRKLAN/531min.txt
        2. NO USB PORT, must save to network

d. IC Computer
    i. My network places/turpinlab/user-pass on tower
    ii. Take file for analysis
    iii. Open in excel – cut and paste in one set of columns to make continuous plot
    iv. Analyze and save data as necessary

ATTACHMENTS

5.6.1 Creating a New Sequence

The following two methods are available for creating a new sequence:

- Use the Sequence Wizard if the program and quantification method have already been created.
- Use the Application Wizard if you want to create a new program and quantification method, in addition to the sequence.

Using the Sequence Wizard

1. Click **Create Sequence** on the **Sequence Control** panel (see Figure 5-7).

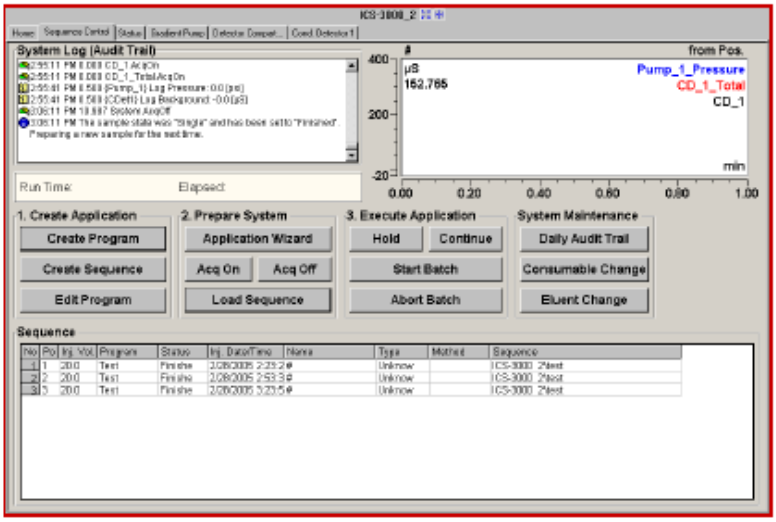

Figure 5-7. Sequence Control Panel

2. Complete the steps in the Sequence Wizard, adding the desired number of samples and standards to the list. For help at any time, click the **Help** button on the Sequence Wizard page.

Using the Application Wizard

1. Click **Application Wizard** on the **Sequence Control** panel
2. Select a suppressor type (if used) and then select an application template from the list.

   NOTE **Instead of selecting an application template, you can use the Virtual Column Separation Simulator. Refer to the Chromeleon Help for details.**

3. Click **Next>** and select the **in a new sequence via Sequence Wizard** option.
4. Click **Next>** to go to the Sequence Wizard.
5. Complete the steps in the Sequence Wizard, adding the desired number of samples and standards to the list. For help at any time, click the **Help** button on the Sequence Wizard page.

   After you finish the Sequence Wizard, a sequence is created and a program appropriate for the selected application is copied to the sequence. If you are using Chromeleon, a quantification method is also copied to the sequence.

   NOTE **Refer to Chromeleon or Chromeleon Xpress online Help for details about the Sequence and Application Wizards.**

Name	**Date**	**Background Signal**	**Pressure**	**Remaining OH**	**Lamps used**	**Column Temperature**	**Suppressor Current**	**Calibration ***

Appendix D.5

Sample Data Sheet

Date:		Light turned on:	
Experiment name:		Stirring setting:	

H_2O_2 Conc.: (amount)		Batch Number:	
H_2SO_4 Conc.:		Batch Number:	
Organic Conc.:		Batch Number:	

Solution Preparation: _____ Solution in vessel: _____

Time	t = min	Sample ID	Temp. (°C)	pH	Comments

References

1. Aiken, A. C., DeCarlo, P. F., Kroll, J. H., Worsnop, D. R., Huff- man, J. A., Docherty, K., Ulbrich, I. M., Mohr, C., Kimmel, J. R., Sueper, D., Zhang, Q., Sun, Y., Trimborn, A., Northway, M., Ziemann, P. J., Canagaratna, M. R., Onasch, T. B., Alfarra, R., Prevot, A. S. H., Dommen, J., Duplissy, J., Metzger, A., Baltensperger, U., and Jimenez, J. L.: O/C and OM/OC ratios of primary, secondary, and ambient organic aerosols with high resolution time-of-flight aerosol mass spectrometry, Environ. Sci. Technol., 42, 4478–4485, 2008.

2. Altieri, K. E., Carlton, A. G., Lim, H. J., Turpin, B. J., and Seitzinger, S.: Evidence for oligomer formation in clouds: Reactions of isoprene oxidation products, Environ. Sci. Technol., 40, 4956–4960, 2006.

3. Altieri, K. E., Seitzinger, S. P., and Carlton, A. G.: Oligomers formed through in-cloud methylglyoxal reactions: Chemical composition, properties, and mechanisms investigated by ultra- high resolution FT-ICR mass spectrometry, Atmos. Environ., 42, 1476–1490, 2008.

4. Altieri, K. E., Turpin, B. J., and Seitzinger, S. P.: Composition of dissolved organic nitrogen in continental precipitation investigated by ultra-high resolution FT-ICR mass spectrometry, Environ. Sci. Technol., 43, 6950–6955, 2009.

5. Anastasio, C. and McGregor, K. G.: Chemistry of fog waters in California's Central Valley: 1. In situ photoformation of hydroxyl radical and singlet molecular oxygen, Atmos. Environ., 35, 1079–1089, 2001.

6. Arakaki, T. and Faust, B. C.: Sources, sinks, and mechanisms of hydroxyl radical (OH) photoproduction and consumption in authentic acidic continental cloud waters from Whiteface Mountain, New York: The role of the Fe(r) (r = II, III) photochemical cycle, J. Geophys. Res., 103(D3), 3487–3504, 1998.

7. Arakaki, T., Kuroki, Y., Okada, K., Nakama, Y., Ikota, H., Kinjo, M., Higuchi, T., Uehara, M., and Tanahara, A.: Chemical composition and photochemical formation of hydroxyl radicals in aqueous extracts of aerosol particles collected in Okinawa, Japan, Atmos. Environ., 40, 4764–4774, 2006.

8. Bigelow, D. S., Dossett, S. R., and Bowersox, V. C.: Instruction Manual NADP/NTN site selection and installation, National Atmospheric Deposition Program, 2001.

9. Blando, J. D., Secondary formation of organic particulate matter in the Smoky Mountains, 1999.

10. Blando J. and Turpin, B.: Secondary organic aerosol formation in cloud and fog droplets: a literature evaluation of plausibility, Atmos. Environ., 34, 1623–1632, 2000.

11. Bond, T. C., Streets, D. G., Yarber, K. F., Nelson, S. M., Woo, J. H., Klimont, Z.: A technology-based global inventory of black and organic carbon emissions from combustion, J. Geophys. Res., 109, D14203, 2004.

12. Brueggemann, E., Gnauk, T., Mertes, S., Acker, K., Auel, R., Wieprecht, W., Moeller, D., Collett, J.L., Chang, H., Galgon, D., Chemnitzer, R., Rued, C., Junek, R., Wiedensohler, W., Herrmann, H., Schmucke hill cap cloud and valley stations aerosol characterization during FEBUKO (I): particle size distribution, mass, and main components, Atmos. Environ., 39, 4291-4303, 2005.

13. Carlton, A. G., Turpin, B. J., Altieri, K., Seitzinger, S., Mathur, R., and Roselle, S.: CMAQ model performance enhanced when in- cloud secondary organic aerosol is included: Comparisons of organic carbon predictions with measurements, Environ. Sci. Technol., 42, 8798–8802, 2008.

14. Carlton, A. G., Turpin, B. J., Altieri, K., Seitzinger, S., Reff, A., Lim, H., Ervens, B.: Atmospheric oxalic acid and SOA production from glyoxal: results of aqueous photooxidation experiments, Atmos. Environ., 41, 7588–7602, 2007.

15. Chang, D. P.Y., and Hill, R. C.: Retardation of aqueous droplet evaporation by air pollutants, Atmos. Environ., 14, 803-807, 1980.

16. Chen, J., Griffin, R. J., Grini, A., and Tulet, P.: Modeling secondary organic aerosol formation through cloud processing of organic compounds, Atmos. Chem. Phys., 7, 5343–5355, 2007.

17. Davidson, C. I., Phalen, R. F., and Solomon, P. A.: Airborne Particulate Matter and Human Health: A Review, Aerosol Sci. Technol., 39:8, 737-749, 2005.

18. Donahue, N. M., Robinson, A. L., Stanier, C. O., and Pandis, S. N.: Coupled partitioning, dilution, and chemical aging of semivolatile organics, Environ. Sci. Technol., 40, 2635–2643, 2006.

19. EPA, US, 2004. Air Quality Criteria for Particulate Matter. US Environmental Protection Agency, Research Triangle Park.

20. Facchini, M. C., Mircea, M., Fuzzi, S., and Charlson, R. J.: Cloud albedo enhancement by surface-active organic solutes in growing droplets, Nature, 401(6750), 257–259, 1999.

21. Facchini, M. C., Rinaldi, M., Decesari, S., Carbone, C., Finessi, E., Mircea, M., Fuzzi, S., Ceburnis, D., Flanagan, R., Nilsson, E. D., Leeuw G., Martino, M., Woeltjen, J., and O'Dowd, C. D.: Primary submicron marine aerosol dominated by insoluble organic colloids and aggregates, Geophys. Res. Lett., 35, L17814, 2008.

22. Faust, B. C., and Allen, J. M.: Aqueous-phase photochemical formation of hydroxyl radical in authentic cloudwaters and fogwaters, Environ. Sci. Technol., 27, 1221–1224, 1993.

23. Feng, J. S., and Moller, D.: Characterization of water-soluble macromolecular substances in cloud water, J. Atmos. Chem., 48, 217– 233, 2004.

24. Fu, T-M., Jacob, D., and Heald, C. L.: Aqueous-phase reactive up- take of dicarbonyls as a source of organic aerosol over Eastern North America, Atmos. Environ., 43, 1814–1822, 2009.

25. Fu, T-M., Jacob, D. J., Wittrock, F., Burrows, J. P., Vrekous- sis, M., and Henze, D. K.: Global budgets of atmospheric glyoxal and methylglyoxal, and implications for formation of secondary organic aerosols, J. Geophys. Res., 113, D15303, 2008.

26. Graber, E. R. and Rudich, Y.: Atmospheric HULIS: How humic-like are they? A comprehensive and critical review, Atmos. Chem. Phys., 6, 729–753, 2006.

27. Graedel, T.E., and Goldberg, K.I.: Kinetic studies of raindrop chemistry I. Inorganic and organic processes, J. Geophys. Res., 88, 865-882, 1983.

28. Graedel, T.E., and Weschler, C.J.: Chemistry within aqueous atmospheric aerosols and raindrops, Rev. Geophys.,19, 505-519, 1981.

29. Graedel, T.E., Weschler, C.J., and Mandich, M.L.: The influence of transition metal complexes on atmospheric droplet acidity, Nature, 317, 240-245, 1985.

30. Graedel, T.E., Mandich, M.L., and Weschler, C.J.: Kinetic model studies of atmospheric droplet chemistry 2. Homogeneous transition metal chemistry in raindrops, J. Geophys. Res., 91, 5205-5221, 1986

31. Hallquist, M., Wenger, J. C., Baltensperger, U., Rudich, Y., Simpson, D., Claeys, M., Dommen, J., Donahue, N. M., George, C., Goldstein, A. H., Hamilton, J. F., Herrmann, H., Hoffmann, T., Iinuma, Y., Jang, M., Jenkin, M. E., Jimenez, J. L., Kiendler-Scharr, A., Maenhaut, W., McFiggans, G., Mentel, T. F., Monod, A., Prevot, A. S. H., Seinfeld, J. H., Surratt, J. D., Szmigielski, R., and Wildt, J.: The formation, properties and impact of secondary organic aerosol: current and emerging issues, Atmos. Chem. Phys., 9, 5155–5236, 2009.

32. Harrison, R. M., and Yin, J.: Particulate matter in the atmosphere: which particle properties are important for its effects on health?, Sci. Total Environ., 249, 85–101, 2000.

33. Heald, C. L., Jacob, D. J., Park, R. J., Russell, L. M., Huebert, B. J., Seinfeld, J. H., Liao, H., and Weber, R. J.: A large organic aerosol source in the free troposphere missing from current models, Geophys. Res. Lett., 32, L18809, 2005.

34. Henze, D. K., Seinfeld, J. H., Ng, N. L., Kroll, J. H., Fu, T.-M., Jacob, D. J., and Heald, C. L.: Global modeling of secondary organic aerosol formation from aromatic hydrocarbons: high- vs. low-yield pathways, Atmos. Chem. Phys., 8, 2405-2420, 2008.

35. Herrmann, H., Tilgner, A., Barzaghi, P., Majdik, Z., Gligorovski, S., Poulain, L., and Monod, A.: Towards a more detailed description of tropospheric aqueous phase organic chemistry: CAPRAM 3.0, Atmos. Environ., 39, 4351–4363, 2005.

36. Intergovernmental Panel of Climate Change (IPCC), Climate Change 2001: The Scientific Basis, edited by J. T. Houghton and D. Yihui, Cambridge Univ. Press, New York, 2001.

37. Jimenez, J. L., Canagratna, M. R., Donahue, N. M., Prevot, A. S. H., Zhang, Q., Kroll, J. H., DeCarlo, P. F., Allan, J. D., Coe, J., Ng, N. L., Aiken, A. C., Docherty, K. S., Ulbrich, I. M., Grieshop, A. P., Robinson, A. L., Duplissy, J., Smith, J. D., Wilson, K. R., Lanz, V. A., Hueglin, C., Sun. Y. L., Tian, J., Laaksone, A., Raatikainen, T., Rautianen, J., Vaattovaara, P, Ehn, M., Kulmala, M., Tomlinson, J. M., Collins, D. R., Cubison, M. J., Dunlea, E. J., Huffman, J. A., Onasch, T. B., Alfarra, M. R., Williams, P. I., Bower, K., Kondo, Y., Schneider, J., Drewnick, F., Borrmann, S., Weimer, S., Demerjian, K., Slacedo, D., Cottrell, L., Griffin, R., Takami, A., Miyoshi, T., Hatakeyama, S., Shimono, A., Sun, J. Y., Zhang, Y. M., Dzepina, K., Kimmel, J. R., Sueper, D., Mid- dlebrook, A. M., Kolb, C. E., Baltensperger, U., and Worsnop, D. R.: Evolution of organic aerosols in the atmosphere, Science, 326, 1525–1529, 2009.

38. Kanakidou, M., Seinfeld, J. H., Pandis, S. N., Barnes, I., Dentener, F. J., Facchini, M. C., Van Dingenen, R., Ervens, B., Nenes, A., Nielsen, C. J., Swietlicki, E., Putaud, J. P., Balkanski, Y., Fuzzi, S., Horth, J., Moortgat, G. K., Winterhalter, R., Myhre, C. E. L., Tsigaridis, K., Vignati, E., Stephanou, E. G., and Wilson, J.: Organic aerosol and global climate modelling: a review, Atmos. Chem. Phys., 5, 1053–1123, 2005,

39. Karamchandani, P., and Venkatram, A.: The role of non-precipitating clouds in producing ambient sulfate during summer: Results from simulations with

the Acid Deposition and Oxidant Model (ADOM), Atmos. Environ., 26, 1041-1052, 1991.

40. Kawamura, K., and Ikushima, K.: Seasonal changes in the distribution of dicarboxylic acids in the urban atmosphere, Environ. Sci. Technol., 27, 2227–2235, 1993.

41. Kawamura, K. and Sakaguchi, F.: Molecular distributions of watersoluble dicarboxylic acids in marine aerosols over the Pacific Ocean including tropics, J. Geophys. Res., 104, 3501–3509, 1999.

42. Kettle, A. J., and Andreae, M.O.: Flux of dimethylsulfide from the oceans: A comparison of updated data sets and flux models, J. Geophys. Res., 105, 26793–26808, 2000.

43. Krivácsy, Z., Kiss, G., Varga, B., Galambos, I., Sárvári, Z., Gelencsér, A., Molnár, Á., Fuzzi, S., Facchini, M. C., Zappoli, S., Andracchio, A., Alsberg, T., Hansson, and H. C., Persson L.: Study of humic-like substances in fog and interstitial aerosol by size-exclusion chromatography and capillary electrophoresis, Atmos. Environ., 34, 4273-4281, 2000

44. Likens, G. E., Edgerton, E. S., and Galloway, J. N.: The composition and deposition of organic carbon in precipitation, Tellus B, 35B, 16-24, 1983.

45. Lim, H. J., Carlton, A. G., and Turpin, B. J.: Isoprene forms secondary organic aerosol through cloud processing: Model simulations, Environ. Sci. Technol., 39, 4441–4446, 2005.

46. Lim, Y. B., Tan, Y., Perri, M. J., Seitzinger, S. P., and Turpin, B. J.: Aqueous chemistry and its role in secondary organic aerosol (SOA) formation, Atmos. Chem. Phys., 10, 10521–10539, 2010.

47. Mader, B.T., Yu, J.Z., Xu, J.H., Li, Q.F., Wu, W.S., Flagan, R.C., and Seinfeld, J.H.: Molecular composition of the water-soluble fraction of atmospheric carbonaceous aerosols collected during ACE-Asia, J. Geophys. Res., 109, D06206, 2004.

48. McHenry, J. N., and Dennis, R. L.: The relative importance of oxidation pathways and clouds to atmospheric ambient sulfate production as predicted by the regional acid deposition model, J. Appl. Meteor., 33, 890–905, 1994.

49. Metzgera, A., Verheggenb, B., Dommena, J., Duplissya, J., Prevota, A. S. H., Weingartnera, E., Riipinenc, I., Kulmalac, M., Spracklend, D. V., Carslawd, K. S., and Baltenspergera, U.: Evidence for the role of organics in aerosol particle formation under atmospheric conditions, PNAS, 107, 6646-6651, 2010.

50. Munger, J. W., Collett, J., Daube Jr., B. C., and Hoffman, M. R.: Fogwater chemistry at Riverside California, Atmos. Environ., 24, 185–205, 1990.

51. Munger, J. W., Jacob, D. J., Daube, B. C., Horowitz, L. W., Keene, W. C., and Heikes, B. G.: Formaldehyde, glyoxal, and methylglyoxal in air and cloudwater at a rural mountain site in central Virginia, J. Geophys. Res., 100, D5, 9325-9333, 1995.

52. Myriokefalitakis, S., Tsigaridis, K., Mihalopoulos, N., Sciare, J., Nenes, A., Kawamura, K., Segers, A., and Kanakidou, M.: In-cloud oxalate formation in the global troposphere: a 3-D modeling study, Atmos. Chem. Phys., 11, 5761–5782, 2011.

53. Noziere, B., Dziedzic, P., and Cordova, A.: Formation of secondary light-absorbing "fulvic-like" oligomers: A common process in aqueous and ionic atmospheric particles?, Geophys. Res. Lett., 34, L21812, 2007.

54. Perri, M. J., Seitzinger, S., and Turpin, B. J.: Secondary organic aerosol production from aqueous photooxidation of glycoalde- hyde: laboratory experiments, Atmos. Environ., 43, 1487–1497, 2009.

55. Pope III, C. A. and Dockery, D. W.: Health Effects of Fine Particulate Air Pollution: Lines that Connect, J. Air Waste Manage., 56, 709–742, 2006.

56. Riipinen, I., Sihto, S.-L., Kulmala, M., Arnold, F., Dal Maso, M., Birmili, W., Saarnio, K., Teinilä, K., Kerminen, V.-M., Laaksonen, A., and Lehtinen, K. E. J.: Connections between atmospheric sulphuric acid and new particle formation during QUEST III–IV campaigns in Heidelberg and Hyytiälä, Atmos. Chem. Phys., 7, 1899-1914, 2007;

57. Seigneur, C., and Saxena, P.: A study of atmospheric acid formation in different environments, Atmos. Environ., 18, 2109-2124, 1984.

58. Seinfeld, J. H., and Pankow, J. F.: Organic atmospheric particulate material, Ann. Rev. Phys. Chem., 54, 121–140, 2003.

59. Shapiro, E. L., Szprengiel, J., Sareen, N., Jen, C. N., Giordano, M. R., and McNeill, V. F.: Light-absorbing secondary organic mate- rial formed by glyoxal in aqueous aerosol mimics, Atmos. Chem. Phys., 9, 2289–2300, 2009.

60. Smith, J. N., Dunn, M. J., VanReken, T. M., Iida, K., Stolzenburg, M. R., McMurry, P. H., and Huey, L. G.: Chemical composition of atmospheric nanoparticles formed from nucleation in Tecamac, Mexico: Evidence for an important role for organic species in nanoparticle growth, Geophys. Res. Lett., 35, L04808, 2008.

61. Sorooshian, A., Lu, M.-L., Brechtel, F. J., Jonsson, H., Feingold, G., Flagan, R. C., and Seinfeld, J. H.: On the source of organic acid aerosol layers above clouds, Environ. Sci. Technol., 41, 4647– 4654, 2007.

62. Sorooshian, A., Ng, N. L., Chan, A. W. H., Feingold, G., Flagan, R. C., and Seinfeld, J. H.: Particulate organic acids and overall water-soluble aerosol composition measurements from the 2006 Gulf of Mexico Atmospheric Composition and Cli- mate Study (GoMACCS), J. Geophys. Res., 112, D13201, 2007.

63. Tan, Y., Perri, M. J., Seitzinger S. P., and Turpin, B. J.: Effects of precursor concentration and acidic sulfate in aqueous glyoxal-OH radical oxidation and implications for secondary organic aerosol, Environ. Sci. Technol., 43, 8105–8112, 2009.

64. Tan, Y., Carlton, A. G., Seitzinger, S. P., and Turpin, B. J.: SOA from methylglyoxal in clouds and wet aerosols: Measurement and prediction of key products, Atmos. Environ., 44, 5218-5226, 2010.

65. Tsigaridis, K., and Kanakidou, M.: Global modelling of secondary organic aerosol in the troposphere: a sensitivity analysis, Atmos. Chem. Phys., 3, 1849–1869, 2003.

66. Turpin, B. J., and Huntzicker, J. J.: Identification of secondary organic aerosol episodes and quantitation of primary and secondary organic aerosol concentrations during SCAQS, Atmos. Environ., 29, 3527–3544, 1995.

67. Turpin, B.J., Huntzicker, J.J.: Secondary formation of organic aerosol in the Los Angeles Basin: a descriptive analysis of organic and elemental carbon concentrations, Atmos. Environ., 25A, 207-215, 1991.

68. Turpin, B. J., Saxena, P., and Andrews, E.: Measuring and simulating particulate organics in the atmosphere: problems and prospects, Atmos. Environ., 34, 2983–3013, 2000.

69. Twomey, S.: Pollution and Planetary Albedo, Atmos. Environ., 8, 1251–1256, 1974.

70. Twomey, S. A. (1991) Aerosols, clouds, and radiation. Atmospheric Environment 25A, 2435-2442.

71. Ulbrich, I. M., Canagaratna, M. R., Zhang, Q., Worsnop, D. R., and Jimenez, J. L.: Interpretation of organic components from positive matrix factorization of aerosol mass spectrometric data, Atmos. Chem. Phys., 9, 2891–2918, 2009.

72. Valverde-Canossa, J., Wieprecht, W., Acker, K., Moortgat, G.K., 2005. H2O2 and organic peroxide measurements in an orographic cloud: the FEBUKO experiment. Atmospheric Environment 39, 4279–4290.

73. Wolff G.T., Monson, P.R., Ferman, M.A., 1979. On the nature of the diurnal variation of sulfates at rural sites in the eastern United States. Environmental Science and Technology 13, 1271-1276.;

74. Yu, L. E., Shulman, M. L., Kopperud, R., and Hildemann, L. M.: Characterization of organic compounds collected during the southeastern aerosol and visibility study: Water-soluble organic compounds, Environ. Sci. Technol., 39, 707–715, 2005.

75. Zappoli, S., Andracchio, A., Fuzzi, S., Facchini, M. C., Gelencse´r, A., Kiss, G., Krivacsy, Z., Molnar, A., Meszaros, E., Hansson, H. C., Rosman, K., and Zebuhr, Y.: Inorganic, organic and macro- molecular components of fine aerosol in different areas of Europe in relation to their water solubility, Atmos. Environ., 33, 2733– 2743, 1999.

76. Zhang, Q., Alfarra, M. R., Worsnop, D. R., Allan, J. D., Coe, H., Canagaratna, M. R., and Jimenez, J. L.: Deconvolution and quantification of hydrocarbon-like and oxygenated organic aerosols based on aerosol mass spectrometry, Environ. Sci. Technol., 39, 4938–4952, 2005a.

77. Zhang, Q., Jimenez, J. L., Canagaratna, M. R., Allan, J. D., Coe, H., Ulbrich, I., Alfarra, M. R., Takami, A., Middlebrook, A. M., Sun, Y. L., Dzepina, K., Dunlea, E., Docherty, K., DeCarlo, P. F., Salcedo, D., Onasch, T., Jayne, J. T., Miyoshi, T., Shi- mono, A., Hatakeyama, S., Takegawa, N., Kondo, Y., Schnei- der, J., Drewnick, F., Weimer, S., Demerjian, K., Williams, P., Bower, K., Bahreini, R., Cottrell, L., Griffin, R. J., Rautiainen, J., and Worsnop, D. R.: Ubiquity and dominance of oxygenated species in organic aerosols in anthropogenically-influenced northern hemisphere mid-latitudes, Geophys. Res. Lett., 34, L13801, 2007.

78. Zuo, Y., and Holgné, J.: Formation of hydrogen peroxide and depletion of oxalic acid in atmospheric water by photolysis of iron(III)-oxalato complexes, Environ. Sci. Technol., 26, 1014 –1022, 1992.